THE
PHYSICAL REVIEW
A Journal of Experimental and Theoretical Physics Established by E. L. Nichols in 1893
VOL. 60, NO. 8 OCTOBER 15, 1941 SECOND SERIES

Production and Isotopic Assignment of Long-Lived Radioactive Sulfur

MARTIN D. KAMEN
Radiation Laboratory, University of California, Berkeley, California
(Received September 3, 1941)

Thick-target yields for the three important nuclear processes giving rise to the long-lived radioactive sulfur isotope are reported. The cross sections calculated from yield values favor the assignment of the activity to S^{35}. The upper limit for the negative electrons emitted by active sulfur is found by absorption measurements in Al and Cellophane to be 120 ± 15 kev. The half-life is 88 ± 3 days. It is concluded that neutron irradiation of carbon tetrachloride affords the most efficient means whereby samples of radioactive sulfur adequate for tracer work may be obtained. The chemical extraction of the sulfur is described and the application of the procedure to large scale production found feasible. Some preliminary investigations on the chemistry of the recoil sulfur produced in the nuclear reactions studied are reported. It is observed that resonance neutrons (absorbed by Cd) are effective in producing sulfur by the (n, p) process analogous to the $N^{14}(n, p)C^{14}$ reaction.

INTRODUCTION

IN 1936, E. B. Andersen[1] found a radioactive sulfur isotope (half-life ~80 days) by irradiating carbon tetrachloride with neutrons. Somewhat later, Libby and Lee[2] investigated the beta-ray spectrum using a screen-wall counter and observed the upper limit to be 107 ± 20 kev. While several articles of a chemical or biochemical nature involving the use of radioactive sulfur as a tracer appeared after 1936, no further studies of the physical properties of this interesting isotope were published. The present report discusses data on the yields and cross sections for the important nuclear reactions concerned in the production of radioactive sulfur. These data may be used not only for isotopic assignment of the activity but also for consideration of the most efficient methods for production of tracer sulfur. Such information should be of interest in view of the increasing importance of radioactive sulfur as a tracer in biochemical investigations.[3-6]

YIELDS OF NUCLEAR REACTIONS

The production of radioactive sulfur by deuteron or neutron activation of sulfur and chlorine has been studied. The reactions of importance from the standpoint of tracer pro-

[1] E. B. Andersen, Zeits. f. physik. Chemie **B32**, 237 (1936).
[2] W. F. Libby and D. D. Lee, Phys. Rev. **55**, 245 (1939).
[3] Borsook, Keighley, Yost, and McMillan, Science **86**, 525 (1937).
[4] H. Tarver and C. L. A. Schmidt, J. Biol. Chem. **130**, 67 (1937).
[5] H. Borsook, J. B. Hatcher, and D. M. Yost, J. App. Phys. **12**, 325A (1941).
[6] H. Tarver and C. L. A. Schmidt, J. App. Phys. **12**, 323A (1941).

duction may be written[7]

$$_{16}S^{34}+{}_{1}D^{2}\rightarrow{}_{16}S^{35}+{}_{1}H^{1} \quad (1)$$

$$_{17}Cl^{37}+{}_{1}D^{2}\rightarrow{}_{16}S^{35}+{}_{2}He^{4} \quad (2)$$

$$_{17}Cl^{35}+{}_{0}n^{1}\rightarrow{}_{16}S^{35}+{}_{1}H^{1} \quad (3)$$

when S^{35} is assumed to be the proper isotope assignment (see discussion below). The yield data for these reactions at various bombarding energies have been summarized in Table I.

For reaction (1) the thick-target yields at ~8 and ~14 Mev bombarding energy relative to the yield at 5 Mev have been tabulated. The leveling off of the yield above 8 Mev was taken to indicate that the cross section for the (d, p) process had become independent of the bombarding energy.

All activities were measured with a Lauritsen electroscope. The sensitivity of this instrument for sulfur radiation was determined by calibration with a sample of active sulfur as $BaSO_4$ which had been counted in a screen-wall counter, the efficiency of which was known to ~50 percent. Consequently the conversion of the counts/min. to microcuries was considered good to within the limits of error given in Table I under the cross section values. Work now in progress should make it possible to arrive at more precise yield values.

Absorption measurements were made with aluminum and Cellophane and the upper limit of the sulfur radiation determined as 120±15 kev. The measurements showed that γ-rays accounted for less than 10 percent of the total radiation. A sample chemically purified and followed over 9 months gave for the half-life a value of 88±3 days.[8]

TABLE I. *Yield of radioactive sulfur.*

Reaction	Target	Beam Energy	Relative Yield	Av. Yield (μc/μamp. hr.)	Cross Section (cm^2)
$S^{34}(d, p)S^{35}$	FeS	5 Mev 8 Mev 14 Mev	1 15±3 50±5	0.075	$7\pm3\times10^{-27}$
$Cl^{37}(d, \alpha)S^{35}$	RbCl	14 Mev	—	0.014	$1\pm0.5\times10^{-27}$
$Cl^{35}(n, p)S^{35}$	CCl_4	0–20 Mev	—	0.11*	$2\pm1\times10^{-27}$

* Obtained with 5 gallons of CCl_4 directly in neutron beam from beryllium target bombarded with 12–16 Mev deuterons from 60-inch cyclotron. In calculating the cross section the neutron-deuteron ratio in the exposed region was taken as 3.5×10^{-3}. The writer is indebted to Dr. E. Segrè and Mr. H. P. Yockey for this datum based on their recent unpublished investigation of the neutron yield from the $Be^9(d, n)B^{10}$ reaction at ~14 Mev. Dr. Willis Lamb of Columbia University was kind enough to check the cross section calculations made for this report.

Isotopic Assignment

The normal isotopic composition of sulfur is S^{32} (95 percent), S^{33} (0.74 percent), S^{34} (4.2 percent) and S^{36} (0.016 percent). The activity may therefore be assigned either to S^{35} or S^{37}. The proper assignment, which has been left unsettled[9] up to now, may be inferred from a consideration of the yield data on reaction (1). If the cross section for the (d, p) reaction is calculated on the basis that S^{34} is the target, a value of 7×10^{-27} cm^2 is obtained. If S^{36} is assumed as the reacting nucleus, this figure must be multiplied by a factor of 220 giving for the cross section a value close to 10^{-24} cm^2. No cross sections for the (d, p) reaction are known to be this high. In Table II some representative values for various nuclei in the neighborhood of sulfur are given. The highest cross sections known occur with the very light elements (i.e., H, Li, Be, etc.), and no value higher than $3\text{–}5\times10^{-25}$ cm^2 has been found. The upper limit for the cross section of reaction (2) based on the nuclear radii of the deuteron and sulfur nucleus may be calculated to be roughly 5×10^{-25} cm^2. From Table II it can be seen that none of the nuclei in the immediate neighborhood of sulfur show cross sections greater than one-tenth of the upper limit. This is to be expected even at the high energies of the bombarding particles used because of the large number of competing reactions possible. It seems quite unlikely, therefore, that the active isotope of sulfur originates from the (d, p) reaction on S^{36}. The activity may, therefore, be considered as arising from S^{35}.

[7] Reaction (1) was first noted by McMillan (unpublished work) who repeated earlier investigations by Sagane, the latter having failed to find a long-lived sulfur activity by deuteron bombardment of sulfur because of low bombarding energies used as well as insufficient bombardment, cf. R. Sagane, Phys. Rev. **50**, 1141 (1936); Cooley, Yost and McMillan, J. Am. Chem. Soc. **61**, 2970 (1939). Reaction (2) was established by the writer in the course of the present investigation. Reaction (3) was responsible for the initial discovery by Andersen.

[8] D. M. Yost (unpublished measurements) has independently found a value in close agreement with this.

[9] R. D. O'Neal and M. Goldhaber, Phys. Rev. **59**, 109A (1941).

TABLE II. *Cross sections and yields for various elements.*

ACTIVE ATOM	REACTION	TARGET	AV. YIELD 16 MEV (μc/μamp. hr.)	CROSS SECTION (cm^2)
$Mg^{27}(\beta^-, \gamma, \tau=10$ min.)	$Mg^{26}(d, p)Mg^{27}$	Mg metal	2800	$1.0\pm0.5\times10^{-26}$
$P^{32}(\beta^-, \tau=14.3$ days)	$P^{31}(d, p)P^{32}$	Red phosphorus	120	$7.3\pm2\times10^{-26}$
$K^{42}(\beta^-, \gamma, \tau=12.4$ hr.)	$K^{41}(d, p)K^{42}$	K metal	35.0	$4\pm2\times10^{-26}$
$Fe^{59}(\beta^-, \gamma, \tau=47$ days)	$Fe^{58}(d, p)Fe^{59}$	Fe metal	0.03	$2\pm1\times10^{-27}$

Through the generosity of Dr. J. W. Kennedy and Dr. G. T. Seaborg, a sample of silver chloride enriched in the Cl^{35} isotope[10] has been made available recently. By studying the production of active sulfur from this sample with reaction (3) it is hoped to confirm the assignment made above.

PRODUCTION OF TRACER SULFUR

(a) Deuteron activation of sulfur

The cross section for $S^{34}(d, p)S^{35}$ was found to be the largest among the three reactions listed as important for production of S^{35}. In practice, however, three factors militated seriously against use of this process, *viz.*: (1) Low isotope abundance of S^{34}. (2) Low specific activity obtainable because of dilution by target sulfur. (3) Tendency of sulfur or sulfides to volatilize or sputter under atomic ion bombardment. Hence, from (1) only 1/25 of the beam could be effective in producing S^{35}. Thus it was found that several milliampere hours of bombardment were necessary to produce satisfactory tracer samples from deuteron bombardment of sulfur. Much difficulty was experienced in preparing targets which could withstand the large beam currents required to adequately activate sulfur in a reasonable period of bombardment. Sulfur, itself, proved entirely unusable, volatilizing even in helium and under optimum cooling conditions when the power input to the target approached $\sim$80 watts/cm^2. Thus, if 100 microampere hours' bombardment at 8 Mev produced the minimum activity desirable in the gram of sulfur required to stop the beam effectively, an exposure of $\sim$10 hours was required. Metal sulfides were found to be the only practicable kind of target material for deuteron activation. Fusion of FeS onto a knurled copper surface which could be water-cooled produced a target which withstood $\sim$1 kw/cm^2 of beam power before appreciably deteriorating. However, for such performance the bombardment was required to take place in helium. In vacuum the sulfide showed a tendency to sputter and give off large quantities of gas which rendered beam operation difficult. It was found that the use of sulfides as internal targets was limited to circulating currents of $\sim100\mu$ amp./cm^2 at 8 Mev.

It was shown chemically that all the activity produced by bombardment of sulfur retained the valence state of the target material. McMillan[11] had found that active sulfur could be dissolved in CS_2 quantitatively and separated from the phosphorus arising from the $S^{34}(d, \alpha)P^{32}$ reaction by shaking with dilute HNO_3, which effectively removed the active phosphorus. This experiment was repeated with carrier $S^=$, and separately with carrier $SO_4^=$ and $SO_3^=$. No activity could be extracted with $SO_4^=$ or $SO_3^=$. A small activity came with the $S^=$ presumably by exchange or through formation of polysulfides.[12] When sulfides were bombarded, all of the activity could be removed by acidification with dilute HCl; such behavior was to be expected since all recoil sulfur could end its career as $S^{*=}$ by electronic interchange with the $S^=$ present as target material.

In carrying out the bombardments of ferrous sulfide for yields determinations, a bell-jar type target was used so that sulfide lost by volatilization could be recovered and error in the yield measurements from this cause avoided.

[10] J. W. Kennedy and G. T. Seaborg, Phys. Rev. **57**, 843 (1940).

[11] E. M. McMillan, reference 7. This method depends on the fact that sulfur does not exchange with CS_2, cf. Cooley, Yost and McMillan, reference 7.

[12] H. H. Voge, J. Am. Chem. Soc. **61**, 1032 (1939).

(b) Deuteron activation of chlorine

Reaction (2) was investigated with rubidium chloride as target. This choice was motivated by the demand for active rubidium as well as sulfur and by the difficulty in using chlorine in any form other than chloride. The disadvantages inherent in deuteron activation of sulfur which have been discussed above were either absent or present to a lesser extent. Thus, the isotope abundance of Cl^{37} was 25 percent as against 4 percent for S^{34}. No dilution because of presence of inactive sulfur could occur. The fair heat conductivity (good compared with the sulfide) and high melting point of the chloride produced a target superior to any of the sulfides tried. On the other hand, the cross section for the (d, α) reaction proved to be some five to ten times lower than that for the (d, p) reaction at 14 Mev.

Nevertheless, reaction (2) could be used profitably for production of tracer sulfur, especially if the metal ion used as target in conjunction with chloride was useful as in the case of rubidium. Bombardment of RbCl for 700 microampere hours[13] at 16 Mev produced 17 microcuries of S^{35}. Such a sample could be recovered in one milligram or less of sulfur and could withstand a dilution of $10^4 - 10^5$ depending on the conditions of measurement. It was found by acidification with dilute HCl that over 95 percent of the recoil sulfur was present as $S^=$. No sulfide was lost during bombardment of the chloride unless the beam power rose to $\sim$500 watts/cm^2 in which case volatilization or sublimation occurred to the extent of 10 percent of the total target material over the period of bombardment ($3\frac{1}{2}$ hours).

(c) Neutron activation of chlorine

This method proved to be the most efficient of the three mentioned. Both high specific and total activities could be realized by exposure of carbon tetrachloride to the neutrons from the 60-inch cyclotron. Both the cross section and isotope abundance were favorable for obtaining large quantities of S^{35}. In addition the chemical manipulations required to extract the active sulfur from the carbon tetrachloride most efficiently proved simple.

Andersen[1] had shown that active sulfur could be concentrated by distillation of the irradiated CCl_4 from inactive sulfur mixed with the chloride prior to bombardment, the active sulfur remaining in the residue with the carrier S. Voge[14] found that only $\sim$one-third of the active sulfur could be recovered as S atoms by this procedure. In this laboratory a similar result was obtained, no more than 30 percent of the active sulfur being recovered as S despite repeated extraction with carrier. It was evident that the major fraction of the S^{35} was held in chemical combination. A number of experiments without carrier were made to ascertain, if possible, the chemical nature of the end products formed by the recoil sulfur. Extraction with cold alkali failed to remove more than 10 percent of the volatile material. Hot alkali was more efficient, the recovery amounting to 30 percent. However, no precautions to exclude air were taken, and, as the active molecules were found to be readily oxidizable (cf. below), it was concluded that the improvement in extraction with hot alkali was due mainly to accelerated oxidation by air. It was suspected that oxidation and not hydrolysis accounted for most of the separability of the sulfur since by bubbling Cl_2 through the CCl_4 with a small quantity of water present 10 percent of the material could be extracted just as with cold alkali. Addition of cold alkali to the chlorine-saturated CCl_4 raised the recoverable sulfur to 25 percent. To extract completely the activity from the CCl_4, it was found necessary to use heat as well as oxidizing agents; H_2O_2, Cl_2, $KMnO_4$ or Br_2 appeared equally good. Permanganate was decided against because almost complete loss of the active $SO_4^=$ formed by oxidation occurred due to occlusion on the MnO_2 formed from the permanganate. It was found that refluxing of the CCl_4 with alkaline hypobromite with subsequent recovery of the sulfate in the aqueous layer constituted a satisfactory procedure. All of these experiments suggested that most of the active molecules were more

[13] An attempt was made to detect Cl^{36} in this sample. No detectable long-lived activity arising from the $Cl^{35}(d, p)Cl^{36}$ reaction was found. Assuming a cross section of $\sim 1 \times 10^{-26}$ cm^2, it was possible to set the half-life of this isotope at $>10^5$ years.

[14] H. H. Voge, reference 12. See also H. H. Voge and W. F. Libby, J. Am. Chem. Soc. **59**, 2474 (1937).

akin to a compound like $CSCl_2$ than to one like Cl_2S_2, inasmuch as a compound like the latter would have been completely extractable in hot alkali.

It was noted that little if any active sulfur was lost by reaction with the tin walls of the containers in which the CCl_4 was bombarded.

To obtain the highest specific activities (about one millicurie of active sulfur in 1–10 milligrams), it was found advisable to remove all sulfur impurities from the CCl_4 prior to irradiation. Analyses of the technical grade of CCl_4 showed amounts of such impurity as high as 30 milligrams S/liter. C.P. grades assayed less than one-tenth of this figure. Hence, it was necessary to redistill CCl_4 from alkaline hypobromite before exposure to neutrons.

It was found that the hypobromite process could be applied to the working of very large quantities of CCl_4. With facilities made available through the cooperation of Professor M. Randall in the Department of Chemistry[15] the feasibility of recovering very small quantities of sulfur high in activity from as much as 100 gallons of CCl_4 was investigated. As little as one gallon of a solution of one normal NaOH containing 3 cc Br_2 extracted 10 milligrams of activated sulfur completely from 110 gallons of CCl_4. No attempt was made to ascertain the minimum time required for complete extraction but periods of 2 to 4 hours were found sufficient.

Some corrosion of the kettle because of exposed surfaces of iron occurred during refluxing and subsequent distillation resulting in the deposition of large amounts of iron oxide. This precipitate was dissolved and analyzed for sulfate, but less than one percent of the active sulfate was occluded (i.e., the loss of sulfate in some 200 grams of Fe_2O_3 amounted to <0.1 milligrams as S). As was anticipated, active phosphorus occluded to a much larger extent ($\sim$50 percent) because of the insolubility of $FePO_4$. In all of the analyses, phosphate was removed as magnesium ammonium phosphate before acidification and precipitation of the sulfate with barium.

Preliminary investigations showed that the $Cl^{35}(n, p)S^{35}$ reaction possessed a marked sensitivity to slow neutrons. Two half-pint cans of CCl_4, one completely wrapped in Cd, were placed in a paraffin box and irradiated with neutrons. The activity of sulfur from the Cd-coated can was one-sixth that from the control. While no value for the slow neutron cross section was obtained, it was very interesting to note that the (n, p) reaction on Cl^{35} could take place with slow neutrons. While the reaction is exothermic by $\sim$680 kev, the potential barrier against proton escape is high ($\sim$5 Mev). It was not expected that any appreciable slow neutron effect would be found. No attempt to enhance the yield by interposition of paraffin between CCl_4 cans was made, but an improvement in production of sulfur by this means should be possible in view of the above result. The experiments are being repeated with antimony chloride in a manner similar to the method of O'Neal and Goldhaber.[16]

It may be noted that competition by the (n, p) reaction could lower considerably the yield of Cl^{36} from the (n, γ) reaction on Cl^{35} especially if the (n, p) reaction occurs, as appears likely, with slow as well as fast neutrons. The reaction $Cl^{35}(n, p)S^{35}$ appears to be closely analogous to the $N^{14}(n, p)C^{14}$ reaction which also occurs with slow neutrons.[17]

The writer is indebted to Mr. G. Friedlaender for aid in the slow neutron experiments. The progress of the research has been greatly accelerated by the interest and encouragement of Professor E. O. Lawrence and the cooperation of the staff of the Radiation Laboratory. Financial aid from the Rockefeller Foundation made this work possible.

[15] The W.P.A. through a local project under supervision of Professor M. Randall aided in setting up the glass-lined iron still. Credit is due Mr. H. W. Koopman, whose assistance in operating the apparatus contributed much to the successful prosecution of this work.

[16] R. D. O'Neal and M. Goldhaber, Phys. Rev. **58**, 574 (1940).

[17] Cf. S. Ruben and M. D. Kamen, Phys. Rev. **59**, 349 (1941) for a discussion of the $N^{14}(n, p)C^{14}$ reaction.

Protons from Deuteron Bombardment of C^{13}

R. F. HUMPHREYS AND W. W. WATSON
Sloane Physics Laboratory, Yale University, New Haven, Connecticut

(Received August 25, 1941)

Comparison of the proton groups emitted under deuteron bombardment by a target of ordinary carbon and by one enriched 25 times in C^{13} shows the existence of an excited state of C^{14} at 5.24±0.29 Mev. This state serves as a possible source for the known 5.5-Mev γ-rays. There is no evidence of any lower-lying excited level in the C^{14} nucleus.

A CONSIDERABLE amount of research has been done on the nuclear reactions involving carbon. Much of this has been reviewed by Bennett, Bonner, Hudspeth, Richards and Watt in a paper[1] which describes additional work employing samples of carbon both enriched and depleted in C^{13}. A summary of the results obtained up to the present time of deuteron bombardment of carbon is given in Table I. In each case the assignment of a reaction to the particular isotope was made by Bennett *et al.* with the aid of targets of altered isotope ratios. A search was made by these authors for proton groups of energy less than 6.6 Mev which might represent an excited state of C^{14}, and thus account for the 5.5-Mev γ-ray. Since none was found the γ-ray was ascribed to an excited state of N^{14} formed in the reaction $C^{13}(dn)N^{14*}$. In the present work which likewise uses targets enriched in one isotope an excited state of C^{14} of energy 5.24 Mev above ground has been found. This offers an alternative explanation for the source of the 5.5-Mev γ-rays.

TABLE I. *Summary of previous results of deuteron bombardment of* C.

Initial Nucleus	Emitted Particle	Energy	Reaction	Energy Released (Q)
C^{12}	γ-ray	3.0±0.2 Mev	$C^{12}(dp)C^{13*}$ $C^{13*}(\gamma)C^{13}$	
	n	0.9 Mev	$C^{12}(dn)N^{13}$	−0.19±0.05 Mev
	P	2.9 Mev	$C^{12}(dp)C^{13}$	2.71±0.05 Mev
		0.8 Mev	$C^{12}(dp)C^{13*}$	−0.52±0.07 Mev
C^{13}	γ-ray	5.5±0.2 Mev	$C^{13}(dp)N^{14*}$ $N^{14*}(\gamma)N^{14}$	
	n	1.49±0.03 Mev	$C^{13}(dn)N^{14*}$	0.40±0.05 Mev
	P	6.6 Mev	$C^{13}(dp)C^{14}$	6.09±0.2 Mev

[1] W. E. Bennett, T. W. Bonner, E. Hudspeth, H. T. Richards and B. E. Watt, Phys. Rev. **59**, 781 (1941). This paper contains references to previous work on carbon.

EXPERIMENTAL PROCEDURE

The carbon targets were prepared from methane gas in which the C^{13} content had been raised to about 27 percent in a multistage thermal diffusion apparatus.[2] A Nier-type 60° mass spectrometer was used to determine the C^{13} : C^{12} abundance ratio. Some 1500 cm³ of this CH_4 enriched in C^{13} to this or a greater extent were passed through a silent discharge under conditions found to give a maximum yield of acetylene. This "heavy" acetylene was desired for spectroscopic experiments. The considerable residue of tar and carbon occurring in this discharge tube was carefully removed and deposited as a mixture in ethyl ether onto gold foil. The result was a somewhat non-uniform, sufficiently durable, "thick" layer of carbon. As judged by the proton groups resulting from deuteron bombardment, this target contained no appreciable amount of N, O or any other light element as

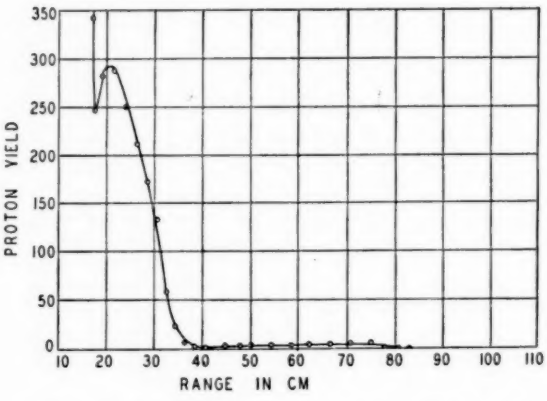

FIG. 1. Proton yield from ordinary carbon, C^{12} : C^{13} ratio 93.3 : 1, bombarded by deuterons.

[2] W. W. Watson, Science **93**, 473 (1941).

impurity. For control experiments other targets were prepared in identical fashion with pure ordinary methane. As an additional check a similar appearing deposit on gold foil was made from some "extra-pure" spectroscopic carbon.

These targets were placed at 45° to a beam of deuterons of 3.82±0.07-Mev energy from the cyclotron. The emitted protons were counted at 90° to the incident deuterons with three proportional counters used in coincidence.[3] With 1.5 microamperes of deuterons the proton yield was enough to necessitate use of diaphragms reducing the count by factors of 200–1000. To increase the resolving power considerable effort was expended to "peak-up" the groups—i.e., to employ the counters more as differential rather than integral counters.

Results

Figure 1 indicates the protons from the bombardment of ordinary carbon; Fig. 2 resulted when the C^{12} : C^{13} ratio was changed from 100 : 1 to 3 : 1; Fig. 3 is an enlargement of the

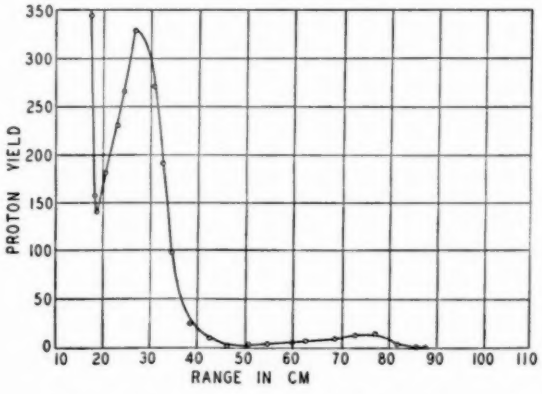

FIG. 2. Proton yield from enriched carbon, C^{12} : C^{13} ratio ~3 : 1, bombarded by deuterons.

$C^{13}(dp)C^{14}$ proton group in Fig. 2. Comparison of Figs. 1 and 2 indicates strongly that the 19 cm and 85 cm groups arise from C^{13}. Likewise, Fig. 3 shows only a single group between 35 cm and 85 cm range. The three groups found, when reduced to their mean ranges,[4] correspond to energies of 3.60±0.10 Mev, 5.21±0.08 Mev and 8.55±0.05 Mev. This gives the following Q values:

$$C^{12}(dp)C^{13} \quad Q=2.38\pm0.15 \text{ Mev}$$
$$C^{13}(dp)C^{14*} \quad Q^*=0.58\pm0.17 \text{ Mev}$$
$$C^{13}(dp)C^{14} \quad Q=5.82\pm0.12 \text{ Mev}$$

and indicates an excited state in C^{14} of 5.24±0.29 Mev. This is thus a possible source for the 5.5±0.2-Mev γ-rays.

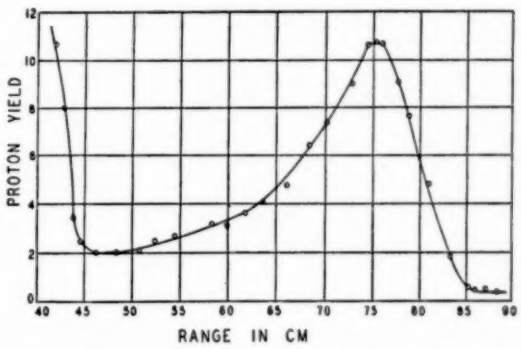

FIG. 3. The long range protons from $C^{13}(dp)C^{14}$ of Fig. 2 magnified by a factor of 25.

Discussion

It is difficult to estimate proton yields from overlapping groups. However, a rough estimate indicates that protons leaving C^{14} in an excited state must be some 50 to 100 times more abundant than those leaving C^{14} in the ground state. In substantiation of this it should be noted that Bennett *et al.*[1] found the 5.5-Mev γ-rays approximately 70 times as numerous as the long range protons. Failure of these authors to find the group resulting in the excited state of C^{14} may lie in the appreciably smaller dispersion offered by a deuteron beam of 1.5 Mev as compared with one of 3.8 Mev.

It is not possible to say unambiguously that 5.24 Mev is the first excited level of C^{14}, since a group coinciding with the C^{12} protons cannot be ruled out. Such a group would lead to a state of 3.44±0.27 Mev above ground. Feenberg and Phillips[5] have predicted with the aid of the Hartree model an excited ^1D state some 1.7 Mev above the ^1S ground state. This corresponds to a proton range of 60 cm. Figure 3 indicates no possibility of such a group of appreciable intensity. A calculation using the single particle

[3] The details of this technique will be published shortly by E. Pollard and one of us (RFH).

[4] M. S. Livingston and H. A. Bethe, Rev. Mod. Phys. **9**, 245 (1937).

[5] E. Feenberg and M. Phillips, Phys. Rev. **51**, 597 (1937).

model puts an upper limit for the ^1D state of 9 Mev.[6] This would lend some support to assuming the first excited level reasonably high. The lack of a γ-ray corresponding to the transition 5.2→3.4 Mev likewise discourages the existence of this 3.4 level.

[6] We are grateful to Professor Henry Margenau for this calculation.

Whether the $C^{13}(dp)C^{14*}$ is the sole source of the 5.5-Mev γ-rays or simply competes with the $C^{13}(dn)N^{14*}$ reaction it is not possible to say. Gamma-ray-proton coincidence measurements would be helpful in this respect.

We wish to make grateful acknowledgement to the George Sheffield Fund for a grant in support of the cyclotron operation.

OCTOBER 15, 1941 PHYSICAL REVIEW VOLUME 60

A Study of the Radiations from the Disintegration of Br^{82}

A. ROBERTS, J. R. DOWNING AND M. DEUTSCH
Massachusetts Institute of Technology, Cambridge, Massachusetts

(Received August 25, 1941)

The radiations from the 36-hour activity ascribed to Br^{82} have been studied by coincidence methods, absorption, and spectrometer techniques. The beta-ray spectrum is simple, and its endpoint is at 0.465 ± 0.01 Mev. Each beta-ray is accompanied by three cascade gamma-rays of energies 0.547 ± 0.01, 0.787 ± 0.015, and 1.35 ± 0.03 Mev. Neither orbital electron capture to Se^{82} nor internal conversion of the gamma-rays is observed. Coincidence measurements made on the beta-ray spectrometer yield independent confirmatory evidence of the simplicity of the beta-ray spectrum. Some considerations concerning the excited states of Kr^{82} obtained in this disintegration are presented.

INTRODUCTION

THE 36-hour slow neutron-induced activity of bromine has been assigned to Br^{82}, and emits a large number of gamma-rays in addition to moderately soft beta-rays. The purpose of the experiments to be described was a study of the radiations from Br^{82}, with the object of determining the modes of disintegration, the energy of the radiations, and, if possible, the resulting energy levels in the product nucleus Kr^{82}.

APPARATUS

Two essentially similar coincidence amplifiers were used in the course of this work. Each of these was of the conventional resistance-coupled pentode type, basically similar to the amplifier described by Langer and Whitaker.[1] In place of cathode biasing, the grid bias on each amplifier stage was separately adjustable. The output of the Rossi coincidence stage was fed into an 885 thyratron mixer, and also into a pulse equalizing amplifier. Grid circuit constants were adjusted to give the sharpest pulses consistent with full saturation of the grids of the Rossi stage. Grid, screen, and plate voltages were obtained from stabilized voltage supplies. Preamplifier stages of Neher-Harper, Neher-Pickering, and modified Neher-Pickering[2] types were used. Separate stabilized high voltage supplies were used for the counters. To obtain individual rates, the pulse equalizing amplifier was used to feed a scale-of-32. Coincidences were counted with the 885 thyratron mixer, which was connected as a self-quenching scale-of-1. The coincidence resolving time was continuously variable by means of the grid bias on the 885. The individual amplifiers of each coincidence amplifier were checked under operating conditions for relative phase shifts by connecting their outputs respectively

[1] L. M. Langer and M. D. Whitaker, Phys. Rev. **51**, 713 (1937).

[2] In this modification, due to Dr. A. F. Kip, the screen battery is replaced by a 5-megohm resistor connected between plate and screen and a 0.5 mf condenser connected between screen and cathode. This is the most satisfactory preamplifier we have used.

to the horizontal and vertical deflecting plates of a cathode-ray oscilloscope. Lack of relative phase shift was verified by the observation that true coincidences gave straight lines through the origin at an angle of 45°.

Counters

The beta-ray counters used were made with brass tubing cathodes of various lengths, $\frac{1}{8}$-inch wall thickness and $\frac{7}{8}$-inch inside diameter, with a mica window on one end. Some of the early counters were filled with air, but all the later work was done with counters filled with tank helium to a pressure just below atmospheric. This permitted the use of quite thin windows (10–15 microns) of large area.

The gamma-ray counters used had metal cathodes sealed in glass envelopes. The cathodes were all $4\frac{1}{2}$ inches long, $\frac{3}{4}$-inch diameter. For most of the work, a thin solid copper cathode (0.010 inch) was used. In later work we found distinct advantages in using copper screen and platinum screen cathodes.[3] For absorption coincidence measurements, the beta- and gamma-counters were mounted in a horizontal plane at right angles, as shown in Fig. 1. This arrangement gave a relatively low cosmic-ray coincidence background, and could be used for both beta-gamma and gamma-gamma coincidences. The apparatus was designed to accommodate interchangeable source-holders, so that sources could be removed and accurately replaced.

With the best of these counters and the modified Neher-Pickering preamplifier circuit, it was possible to count without appreciable loss up to 20,000 counts per minute. Continued operation at this counting rate for many hours caused no change as large as 3 percent in the counting rate.

The magnetic lens beta-ray spectrometer used in this work has been briefly described,[4] and a more complete description is in preparation.

Procedure

Adjustment of amplifier

It was found that after the amplifiers had been adjusted for zero relative phase shift, changing counters did not alter the phase of the signal. In adjusting to zero relative phase shift, two counters were used, and beta-rays sufficiently energetic to penetrate both were obtained from either K^{42} or As^{76}. This method permitted the verification of zero phase shift with the counters actually used in the experiment.

Adjustment of coincidence resolving time

It was found that after the amplifier had been adjusted for sharp pulses and zero relative phase

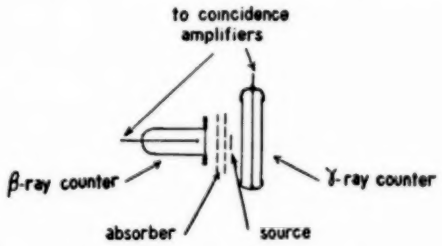

FIG. 1. Arrangement of counters for absorption experiments.

shift, the coincidence pulses obtained from the Rossi stage had a definite maximum height determined by the circuit constants. True coincidences had the greatest height, and partial coincidences were smaller. Thus adjustment of the bias on the 885 made it possible to suppress partial coincidences, and thus to vary the coincidence resolving time. Variation of the bias gave a range from 0 to 6 microseconds.

It has been pointed out by Dunworth[5] and others, that the appearance of the voltage pulse across a counter is not coincident with the entrance of the ionizing radiation, but that it follows it after a certain time lag. This time lag is not constant in any counter, but has a characteristic distribution of values depending upon the construction of the counter. By using a source of high energy beta-rays as described above, we determined for each pair of counters used the resolving time at which true coincidences began to be lost, in much the same fashion as is described by Rotblat.[6] We preferred to run at a resolving time slightly longer than this, so that slight changes in the resolving time or in the counters would not affect the true-coincidence rate. In practice, if a change in

[3] R. D. Evans and R. A. Mugele, Rev. Sci. Inst. **7**, 441 (1936).
[4] M. Deutsch, Phys. Rev. **59**, 684A (1941).
[5] J. V. Dunworth, Nature **144**, 152 (1939).
[6] J. Rotblat, Proc. Roy. Soc. **A177**, 260 (1941).

resolving time was discovered, the data were discarded and the trouble in the amplifier repaired. Resolving times used were ordinarily between 3 and 4 microseconds. This is somewhat longer than the resolving times used by other workers, and the difference may be partially attributed to the fact that our counters are somewhat larger than those usually used.

In this type of amplifier, the size and shape of the output pulse and thus the resolving time should be independent of the individual counting rates. We verified this for our apparatus up to the highest counting rates used.

Coincidence data with the beta-ray spectrometer

In the short magnetic lens type of beta-ray spectrometer, both the source and the beta-ray counter are outside the magnetic field and are well separated. In taking beta-gamma coincidences, a gamma-ray counter was placed directly behind the source, while beta-rays focused by the spectrometer were counted in the usual way. This method has the advantage of measuring coincidences of gamma-rays with beta-rays of a narrow range of energy. In correcting data taken with the spectrometer, the number of gamma-gamma and cosmic-ray coincidences is negligible, since the counters are so far apart.

Measurement of gamma-ray energies

After the rest of the experiment had been completed,[7] it was found possible to measure the energies of the various gamma-rays in the spectrometer.[8] For this purpose, a source was prepared whose gamma-ray activity was at least equivalent to that of 5 to 10 micrograms of radium. This source was sandwiched between layers of copper of sufficient thickness to absorb all the beta-rays, and a radiator of either aluminum or lead placed directly over the front face of the source, according to whether it was desired to measure only Compton recoils or Compton recoils plus photoelectrons.

Preparation of Br^{82} sources

In preparing sources, acetylene tetrabromide $C_2H_2Br_4$ was irradiated by slow neutrons from the M. I. T. cyclotron, and the active bromine precipitated out as AgBr, according to a method previously described.[9] No carrier was added, and the total precipitate was usually about 10–20 mg. The AgBr was dissolved in ammonia, and the source was prepared by evaporating the solution on a thin cover glass. Sufficient time was allowed for the 4-hour period of Br^{80} to disappear.

Results

The fraction of recorded beta-rays giving recorded beta-gamma coincidences as a function of absorber in front of the beta-ray counter is shown in Fig. 2. Sufficient absorber was placed in front of the gamma-ray counter to prevent counting beta-rays in it. The data have been corrected for random coincidences, cosmic-ray background, and gamma-gamma coincidences

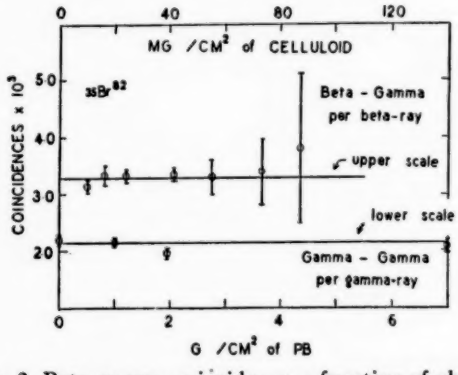

FIG. 2. Beta-gamma coincides as a function of absorber in front of the beta-counter, and gamma-gamma coincidences as a function of absorber in front of the beta-counter, used to count gamma-rays. The point for zero absorber in the gamma-gamma coincidence curve is taken with sufficient celluloid to cut out all the beta-rays.

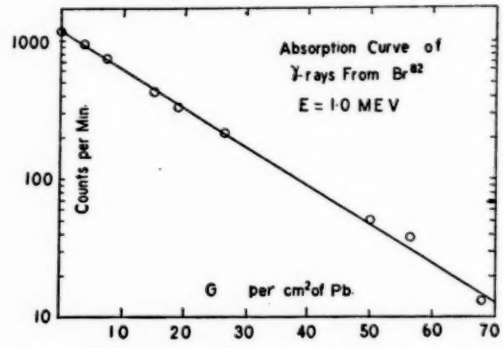

FIG. 3. Absorption of the gamma-rays measured in a single gamma-ray counter. The counter and source were eight inches apart.

[7] J. R. Downing and A. Roberts, Phys. Rev. **59**, 940A (1941).

[8] M. Deutsch and A. Roberts, Phys. Rev. **60**, 362 (1941).

[9] A. Roberts and J. W. Irvine, Jr., Phys. Rev. **53**, 609 (1938).

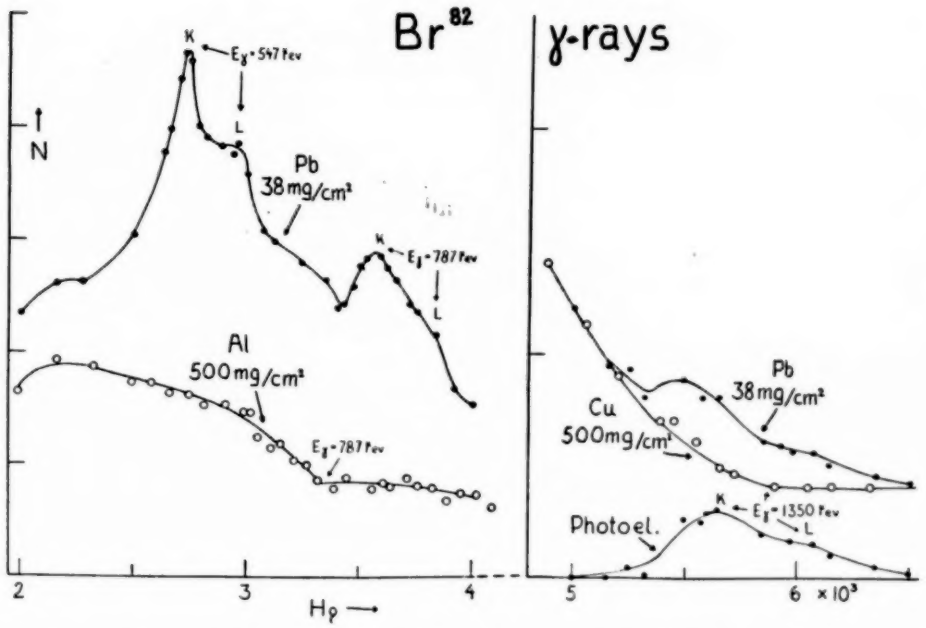

FIG. 4. Typical secondary electron spectra from Br^{82} gamma-rays. Scales adjusted to separate curves. Curve marked "photoel." represents difference between Cu and Pb radiators.

from gamma-rays registered in the beta-counter. The data represent one of several such runs taken with different counters, amplifiers, and geometry. All runs gave a constant number independent of absorber thickness.

Figure 2 shows also a plot of the fraction of recorded gamma-rays giving recorded gamma-gamma coincidences, as a function of the amount of absorber in front of the beta-counter (used to count gamma-rays). This curve is also flat over the region measured, and has been repeatedly verified.

Figure 3 shows an absorption curve of the gamma-rays registered by a single gamma-ray counter. Figure 4 shows a plot of the spectrum of secondary electrons from lead and aluminum produced by the gamma-rays, as measured in the spectrometer. Figure 5 shows the beta-ray spectrum, and also the coincidence spectrum, i.e., the number of beta-gamma coincidences registered as a function of beta-ray momentum. The end-point of the beta-ray spectrum is at 0.465 ± 0.01 Mev, both by inspection and by extrapolation of the Fermi plot, which is shown in Fig. 6.

A search was made for characteristic x-rays, and none was found. This rules out any appreciable branching of Br^{82} to the stable Se^{82} by orbital electron capture. We estimate that not more than 5 percent of the Br^{82} can decay by this process. The absence of x-rays also rules out internal conversion which might have escaped detection in the spectrometer.

Discussion of Results

Since the fraction of beta-rays giving observed beta-gamma coincidences is independent of beta-ray energy, we conclude that all beta-rays are associated with the same number of gamma-

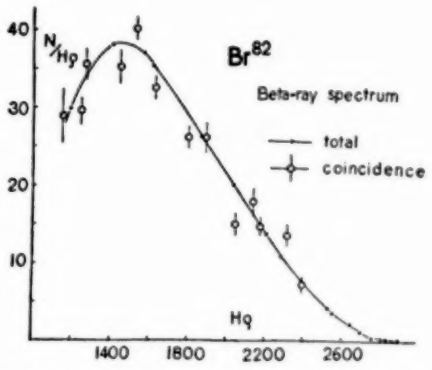

FIG. 5. The beta-ray spectrum and the beta-gamma coincidence spectrum of Br^{82} as taken on the spectrometer. The curves are plotted with arbitrary ordinates.

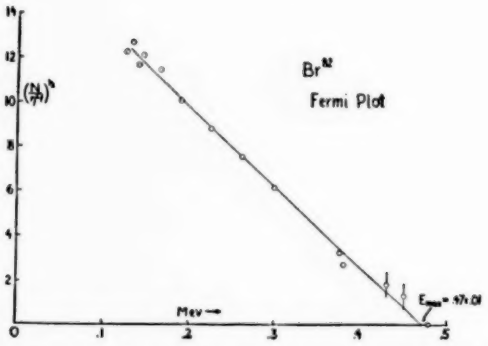

FIG. 6. Fermi plot of the beta-ray spectrum of Br^{82}. The $f(Z, n)$ function is for $Z=35$, not the usual $Z=0$ approximation.

rays. Thus the beta-ray spectrum must be simple. The Fermi plot bears this out.

Since gamma-gamma coincidences are observed, there must be more than one gamma-ray per disintegration. Since the absorption of the gamma-gamma coincidences shows a constant fraction of the gamma-rays yielding gamma-gamma coincidences, we can conclude that no gamma-ray considerably softer than the average is necessary for gamma-gamma coincidences. The simple exponential character of the gamma-ray absorption curve also indicates the absence of any strong lower energy radiation, and indicates also an average energy of about 1.0 Mev for the gamma-rays. This observation is borne out by the measurement of the gamma-ray energies from the secondary electron spectrum. The energies are 0.547 ± 0.01, 0.787 ± 0.015, and 1.35 ± 0.03 Mev. The inability of the absorption measurements to disclose the complexity of the gamma-ray spectrum is worth notice.

The problem is now to assign the number of gamma-rays accompanying each disintegration. In our preliminary report,[7] we concluded that three cascade gamma-rays accompany each beta-ray, on the ground that the ratio of beta-gamma to gamma-gamma coincidences was 1.5 and from a corroborative check on the efficiency of the counter by means of the 0.85 Mev gamma-ray of Mn^{56}. This conclusion was based upon the assumption of approximately equal energy of all three gamma-rays, and it is now possible to check the conclusion without making such an assumption.

Dunworth[10] has published a curve showing the efficiency of a brass cathode gamma-ray counter as a function of energy in agreement with a theoretical curve of v. Droste, shown in Fig. 7. The points shown give the efficiency of our copper cathode gamma-ray counter. From the efficiency of the gamma-ray counter, certain conclusions can now be drawn concerning the gamma-ray emission.

The value 3.28×10^{-3} beta-gamma coincidence per beta-ray represents the sum of the gamma-counter efficiencies for detecting the gamma-rays associated with beta-rays. This value will represent a weighted mean of competing modes of decay for the excited states, if such competing modes exist. Under the assumption of cascade emission of the three gamma-rays, the observed value of 3.28×10^{-3} is to be compared with 3.32×10^{-3}, which is the sum of the efficiencies for detecting the three gamma-rays, as read off the efficiency curve, Fig. 7. Furthermore, if we calculate what the gamma-gamma coincidence rate should be (it is given by

$$\sum_{\substack{1\\ i\neq j}}^{3} \epsilon_i\epsilon_j \Big/ \sum_{1}^{3} \epsilon_i$$

where ϵ_i is the efficiency for detecting the ith gamma-ray), the value turns out to be 1.94×10^{-3}, compared with the observed value 2.14×10^{-3}. Taken together, these observations afford almost certain proof that the three gamma-

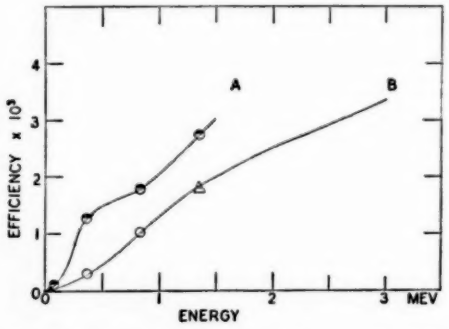

FIG. 7. Variation of efficiency of gamma-ray counters with energy of gamma-rays. Curve for copper cathode (B) derived theoretically by v. Droste, reference 10. Scale fitted at 0.83 Mev by determining the number of beta-gamma coincidences per high energy beta-ray in Mn^{56} (F. Norling, Phys. Rev. **58**, 277L (1940); also 8). The point at 0.367 Mev was obtained from I^{131}, reference 8, (complete description in preparation). The point at 1.35 Mev is predicted by the assumption of three cascade gamma-rays from Br^{82}. Points for curve A obtained with Pt screen cathode in the same manner as for B.

[10] J. V. Dunworth, Rev. Sci. Inst. **11**, 167 (1940).

rays are in cascade. Any other assignment would predict considerably lower coincidence rates. It also follows that within the experimental error, there is no other gamma-ray in cascade, which might have escaped detection in the spectrometer. It is, of course, possible that the observed energy of 1.35 Mev corresponds to two unresolved gamma-rays, one of which represents a cross-transition competing with the emission of the 0.547 and 0.787 Mev gamma-rays.

Since the observed beta-ray transition ends on an excited state of Kr^{82}, which is about 2.8 Mev above the ground state, a careful search was made for beta-rays emitted in a transition to lower levels, by means of the beta-ray spectrometer. None was found, and we estimate that no higher energy beta-ray spectrum with a relative abundance as high as 2 percent is present.

The above experiments on the disintegration of Br^{82} to Kr^{82} do not supply data concerning the order of emission of the three gamma-rays. There is at present no known method of approach to this problem. Thus we cannot give the correct order of the excited states of Kr^{82} (information on the order of the excited levels might be obtained if the appropriate proton groups were found in a study of the reaction $Br^{79}(\alpha, p)Kr^{82}$). One arbitrarily chosen level scheme is shown in Fig. 8. If, for the moment, we assume this to be the correct designation of the disintegration scheme, then the following considerations are of interest.

The ground state of Kr^{82} probably has zero angular momentum, since Z and A are both even. If one assumes the Fermi theory of beta-disintegration, and more specifically only the Fermi type of interaction, the probability of disintegration is found to vary approximately as the fifth power of the total energy of disintegration. The observed total energy is $0.47+mc^2=0.98$ Mev, and a transition to the assumed next lower state would thus have an energy of about 1. 53 Mev. If the two transitions were equally allowed, the transition to the lower state would be $(1.53/0.98)^5$ or 9.2 times more probable (or even more if any other gamma-ray is the first emitted). It is thus obvious that the transition to the next lower state must be forbidden, as well as to the other still lower states. No detailed theory of the relative probability of forbidden transitions for the Fermi interaction has been given. Thus we can only estimate, from such data as are afforded by Sargent diagrams, the variation of transition probability with increasing change in angular momentum. For the heavy elements, the Sargent curves show a difference of a factor of about 100 between allowed transitions and those assumed to be once forbidden. How this factor will vary with atomic number and energy of disintegration is not known in detail. It seems reasonable to assume that the probability ratio is of the order 100. However, a factor of 100 in the relative probabilities would still permit a high energy spectrum 9 percent as abundant as the low energy spectrum. We must therefore conclude that the higher energy spectra are all at least twice forbidden.

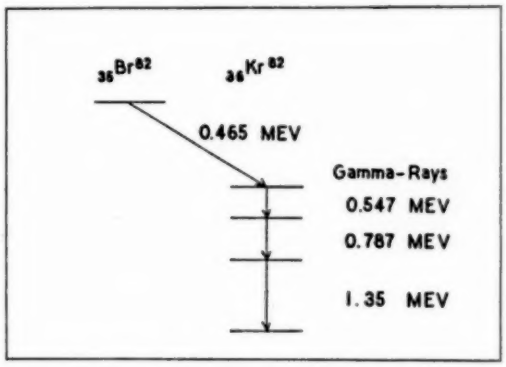

FIG. 8. Proposed energy level diagram for the levels of Kr^{82} observed in the disintegration of Br^{82}.

From the spectra of the gamma-ray secondaries, we find no evidence for any gamma-rays of energy greater than 1.35 Mev. Thus, with the possible exception of a 1.34 (=0.55+0.79) Mev gamma-ray, crossover transitions do not occur in observable amount (i.e., less than 5 percent). There is no evidence that the 1.34 Mev crossover appears (we assume the 0.55 and 0.79 Mev gamma-rays in direct sequence), but the efficiency of the counters is such that a fairly large proportion of the disintegrations could proceed in this manner without much affecting the observed coincidence rates.

If the crossover transitions are thus assumed forbidden, as at least some of them are, considerations as to the angular momentum of the levels in Kr^{82} are in order. Equations for the lifetime of excited levels against electric multi-

pole radiation have been given by Bethe[11] and recently by Lowen.[12] These expressions, derived on the liquid drop model, expressly forbid dipole radiation. Dipole radiation is observed, however, in heavy nuclei, and should be at least as probable in lighter nuclei. If we assume that dipole radiation has about the same probability as quadrupole radiation, then a careful consideration of the lifetimes leads one to the conclusion that the angular momentum of the highest observed Kr^{82} level must be at least 4 units, and that angular momentum of the ground state of Br^{82}, on either the Fermi or the Gamow-Teller selection rules, is also at least 4 units.

Matrix element

Using the universal time constant of the Fermi theory, $\tau=3000$ sec., as given by Gronblom,[13] and the values of the $f(Z, \eta)$ transition probability function given by Evans,[14] we find for the matrix element for the $Br^{82}-Kr^{82}$ transition the value $G^2=0.02$.

Integration of the spectrum

The net efficiency of the gamma-ray counter for the gamma-rays from one disintegration is given by the sum of the efficiencies of the counter (including solid angle, absorber, etc.) for detecting each of these gamma-rays. For example, in the disintegration scheme shown in Fig. 8, the net efficiency is the sum of the efficiencies for the 0.55, 0.79 and 1.35 Mev gamma-rays. In the arrangement used for measuring coincidences in the spectrometer, the gamma-ray counter had a net total efficiency of 4.4×10^{-3} for the gamma-rays of Br^{82}, as measured by coincidences. We can find the number of disintegrations per minute by dividing the number of observed gamma-ray counts per minute by the net efficiency. On the other hand, we can find the number of beta-rays emitted per minute by integrating the beta-ray spectrum (see Fig. 4), and taking into account the transmission of the spectrometer.

In our case, for example, a source giving 3000 gamma-ray counts per minute should have $3000/4.4\times10^{-3}$ or 6.8×10^5 disintegrations per minute. Integrating the upper half of the momentum spectrum for this source,[15] we find that there are 3.1×10^5 beta-rays per minute with $H\rho>1350$ gauss-cm. If one takes into account the approximate symmetry of the Fermi distribution, the total number of beta-rays emitted per minute is found somewhat above 6.2×10^5, provided that the spectrum is a simple one. By comparing this number with the number of disintegrations per minute deduced from the gamma-ray counting rate, we reach the following conclusions: All observed gamma-rays (±10 percent) accompany a simple beta-ray spectrum as shown in Fig. 8; within the error of measurement there is no other mode of disintegration such as a very soft beta-ray spectrum or orbital electron capture accompanied by gamma-rays. This is in agreement with our failure to detect any other mode of disintegration. The coincidence amplifier must detect all or nearly all the true coincidences, since otherwise the number of disintegrations calculated from the net efficiency would have been overestimated.

This method of determining the total number of disintegrations should be useful in extrapolating spectra to low energies.

ACKNOWLEDGMENTS

This research was supported in part by a grant from the John and Mary R. Markle Foundation. We wish to express our thanks to the many members of the laboratory staff who have made helpful suggestions, to Professor M. S. Livingston, Dr. J. H. Buck, and the cyclotron crew for their cooperation, and particularly to Professor Robley D. Evans for his continued interest.

[11] H. A. Bethe, Rev. Mod. Phys. **9**, 226 (1937).
[12] I. S. Lowen, Phys. Rev. **59**, 835 (1941).
[13] B. O. Gronblom, Phys. Rev. **56**, 508 (1939).
[14] R. D. Evans, "Introduction to the atomic nucleus," M. I. T. course notes.

[15] These data represent weighted averages for a number of sources. The reason for using only the upper half of the spectrum is that it is least subject to distortion caused by instrumental effects.

The L Radiation from Sulphur

D. H. Tomboulian and Willoughby M. Cady
Cornell University, Ithaca, New York

(Received August 5, 1941)

The L-emission band from a sulphur target has been studied spectrophotometrically, and the intensity contour of the band has been deduced. The essential features consist of a strong peak at 149 ev, less pronounced structures at about 158 ev, and a broad peak or "tail" around 136 ev, in substantial agreement with previous studies. In contrast with the corresponding bands from the metallic elements of the second row of the periodic table, the drop in intensity on the high energy side of the band occurs gradually. Because of this fact, and perhaps also because of insufficient resolving power, the L_{II} and L_{III} edges have not been separated. A tentative interpretation has been given for the main observed features. No trace of the $L_I - L_{III}$ transition has been found.

THE L spectrum has been investigated by Prins and Takens[1] and by Siegbahn and Magnussen[2] who have carried out wave-length determinations of the characteristic features of the radiation which lies in the spectral range from about 75A to about 85A. Skinner,[3] in his report on the emission bands from certain solids, has published a curve showing the L band of sulphur. The present investigation constitutes a more refined photometric determination of the intensity distribution of the radiation which is emitted when vacancies occur in the L_{II} and L_{III} levels. Information of this type is of value in the study of the level system of the valence electrons in solids, and particular interest attaches to the present study since sulphur is a typical insulator.

Experimental

The general description of the experimental features dealing with the x-ray tube, vacuum spectrograph, and the photometric method have been described previously;[4] only additional techniques and observations related to the study of sulphur will be given here. Because of the high chemical affinity of sulphur towards nickel and copper under conditions of operation of the x-ray tube, the target of the tube, as well as filament leads, were made of stainless steel. This material is not attacked appreciably by sulphur and spot welds readily to the tungsten filament. Yellow crystalline sulphur of high purity was fused in vacuum into an open-ended Pyrex ampule, which was then inserted into the x-ray tube. The sulphur was evaporated by external heating from a tungsten filament placed near the glass container, which was shielded from the heat of the x-ray filament to prevent continuous evaporation during operation of the tube.

Because of the volatile nature and low melting point of sulphur, it was necessary to keep the target cold (−45°C) during bombardment. This was accomplished by circulating alcohol whose temperature had been lowered by the use of solid carbon dioxide. This method of cooling was found to be quite adequate in retaining a deposit of sulphur on the target face for the duration between renewals of the sulphur coating. Indeed, for the particular thickness of target wall ($\frac{1}{32}''$), and size of focal spot (1.2 sq. cm), and a power input of 50 watts, this method of cooling was found to be more efficient than direct liquid-air cooling of the same target for the same power input. (Liquid air boils behind the focal spot, so its own vapor forms a thermally insulating layer. The use by Skinner[5] of a very thick-walled target was intended to mitigate this boiling. That it did so is, however, questionable, since calculation shows that there is no significant fringing of the lines of heat flow in a target wall whose thickness is comparable with the width of the focal spot.)

[1] J. A. Prins and A. J. Takens, Zeits. f. Physik **77**, 795 (1932).
[2] M. Siegbahn and T. Magnussen, Zeits. f. Physik **87**, 291 (1934).
[3] H. W. B. Skinner, Phil. Trans. Roy. Soc. **A239**, 95 (1940).
[4] W. M. Cady and D. H. Tomboulian, Phys. Rev. **59**, 381 (1941).
[5] Reference 3, p. 101.

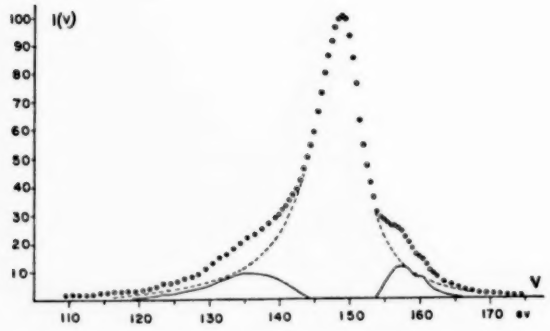

FIG. 1. Relative intensity I(V) in the L band of sulphur. The circles represent experimental determinations.

Five runs were made with varying exposure times (80–320 min.) and tube currents (10–20 ma) at potentials of about 2000 volts. A ballast resistance of 15,000 ohms was placed in series with the target of the tube in order to increase the stability of operation. The pressures in the x-ray tube were higher than those attained while working with aluminum and magnesium.[4]

It is difficult to know whether the deposit of sulphur on the target was orthorhombic. The appearance of the focal spot did vary from run to run both in color and texture. For tube currents of 10 ma the deposit retained a yellowish-white color. For higher currents the focal spot took on a light brownish color and a glossy appearance; upon removal of the target the deposit of sulphur was gummy in nature in these cases. However, upon standing for several hours it seemed to revert to the hard yellow form. A study of sulphur allotropes by Das[6] indicates that the gummy deposit of sulphur, often regarded as amorphous, is really crystalline and gives diffraction patterns identical with those obtained from orthorhombic sulphur. We presume that our spectra are characteristic of this modification. The loss of sulphur by evaporation from the target was found to depend strongly on the tube current. However, for currents equal to, or less than, 20 ma an exploratory run indicated that this loss was not excessive since the x-radiation did not markedly diminish during the first twenty minutes of bombardment after removing the deposit of sulphur.

[6] S. R. Das, Ind. J. Phys. **12**, 163 (1939).

Results and Discussion

The points in Fig. 1 represent a plot of the data showing the intensity distribution of the radiation. The data were prepared by averaging the results of four plates representative of strong and weak exposures as well as high and low tube currents. In obtaining the average, the intensities on the high and low energy side of the main peak were weighted more heavily in the case of dense negatives; while in the case of fainter negatives the intensities near the peak were assigned greater weight. In reducing the plates the wave-length corresponding to the peak was set equal to 83.1A, the value given by Skinner,[7] and in determining the photon energies given in Fig. 1, 12,370 volt-angstroms was used as the conversion factor. Individual densitometer traces from the different runs were in good agreement in regard to the main features of the band. The plates were examined for impurity spectra due to carbon, nickel, chromium, iron and mercury. There was no indication of the presence of these impurities. On the most intense exposure, no trace of the L_I–L_{III} radiation could be found. This line is predicted[8] to be at 203A and would have been detected if its intensity were of the order of 3 percent of that of the main peak.

Comparison with Skinner's curve[7] on the same element indicates good agreement with respect to the wave-length. However, the present results differ widely in intensity from those of Skinner. If, as we believe, our band shape is correct, this discrepancy may perhaps be ascribed to a failure in the adjustment of the photometer, the deflections of which were assumed by Skinner[9] to be approximately proportional to the intensity of the x-radiation causing the blackening on the plate.

The interpretation of the observed band shape is hardly a task for the experimentalist, but we hazard a guess. For this purpose it is convenient to extend the contour of the main peak smoothly to the base line as indicated by the dotted lines in Fig. 1. It is then possible to sketch in the shapes of two component features with maxima at about 136 and 158 ev. If the valence electrons

[7] Reference 3, p. 108.
[8] D. H. Tomboulian and W. M. Cady, Phys. Rev. **59**, 422 (1941).
[9] Reference 3, p. 106.

of sulphur can be classified crudely as belonging to $3s$ and $3p$ bands, then the L-emission spectrum should divide itself into two parts corresponding to the electron transitions

$$3s \rightarrow L_{II,III}$$
$$3p \rightarrow L_{II,III}.$$

The main contribution to the band (peak at 149 ev) is to be ascribed to the first of these; while the structure at 158 ev may perhaps be associated with the second transition which should be relatively weak since it is nearly forbidden. The $3s$–$3p$ interval (9 ev) as deduced by this procedure is not in contradiction with the value estimated from x-ray and optical data.

The broad peak at 136 ev may perhaps arise from a "semi-Auger" process[4] in which a $3s$ electron falls into the ionized L shell and a second $3s$ electron is excited into an unoccupied level. In this process a photon is emitted of which the energy is less than the energy loss of the first electron. Such a process would demand that the interval between the main peak and the broad peak be larger than that $3s$–$3p$ interval, and indeed such is the case (13 *vs.* 9 ev).

The authors wish to acknowledge their gratitude to Professor Frederick Seitz of the University of Pennsylvania and to Professor H. Bethe of Cornell University for helpful discussions in connection with this investigation.

OCTOBER 15, 1941 PHYSICAL REVIEW VOLUME 60

The Half-Life of Iodine (128)

D. E. HULL AND HERMAN SEELIG*
School of Chemistry, University of Minnesota, Minneapolis, Minnesota
(Received August 29, 1941)

The half-life of iodine (128) has been measured with high accuracy by means of a G-M counter and amplifying circuit of tested reliability. An absolute calibration of the counter was carried out by a simple method. The half-life was determined from the data by an arithmetical, rather than a graphical method. The results of four closely concordant experiments give for the best value of the half-life, $T = 24.99 \pm 0.02$ minutes. It is suggested that this radio-element can now be used in a quick and convenient calibration of counters or other instruments for measurement of radioactivity.

IN some current experimental work by the writers it has become necessary to know the half-life of iodine (128) with greater accuracy than is characteristic of the values now in the literature. Although this radio-element was among the first discovered by Fermi in his fundamental research on the production of artificial radioactivity by neutron bombardment, and it has been used and studied by researchers too numerous to list here, yet its half-life has not been determined with an accuracy much better than 5 percent. Probably the best value is that given by Livingood and Seaborg,[1] namely, 25 ± 1 min. Of course, this situation is not unique with radio-iodine. The half-lives of very few radio-elements are known with an accuracy better than a few percent. Notable exceptions are the values for radon, determined independently by investigators in two laboratories with excellent agreement;[2,3] for phosphorus[4] (32), and for carbon[5] (11).

Since there is available in this laboratory a G-M counter and amplifier with a known reliability of about 0.2 percent in relative measurements, an attempt has been made to determine the half-life of radio-iodine with an accuracy of this order. The radio-iodine was prepared by slow neutron bombardment of phenyl iodide, concen-

* Now with the duPont Company, Wilmington, Delaware.

[1] J. J. Livingood and G. T. Seaborg, Phys. Rev. **54**, 775 (1938).

[2] W. Bothe, Zeits. f. Physik **16**, 266 (1923).

[3] I. Curie and C. Chamié, J. de phys. et rad. [6] **5**, 238 (1924).

[4] N. B. Cacciapuoti, Nuovo Cimento **15**, 213 (1938).

[5] A. K. Solomon, Phys. Rev. **60**, 279 (1941).

TABLE I. *Half-life of iodine* (128).

Exp. 1	25.01±0.04 min.
2	25.03±0.04
3	24.97±0.04
4	24.97±0.03
Average	24.99±0.02 min.

trated by extraction with aqueous sodium iodide, and precipitated as silver iodide. The precipitate was filtered by suction in a Buchner funnel, was washed and dried with alcohol and ether, and was coated with a thin layer of cellulose nitrate formed from a dilute acetone solution by evaporation. The filter paper was then wrapped snugly around the counter and held firmly in place with rubber bands. Since the radioactive sample was thus held in a fixed position for the duration of the measurements, all corrections for absorption in the precipitate and counter wall and for geometry of the source could be ignored.

The counter used in this work was one of the thin-walled glass type described in a previous paper by one of us.[6] Since the work reported in that paper, however, the counter has been filled with argon instead of air, to a pressure of 5 cm. This change has resulted in two definite advantages: First, the counting plateau has a much smaller slope, only 0.3 percent per volt in contrast with 2.7 percent found with air-filling. Second, the "warming-up" effect described previously is very largely, if not completely, eliminated. It is now possible to count at a rate of 100 per second for an interval long enough to reduce the error due to random distribution to 0.1 percent without any measurable increase in counting rate. The background rate of the counter has been found to be quite constant and reproducible within the random error of about 2 percent. It does not change while the counter is being used at high speeds. The amplifier is of the Neher-Harper type with a vacuum-tube scaling circuit transmitting every eighth pulse to the Cenco recorder.

The counter was calibrated by a modification of a method described by one of us,[6] which is applicable when the counting losses can be represented by the function

$$R/N=e^{-\tau R}. \quad (1)$$

Two bulbs containing the radium D left from the decay of radon were used in the calibration. The first bulb was placed at a convenient distance and the counting rate determined with the desired accuracy. Then, with this bulb still in place, the second bulb was brought up to some point which gave a counting rate of approximately the desired value, and the rate with both in position was measured. Then the first bulb was removed without touching the second, and the rate due to the second alone was determined. No "standard" positions are involved in this method, and there is no question of replacing a radioactive sample so as to reproduce the geometry of a previous measurement. Finally, a measurement of the background rate was made. These four values were substituted in the equation given in the aforementioned paper,

$$\tfrac{1}{2}(R_p^3+R_q^3-R_s^3)\tau^2+(R_p^2+R_q^2-R_s^2)\tau +R_p+R_q-R_s-B=0 \quad (2)$$

TABLE II. *Decay of iodine* (128).

TIME (MIN.)	OBSERVED RATE	CORRECTED FOR LOSSES	CORRECTED FOR BKG.
4	351.4	394.0	392.2
12	289.5	316.9	315.1
20	235.6	252.9	251.1
28	193.5	204.7	202.9
36	156.1	163.2	161.4
44	125.7	130.1	128.3
52	101.6	104.5	102.7
60	82.1	83.9	82.1
68	66.1	67.3	65.5
76	53.6	54.4	52.6
84	42.9	43.4	41.6
92	35.4	35.7	33.9
100	28.4	28.6	26.8
108	23.2	23.3	21.5
116	19.3	19.4	17.6
124	15.7	15.8	14.0
132	12.7		10.9
140	10.60		8.84
148	8.81		7.05
156	7.48		5.72
164	6.32		4.56
172	5.54		3.78
180	4.64		2.88
188	4.15		2.39
196	3.62		1.86
204	3.32		1.56
Bkg.	1.76		

$S_1=1879.6-22.9=1856.7$
$S_2=\ 125.7-22.9=\ 102.8$

$$T=\frac{0.3010\times 104}{\log\frac{1856.7}{102.8}}=24.91 \text{ min.}$$

Corrected for stopwatch error, $T=24.91\times 1.0025$
$=24.97$ min.

[6] D. E. Hull, Rev. Sci. Inst. **11**, 404 (1940).

and the corresponding value of τ, the recovery time constant, was calculated.

The following values of τ were obtained at different total counting speeds as indicated:

R_s	τ in microseconds
77	990±130
108	980±120
156	950± 60
Weighted av.	960± 50

The observed constancy justifies the assumption made that the counting losses can be represented by a simple exponential function.

Three different samples of radio-iodine were measured on this counter. The recorder dial was read at regular intervals while the counter operated continuously from an initial rate of 180 per second down to 10 per second. From these readings the average counting rate during each interval was computed. These observed rates were corrected for counting losses by Eq. (1). The list of corrected counting rates was divided into two halves at the midtime t, and the summation of each part was taken. The background contribution was deducted from each of these, and then the half-life was calculated by the equation

$$T=\frac{0.3010\,t}{\log(S_1/S_2)} \qquad (3)$$

where t is the duration of time for each half of the measurements, S_1 is the sum of the corrected rates found for the first half of the intervals measured, and S_2 is the corresponding figure for the second half. The values of the half-life thus obtained, together with the probable error in each calculated from the number of counts, are listed in Table I.

A fourth sample was measured on a different counter and amplifier with a scale of 64. The calibration of this circuit gave a much smaller τ, but one which was not exactly constant. The value of τ as a function of counting speed on this circuit was found to be represented by the expression

$$\tau=250+0.22R \text{ (in microseconds)} \qquad (4)$$

for rates up to 400 per sec. The activity of the iodine measured on this counter was followed from 400 down to 2 counts per sec., covering a period of eight half-lives. The value obtained in this experiment is given last in Table I.

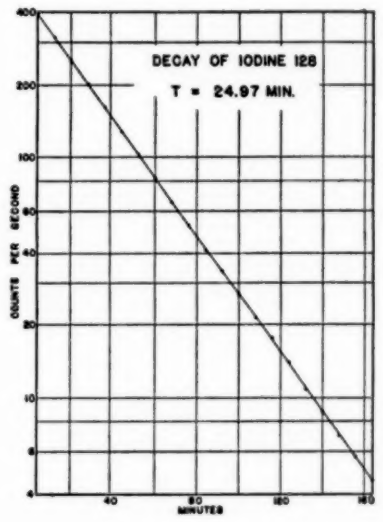

FIG. 1. Sample of data on decay of I^{128}. Corrections for background and losses have been made.

Table II gives the experimental data obtained in this last experiment. In the second column are the observed average counting rates during successive eight-minute intervals. In the next column are shown the rates corrected for counting losses according to Eqs. (1) and (4). The last column shows the measurements corrected for background. A logarithmic plot of the figures in the last column is shown in Fig. 1. The stopwatch used in this experiment ran 0.25 percent slow as compared with an electric clock, so the value of T is finally corrected for this.

It may be pointed out that the accurate knowledge of the half-life of a commonly available radio-element, such as iodine (128), will be useful to many who are using radio-elements in various applications, because a counter or other measuring instrument can be very simply calibrated with sufficient accuracy for most purposes by following the decay of radio-iodine over the useful range of the instrument, plotting the data thus obtained on the usual logarithmic scale, and then drawing a line with slope corresponding to $T=24.99$ min. asymptotic to the curve at low counting speeds. The deviation of the observed curve from the theoretical line at any given higher rate shows the correction to be applied to other measurements made at that rate.

Rotational Analysis of the 2900A Band of CO_2^+

FACUNDO BUESO-SANLLEHÍ*
Ryerson Physical Laboratory, University of Chicago, Chicago, Illinois
(Received August 11, 1941)

A rotational analysis of the CO_2^+ doublet band near λ2896 and λ2882 has been made. The band was photographed in the third order of the 30-foot grating spectrograph at Ryerson Laboratory with a dispersion of 0.22A/mm and a resolving power of 300,000. The structure is explained by a $^2\Sigma^+_u \rightarrow {}^2\Pi_g$ (case *a*, inverted) transition, where the $^2\Pi_g$ is the ground state of CO_2^+. Alternate lines are missing as expected for $^2\Sigma$ in view of the zero spin of the oxygen nuclei. A number of perturbations are observed, which involve displacements and weakening of the lines. These are probably caused by higher vibrational levels of a $^2\Pi_u$ state which lies about 0.8 volts below the $^2\Sigma^+_u$. The values found for the molecular constants of the lower $^2\Pi_g$ state ($B_1=0.3795$ cm^{-1}, $B_2=0.3813$ cm^{-1} and the Λ-doubling coefficient $p=0.004$ cm^{-1}) agree with those found by Mrozowski. For the upper $^1\Sigma^+_u$ state, $B=0.3784$ cm^{-1} and the spin-doubling coefficient $\gamma=0.019$ cm^{-1}. The spin-orbit coupling coefficient A for the $^2\Pi_g$ state is -159.5 cm^{-1}.

INTRODUCTION

THE spectrum of CO_2 has been the object of considerable investigation. From studies of the infra-red and Raman spectra Martin and Barker[1] were able to show that the normal CO_2 molecule is linear, confirming the previous results of Eucken[2] and of Stuart.[3]

Among the first to study the emission spectrum were Fox, Duffendack, and Barker,[4] who found extensive systems of bands from λ2800 to λ5000. They observed that the bands centered at λ2882 and λ2896 (see Fig. 1) were the strongest in the spectrum and presented a different appearance from the other bands. Duffendack and Smith[5] concluded that most of the observed bands could be ascribed to CO_2^+ as the emitter, and estimated the excitation potential of the strong λ2900 doublet band at 19 volts.

This band was first photographed under high dispersion by Duncan.[6] He used a 65-volt arc at 6–15 ma with flowing CO_2 at a pressure of 0.1 mm. His dispersion with a 21-foot grating was 1.2A/mm in the second order. This, however, was not sufficient to resolve the structure fully, but from its appearance he believed that each of the two sub-bands consists of a positive, a negative, and a zero branch. The zero branches he identified with the strong, rather wide lines at 34,517.54 cm^{-1} and 34,678.25 cm^{-1} marked (*b*) and (*a*) in Fig. 1. He concluded, in agreement with Duffendack and Smith, that the excitation potential for the bands must be about 19 volts, and thus correspond to ionization of the molecule.

Schmid[7] photographed the λ2900 band with a 21-foot grating in this laboratory, using a continuous flow of CO_2 through a Back box with magnetic field, and also a hollow cathode without field. He concluded that the transition was a (0,0) band of a $^2\Pi$ (case *a*)$\rightarrow{}^2\Pi$ (case *b*) electronic transition in a linear CO_2^+ molecule,[8] although his resolving power did not permit a satisfactory analysis. He also arranged the lines in *P* and *R* branches, again identifying a *Q* branch in each sub-band with each of the two strong lines mentioned above.

The emitter of the band was more definitely identified as CO_2^+ by Roy and Duffendack.[9] They employed a low voltage arc in mixtures of CO_2 and O_2, with and without the addition of rare gases. Accepting the electron impact value of $I=14.4$ volts given by Smyth[10] for the minimum

* Now at the University of Puerto Rico, Río Piedras, Puerto Rico.

[1] P. E. Martin and E. F. Barker, Phys. Rev. **41**, 291 (1932).
[2] A. Eucken, Zeits. f. Physik **37**, 714 (1926).
[3] H. Stuart, Zeits. f. Physik **47**, 457 (1928).
[4] G. W. Fox, O. S. Duffendack, and E. F. Barker, Proc. Nat. Acad. Sci. **13**, 302 (1927).
[5] O. S. Duffendack and H. L. Smith, Phys. Rev. **34**, 68 (1929).
[6] J. F. Duncan, Phys. Rev. **34**, 1148 (1929).
[7] R. F. Schmid, Zeits. f. Physik **83**, 711 (1933).
[8] The notation and formulas for diatomic molecules are applicable to linear triatomic molecules [cf. R. S. Mulliken, Phys. Rev. **42**, 364 (1932)].
[9] A. S. Roy and O. S. Duffendack, Proc. Nat. Acad. Sci. **19**, 497 (1933).
[10] H. D. Smyth, Rev. Mod. Phys. **3**, 347 (1931).

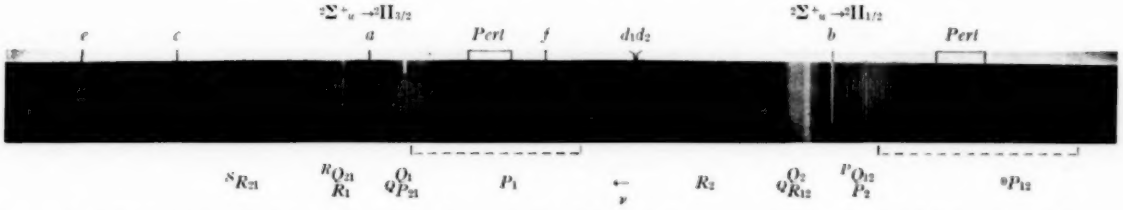

FIG. 1. Spectrogram of the λ2900 doublet band of CO_2^+. The sub-bands are centered near (*a*) ($\nu = 34{,}678.25$ cm^{-1}) and (*b*) ($\nu = 34{,}517.54$ cm^{-1}). The meaning of the letters is given in the text. The portions of the branches shown by dashed brackets under *Perl* are shown enlarged in Fig. 4, while the solid brackets include the lines which show the greatest perturbations.

ionization potential of CO_2, they obtained a value of $I = 18.7$ volts for the excitation potential of the λ2900 band.

From a pair of Rydberg series in the ultraviolet absorption spectrum of CO_2, Henning[11] and Rathenau[12] found an ionization potential of 18.00 ± 0.03 volts which should presumably correspond to ionization of an inner electron.

On the basis of theoretical considerations as to the electron configuration of CO_2, and taking into account the experimental data available, Mulliken[13] concluded that the λ2900 band is most probably a $^2\Sigma^+_u \rightarrow ^2\Pi_g$ transition, with the $^2\Pi_g$ as the normal state of CO_2^+. The electron configuration he gives for the normal state of CO_2 is the following:

$$(1s)^2(1s)^2(1s)^2(2s)^2(2s)^2(\sigma+s+\sigma,\sigma_g)^2(\sigma-\sigma+\sigma,\sigma_u)^2 \times(\pi+\pi+\pi,\ \pi_u)^4(\pi-\pi,\ \pi_g)^4,\ ^1\Sigma^+_g.$$

By identifying the ionization potential of 18 volts as that required for the removal of one of the σ_u electrons from the normal molecule (thus resulting in a $^2\Sigma^+_u$ state for the ion) he was able to predict a minimum I of 13.72 volts for CO_2, a value which is lower than the electron impact values of Mackay[14] and of Smyth.[10] Mulliken's estimate is in exact agreement with the $I = 13.73 \pm 0.01$ volts found later by Price and Simpson[15] from an additional Rydberg series. This energy would then correspond to that required for the removal of a π_g electron from the CO_2 molecule giving the normal state of CO_2^+. The absence of vibrational excitation in Henning's Rydberg series indicates that CO_2^+ in the $^2\Sigma^+_u$ state is linear, and it is reasonable to assume that the same is true for the normal state.

The present writer, in 1936–37, obtained a series of plates in the second order of the 30-foot grating in Ryerson Laboratory, using a water-cooled hollow cathode. The experiments were resumed in 1940 when a new grating with higher resolving power was available, and, with an improved hollow cathode, excellent third-order plates were obtained. These permitted the rotational analysis to be made, confirming Mulliken's prediction. The transition is, in fact, a $^2\Sigma^+_u \rightarrow ^2\Pi_g$ transition in a linear molecule, where the $^2\Pi_g$ is case *a*, inverted.

EXPERIMENTAL

A large portion of the experimental work was done in collaboration with Dr. S. Mrozowski in Ryerson Laboratory in a joint program to cover the complete CO_2 spectrum from λ2800 through the visible.

The λ2900 band was photographed on Eastman Process plates. During the exposures, many of 50-hour duration, constant observation of the barometric pressure was required, since changes of over 2.5 mm Hg cause an appreciable shift of the lines at the high dispersion used. For similar reasons the temperature of the grating was kept constant to within 0.1°C. A bromine filter was used to cut out the second-order spectrum.

The dispersion was 0.22A/mm and the resolving power exceeded 300,000. The theoretical resolving power of 450,000 could not be attained because of the Doppler width of the lines at the high current density used. To obtain a rough estimate of the half-intensity width due to Doppler broadening, an approximate temperature of emission was determined as follows. The J value of the most intense line in each branch was

[11] H. J. Henning, Ann. d. Physik **5**, **13**, 599 (1932).
[12] G. Rathenau, Zeits. f. Physik **87**, 32 (1933).
[13] R. S. Mulliken, J. Chem. Phys. **3**, 720 (1935).
[14] C. A. Mackay, Phys. Rev. **24**, 319 (1924).
[15] W. C. Price and D. M. Simpson, Proc. Roy. Soc. **A169**, 501 (1939).

obtained, and an average value of $J_{max}=38$ was found. There was considerable uncertainty in this determination because of the perturbations discussed later, but the average value should be sufficiently good for the rough approximation desired. The usual formula for the intensity of a line is[16] $I=Cie^{-BJ(J+1)/0.7T}$. The intensity factor i for a given transition may approximately be taken as $(aJ+b)$ (where a and b are small, since the summation rule for the intensity factor of all permissible transitions to or from a given level J requires that $\sum i \sim (2J+1)$). For high J values we may neglect the small additive quantities b in the expression for i and the 1 in the numerator of the exponent of the intensity formula. This approximation gives $T \backsimeq 2BJ_{max}/0.7$. With $B=0.38$ cm^{-1} as shown later and $J_{max}=38$, the effective rotational temperature of emission is found to be about 1600°K. The half-intensity Doppler breadth of the lines is then given by

$$\delta = 1.67(\lambda_0/C)(2RT/\mu)^{\frac{1}{2}} \backsimeq 0.012\text{A},$$

corresponding to a resolving power of $2900/0.012 \backsimeq 240{,}000$, and indicating that the estimated temperature is probably somewhat high.

The source used was a water-cooled hollow cathode operated from a 2000-volt d.c. generator at currents up to 2.3 amperes. At pressures below 1 mm, the discharge was very steady and the CO and CO^+ bands were relatively weak. At higher pressures the discharge became very bright and arc-like, but the added intensity was mainly due to CO.

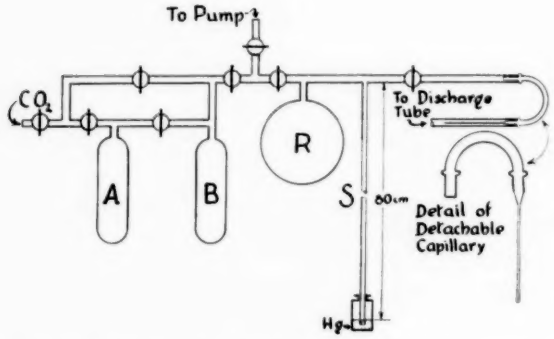

FIG. 2. Diagram of purifying system and flow control. Commercial CO_2 was purified by sublimation and resublimation between A and B by liquid nitrogen. The reservoir R and the capillary permitted regulation of the rate of flow of CO_2 into the discharge tube.

[16] Cf. R. S. Mulliken, Rev. Mod. Phys. **3**, 89 (1931).

A series of exposures with flowing and stagnant gas was made with a Hilger E-3 quartz spectrograph to determine the effect that the rate of flow would have on the relative intensities of the CO_2^+ and CO bands. For the stagnant series the 3-liter discharge tube was filled with CO_2 to the proper pressure and then isolated from the pump. A 2-second exposure was taken as soon as the power was turned on and successive 2-second exposures were taken after the discharge had been going for 10 seconds, 1 minute, 5 minutes, 25 minutes and 2 hours without changing the gas. No change was found in the relative intensities of the CO_2^+ and CO bands in the various exposures. This indicated that equilibrium between the two gases is almost instantly attained and then maintained. Thus it was seen to be useless to keep a fast flow of CO_2 through the discharge tube, and in the subsequent exposures only a small amount was admitted through a leak to replenish that removed by the clean-up action of the discharge. This was a decided advantage considering the long exposures required and the time involved in the purification of the CO_2.

The arrangement shown in Fig. 2 was used to keep the pressure in the discharge tube constant. Commercial CO_2 was purified by sublimation and resublimation between A and B by liquid nitrogen, and stored as solid in B. In this manner no trouble was experienced from impurities and even the λ3064 OH band was absent. A Pyrex capillary was made as shown in the inset. It was held in place as shown in Fig. 2 by Picein wax and could easily be removed to alter its length for adjustment of the rate of flow. Further adjustment was provided by the 2-liter reservoir R into which CO_2 was admitted from B when required, so that the pressure registered by the barometer and safety-valve S at the head of the capillary would permit the proper flow. With this arrangement the tube operated for several hours without attention and required only occasional small additions of CO_2 into the reservoir to maintain its pressure constant within 3–5 cm Hg.

It was hoped that the band might appear more intensely in the presence of helium. However, a series of exposures made with various concentrations of the two gases at various pressures did not show any appreciable increase in the intensity of the CO_2^+ bands.

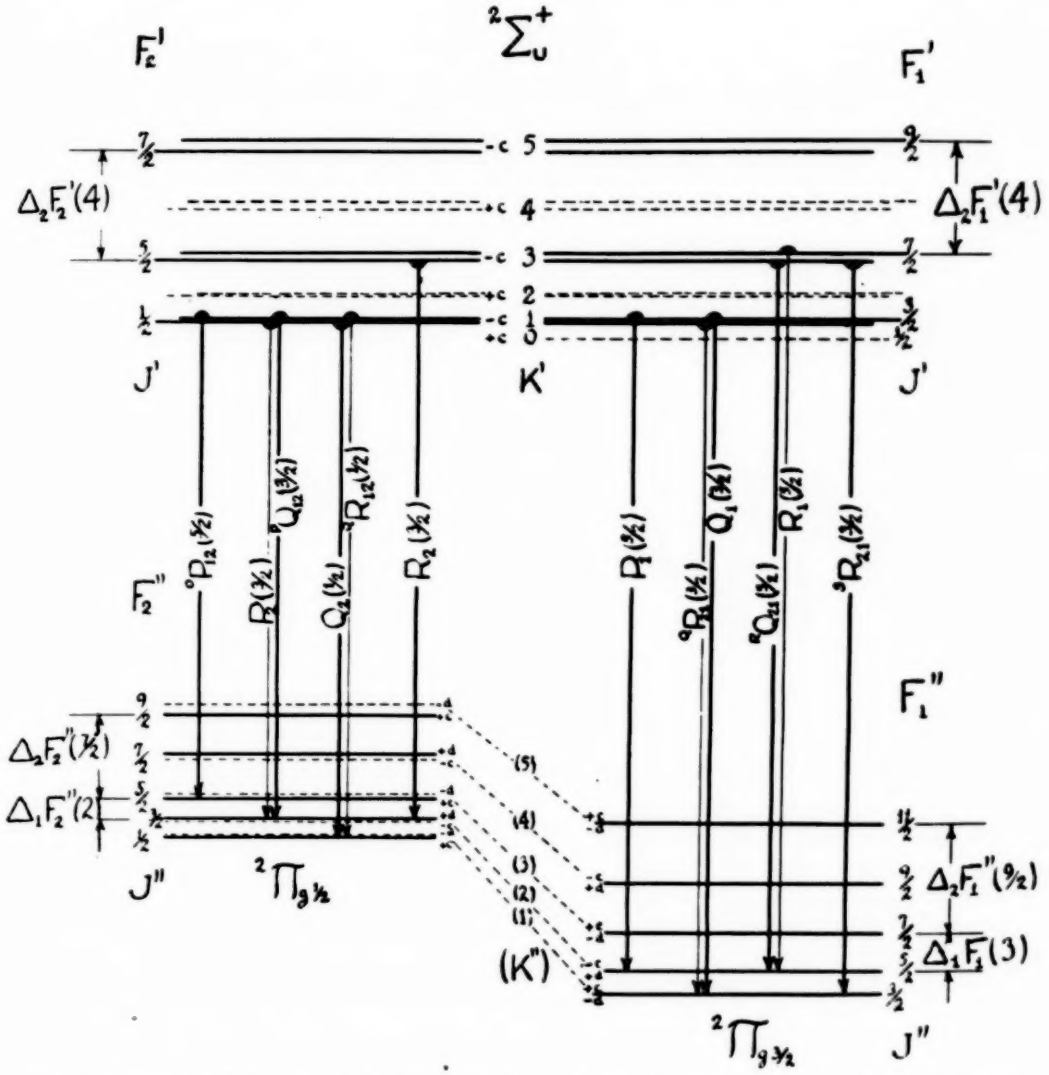

FIG. 3. Energy level diagram of the $^2\Sigma^+_u \rightarrow {}^2\Pi_g$ (inverted case *a*) transition. The + levels of the $^2\Sigma^+_u$ and the − levels of the $^2\Pi_g$ are missing. They are shown by dotted lines. The first line of each branch is given. The Λ-doubling of the $^2\Pi_{1/2}$ and the spin doubling of the $^2\Sigma^+_u$ are greatly exaggerated.

Three plates with different exposures were measured on a linear dispersion scale at the Massachussetts Institute of Technology with Professor Harrison's machine. The second-order iron lines at λ4352.738 and λ4315.087, one near the beginning and the other near the end of the band, were used to set the machine to the proper dispersion and wave-length range. Six readings were obtained for each line, since the plates were measured both forward and backwards. The average of the six readings was then taken, corrected for the non-linearity of the dispersion of the grating, and reduced to vacuum. The correction curve for the deviation from true linear dispersion was obtained directly from the grating formula. The scarcity of standard iron lines in the region covered by the band did not permit the construction of an experimental correction curve, but the theoretical curve used should be sufficiently good to give the absolute wave numbers of the lines to a few hundredths of a wave number throughout the 30A region which includes the band. A greater reliability than this cannot be expected, as the measurements of S. Mrozowski on other bands of CO_2^+ over a wide spectral region have shown. The combination

TABLE I. *Wave numbers in 2900A band of* CO_2^+.

Observed Wave Numbers of Lines	Int.†	Assignment*			Observed Wave Numbers of Lines	Int.†	Assignment*			Observed Wave Numbers of Lines	Int.†	Assignment*			Observed Wave Numbers of Lines	Int.†	Assignment*		
34404.48	1	$^{O}P_{12}$			07.11	6*w*				47.74	2				93.37	1			
11.17	2*w*	—			07.72	7				48.08	3				94.26	1			
11.66	1				08.07	8*w*				48.93	7	29			94.70	2	72		
14.50	1				08.41	5				49.33	4				96.34	2			
15.59	1				08.77	6				49.75	2				97.26	3	70		
16.82	1				09.07	6				50.13	2				97.60	2			
21.56	1	74			09.41	8				50.80	7	31			97.77	2			
22.47	1				09.91	7				51.33	3				99.02	3			
23.34	1				10.28	8				51.99	3				99.72	3	68		
24.50	1				10.78	7				52.52	2				34600.29	2			
24.91	2	72			11.32	7				52.84	7	33			00.93	1			
26.11	1				11.78	6				53.49	2				01.29	1			
27.96	1	70			12.21	8				54.13	3				01.78	1			
28.56	1				12.46	7				54.82	8	35			02.21	3	66		
29.08	1				12.94	5				55.55	4*w*				02.74	1			
30.91	1	68			13.50	6				56.32	4				03.16	1			
31.78	1				13.75	5				56.79	7	37			03.42	1			
32.95	1				14.16	5				57.30	3				03.30	3*w*	64		
33.83	2	66			14.50	4				57.61	3				05.43	1			
35.11	1				14.68	6				58.01	3				06.09	2			
36.42	2	64			15.06	7				58.30	2				06.75	4	62		
37.17	1				15.44	5				58.82	7	39			07.15	3			
37.66	1				15.98	6				59.62	2				07.74	3			
38.74	1				16.35	7				60.04	1				08.61	2			
39.30	2	62			17.06	8				60.33	2				09.01	4	60		
40.37	1				17.54	10*vvw*		(*b*)		60.46	2				09.52	2			
41.05	1				18.48	7*vw*				60.83	5	41			10.41	1			
42.01	2	60			19.28	6				61.30	2				11.17	4	58		
42.63	1				20.06	6				61.59	2				11.89	1			
44.61	2	58			20.80	6*vw*				61.99	2				12.19	2			
45.33	1				21.35	6				62.84	7*w*	43			12.83	2			
47.22	3	56			21.94	6				63.36	3				13.38	5	56		
48.12	1				22.39	8	$^{Q}R_{12}$	Q_2		63.97	4				14.56	1			
49.80	4	54			22.84	8	—	—		64.84	7	45			15.10	2			
51.47	1				23.01	9				65.25	4				15.55	6	54		
52.26	4	52			23.28	8	20?			65.51	2				16.14	3		(*f*)	
54.83	4	50			23.56	8	22			66.00	2				16.53	5			
56.16	1				23.81	8				66.47	4				17.72	6	52		
57.40	5	48			24.12	8	24			66.83	6	47			18.22	2			
59.90	5	46			24.38	8	26	20		67.25	3				18.82	2			
62.45	5	44			24.72	8	28, 30	22		68.85	6	49			19.89	7	50		
65.00	5	42			25.48	10*vvw*		24, 26, 28		69.31	2				21.35	1			
67.80	5	40			25.76	10		30		69.61	3				21.71	2			
68.34	1				26.14	9		32		69.91	3				22.09	6	48		
70.56	1	38			26.67	10*w*	32, 34	34		70.33	1				23.02	2			
71.91	5	36			27.08	9		36		70.79	5	51			23.52	2			
75.00	4	34			27.61	9		38		71.36	3				24.25	7	46		
75.96	3	32			28.10	9		40		71.68	4				25.60	1			
78.96	2	30	$^{P}Q_{12}$	P_2	28.57	9	38	42		72.31	1				26.47	7	44		
81.51	1		—	—	29.09	9	40	44		72.76	5	53			27.30	2			
81.71	5	28	69		29.60	9	42	46		73.64	2*vw*				28.72	6	42		
82.95	1		67		30.00	9	44	48		74.67	5	55			29.52	1			
84.44	5	26	65		30.53	9	46	50		75.12	2				29.96	2			
85.31	2		63		31.03	9	48	52		75.65	3				30.18	1			
85.55	1			59	31.50	9	50	54		76.08	1				31.23	6	40		
86.94	6*vw*	24	61		31.83	9	52	56		76.51	4	57			32.69	2			
87.88	6		59	57	32.21	8	54			78.35	3				33.70	1	38		
89.01	6		57	55	32.82	8				78.66	2	59			34.76	6	36		
89.73	6	22			33.05	7				79.50	2				35.24	1			
90.06	7		55	53	33.51	7				80.13	3				37.58	6	34		
91.14	7		53	51	33.93	6*w*				80.45	2				38.28	4	32		
92.18	8		51	49	34.27	5				80.87	2				39.54	1			
92.52	6	20			34.81	5				81.12	2				40.22	1			
93.21	8		49	47	35.29	2				81.77	4				41.08	4	30		
94.21	8		47	45	35.69	3				82.25	3*w*				41.45	2			
94.68	5				36.13	3				82.95	3*w*				42.71	1			
95.14	8*w*		45	43	36.33	3				83.28	5				43.11	2			
95.86	5				36.64	3				83.73	5				43.60	7	28		
96.31	9		43	41	37.04	3				84.16	4				44.75	3			
97.30	9		41	39	37.66	2				85.17	6*vw*	(d_1)			45.29	2*w*			
98.44	8*w*		39	37	38.15	3				85.88	6*vw*	(d_2)			46.15	6	26		
99.54	8*w*		35	35	38.38	2				86.46	1				46.60	1			
34500.52	8		31	33	39.19	3				86.87	2				47.50	3			
01.16	8		33		39.64	3				87.24	2				48.16	1		Q_1	
01.68	8			31	40.11	2				87.59	2				48.47	7	24	—	
02.13	8		29		40.76	3				87.99	1	P_1			48.77	4			
02.90	8			29	41.29	4				88.44	2	—			49.10	2			
03.33	9		27		41.97	4	R_2			88.97	2	76			49.37	2		71	
03.98	7				42.33	2	—			89.81	2*w*				50.01	3			
04.28	7			27?	42.80	5	21			90.14	2*w*				50.47	4		69	
04.54	9		25		43.28	3				91.05	1				51.08	7	22		
04.92	7				43.95	6	23			91.41	1				51.48	4		67	
05.59	9		23		44.78	2				91.93	2	74			51.97	4			
05.81	8			25?	45.35	6	25			92.23	2				52.35	5		65	
06.04	8				46.16	2				92.80	1				52.69	2			$^{Q}P_{21}$
06.81	9		21	23?	47.05	7*w*	27			93.09	1				53.11	5		63	—

† The letters *w*, *vw*, and *vvw* after the intensities mean wide, very wide and very very wide.

* Under the heading of "Assignment" the J numbering for the lines of the various branches is given. For example, 41 means $J = 41\frac{1}{2}$. The letters in parentheses have the meanings given in the text.

TABLE I—*Continued.*

Observed Wave Numbers of Lines	Int.†	Assignment*		Observed Wave Numbers of Lines	Int.†	Assignment*		Observed Wave Numbers of Lines	Int.†	Assignment*		Observed Wave Numbers of Lines	Int.†	Assignment*	
53.29	4			76.70	6			10.09	3			46.39	3		
53.68	7	20		77.11	4			11.01	7	29		46.81	3		
53.95	6		61	77.48	6			12.05	4			47.44	3w	61	
54.45	5			78.25	10vvw	(a)		13.09	7	31		48.74	3		
54.79	7		59	79.16	2			13.81	3			49.56	4		
55.20	5			79.73	2			14.32	2			50.10	2		
55.37	7		57	80.06	3			14.75	4			50.91	3		
55.84	6			81.52	2			15.39	7	33		51.58	3		
56.12	8		55	81.99	3			16.41	3			52.03	2		
56.41	7			82.52	3			16.82	4			53.01	3		
56.77	8		53	83.02	5w			17.26	4			53.52	2		
57.14	7			83.44	5	R_1	$^RQ_{21}$	17.58	7	35		54.12	2		
57.47	8		51	83.71	6			18.06	3			54.71	1		
57.88	6			84.06	6	18		18.79	3			55.06	3w		
58.12	8		49	84.44	7	20		19.18	4			55.85	1		
58.62	6			84.89	7	22		19.87	7w	37		56.27	1		
58.82	8		47	85.59	7	24	18	20.45	4			57.11	4		
59.32	6			86.10	8	26?	20	21.16	3			58.26	2		
59.46	9		45	86.92	10vw	30	22, 24, 26	22.17	6	39		58.94	2w		
60.01	6			87.38	9		28	22.83	5			60.63	2		
60.17	9		43	87.59	6			23.43	3			61.07	4		
60.72	7			87.88	9		30	23.91	5			62.33	3		
60.88	9		41	88.47	9		32	24.46	6	41		62.61	3		
61.42	8			89.24	10vw	32, 34	34	24.92	6			63.21	3		
61.92	9		39	89.93	9		36	25.48	3			63.62	3		
62.39	9		35	90.70	9		38	25.94	5			63.96	4		
62.95	9w		37, 31	33	91.47	9	36	40	26.82	7	43		64.49	4	
63.31	7			91.87	7	38		27.20	4			64.78	4		
63.74	8		33	92.34	9w	40	42	27.51	3			65.58	4w		
63.99	8			31	93.13	9	42	44	27.91	3			66.10	3	
64.27	8		29	93.96	9	44	46	28.50	4			66.67	5		
64.68	6			94.77	8		48	29.12	6	45		67.21	4vw		
65.02	9			29	95.62	8		50	29.40	5			67.72	4	
65.12	9		27	96.44	8		52	30.28	4			68.52	6		
65.79	8vw			87.27	8	54		30.90	3			69.23	3		
66.00	8			27	98.11	7w	56	31.44	5	47		69.63	4		
66.55	8			98.79	7			32.06	4			70.27	5		
67.07	9		23	99.14	6			32.87	3			70.59	5		
67.51	8			25	99.52	6		33.77	5	49		71.40	4w		
68.13	9		21	99.81	6			35.51	2			72.15	4		
68.76	6			23?	34700.19	6		36.14	4w	51		72.69	5		
69.23	9w		19?		00.59	7		36.85	3			73.45	5		
69.75	5			21?	01.22	6		37.38	2			73.97	5		
69.99	5				01.38	5		37.83	2			74.52	5		
70.43	8				01.79	6		38.48	5	53		74.95	5		
70.73	7				02.12	7w	$^SR_{21}$	39.11	4			75.38	4		
71.01	6				03.08	6w		39.58	4			75.70	3		
71.29	5				03.52	5		40.96	4w	55		76.02	4		
71.68	7				03.82	5	21?	41.58	5			76.43	5		
72.27	5				04.11	6		42.11	4			76.67	6		
72.70	6				04.78	3		42.66	4			77.04	6		
72.99	7w				05.46	7	23	43.09	5	57		77.50	6		
73.72	4				06.16	3		43.59	5			77.81	6		
74.16	6				07.07	5w	25	43.88	5			78.06	6		
74.63	3				08.12	3		44.35	5			78.67	9	(e)	
75.30	5				08.98	7	27	44.81	6						
76.34	5				09.67	2		45.41	5vvw	59	(c)				

differences [see Eqs. (3) and (4)] should show a greater accuracy since they involve lines which are closer together than the interval between the iron standards. Two other iron lines, namely λ4325.768 and λ4307.91 provided a check on the accuracy of the corrections. Table I gives the wave numbers of the lines, together with the estimated intensities, obtained from the amplitudes on the photometric trace.

ANALYSIS

General considerations

The schematic energy level diagram (Fig. 3) shows the first line of each branch for a $^2\Sigma^+_u \rightarrow {}^2\Pi_g$ transition with case *a* inverted $^2\Pi_g$. The antisymmetric levels should be missing because of the zero spin of the oxygen nuclei. These levels are indicated by dotted lines; they correspond to the + rotational levels in the $^2\Sigma^+_u$ and to the − rotational levels in the $^2\Pi_g$ state.

In accordance with the selection rules $\Delta J = 0$ or ± 1 and $+ \rightleftarrows -$, the band should consist of two sub-bands with six branches in each, the separation between the two sub-bands being approximately equal to A, the spin-orbit coupling coefficient for the $^2\Pi_g$ state. The coefficient A is negative for

inverted $^2\Pi$ ($^2\Pi_{3/2}$ lies deeper). The P_2, $^PQ_{12}$ and the Q_2, $^QR_{12}$ branches in the ($^2\Sigma$, $^2\Pi_{1/2}$) sub-band and the $^QP_{21}$, Q_1 and the $^RQ_{21}$, R_1 branches in the ($^2\Sigma$, $^2\Pi_{3/2}$) sub-band should form four series of close pairs [cf. Fig. 3 and Eqs. (1)] with separations $\Delta\nu_{12}(K)=\gamma(K+\frac{1}{2})$ where γ is a small constant; $\Delta\nu_{12}$ corresponds to the spin doubling of the $^2\Sigma^+_u$ levels.[17]

The total energy terms are given by[16,17]

$$^2\Pi_{1/2}: T_{2c}(J)=(T_0''-\tfrac{1}{2}A-\tfrac{1}{4}B_2)-\tfrac{1}{2}p(J+\tfrac{1}{2})+B_2J(J+1)+DJ^2(J+1)^2\cdots, \quad (1a)$$

$$^2\Pi_{1/2}: T_{2d}(J)=(T_0''-\tfrac{1}{2}A-\tfrac{1}{4}B_2)+\tfrac{1}{2}p(J+\tfrac{1}{2})+B_2J(J+1)+DJ^2(J+1)^2\cdots, \quad (1b)$$

$$^2\Pi_{3/2}: T_{1c}(J)=(T_0''+\tfrac{1}{2}A-\tfrac{9}{4}B_1)+B_1J(J+1)+DJ^2(J+1)^2\cdots=T_{1d}(J), \quad (1c)$$

$$^2\Sigma;\ J=K+\tfrac{1}{2}: T_1(J)=T_0'+\tfrac{1}{2}\gamma K+BK(K+1)+DK^2(K+1)^2\cdots$$
$$=T_0'+\tfrac{1}{2}\gamma(J-\tfrac{1}{2})+B(J-\tfrac{1}{2})(J+\tfrac{1}{2})+D(J-\tfrac{1}{2})^2(J+\tfrac{1}{2})^2\cdots, \quad (1d)$$

$$^2\Sigma;\ J=K-\tfrac{1}{2}: T_2(J)=T_0'-\tfrac{1}{2}\gamma(K+1)+BK(K+1)+DK^2(K+1)^2\cdots$$
$$=T_0'-\tfrac{1}{2}\gamma(J+\tfrac{3}{2})+B(J+\tfrac{1}{2})(J+\tfrac{3}{2})+D(J+\tfrac{1}{2})^2(J+\tfrac{3}{2})^2\cdots \quad (1e)$$

where γ is as given above and p is the Λ-doubling constant [$\Delta\nu_{dc}(J)=p(J+\frac{1}{2})$ with p positive in this case; the Λ-doubling of the $^2\Pi_{3/2}$ is expected to be negligibly small[17]]. Schaffer[18] has shown that for linear triatomic molecules D is given by the same type of formula $D=4B^3/\omega^2$ as for diatomic molecules, where here ω refers to the totally symmetrical vibration frequency. Using $B=0.38$ cm^{-1} as shown later, and $\omega=1305$ cm^{-1},[19] one obtains $D=1.3\times10^{-7}$ cm^{-1} for the $^2\Pi_g$ state, and may expect nearly the same for the $^2\Sigma^+_u$ state, since the B values of the two states are almost equal.

The equations for the band lines of the ($^2\Sigma^+_u$, $^2\Pi_{1/2}$) sub-band in such a transition are:[16,17]

$$^OP_{12}(J)=T_1'(J-1)-T_{2c}''(J)=\nu_2+\tfrac{1}{4}(p-3\gamma+3B)-(2B+B_2-\tfrac{1}{2}p-\tfrac{1}{2}\gamma)J$$
$$+(B-B_2)J^2-2(2D'+D'')J^3\cdots, \quad (2a)$$

$$P_2(J)=T_2'(J-1)-T_{2d}''(J)=\nu_2-\tfrac{1}{4}(p+\gamma+B)-(B_2+\tfrac{1}{2}p+\tfrac{1}{2}\gamma)J$$
$$+(B-B_2)J^2-2D''J^3\cdots, \quad (2b)$$

$$^PQ_{12}(J)=T_1'(J)-T_{2d}''(J)=\nu_2-\tfrac{1}{4}(p+\gamma+B)-(B_2+\tfrac{1}{2}p-\tfrac{1}{2}\gamma)J+(B-B_2)J^2-2D''J^3\cdots, \quad (2c)$$

$$Q_2(J)=T_2'(J)-T_{2c}''(J)=\nu_2+\tfrac{1}{4}(p-3\gamma+3B)+(2B-B_2+\tfrac{1}{2}p-\tfrac{1}{2}\gamma)J$$
$$+(B-B_2)J^2+2(2D'-D'')J^3\cdots, \quad (2d)$$

$$^QR_{12}(J)=T_1'(J+1)-T_{2c}''(J)=\nu_2+\tfrac{1}{4}(p+\gamma+3B)+(2B-B_2+\tfrac{1}{2}p+\tfrac{1}{2}\gamma)J$$
$$+(B-B_2)J^2+2(2D'-D'')J^3\cdots, \quad (2e)$$

$$R_2(J)=T_2'(J+1)-T_{2d}''(J)=\nu_2-\tfrac{1}{4}(p+5\gamma-15B)+(4B-B_2-\tfrac{1}{2}p-\tfrac{1}{2}\gamma)J$$
$$+(B-B_2)J^2+2(4D'-D'')J^3\cdots. \quad (2f)$$

The equations for the band lines of the ($^2\Sigma^+_u$, $^2\Pi_{3/2}$) sub-band are obtained from these by replacing the subscripts of T'', ν_2 and B_2 by 1 and putting $p=0$ since the Λ-doubling for the $^2\Pi_{3/2}$ state is negligible. The notation for the branches is then P_1, $^QP_{21}$, Q_1, $^RQ_{21}$, R_1, and $^SR_{21}$, respectively, in order of increasing frequency, as in Eqs. (2). The difference $\nu_1-\nu_2$ is approximately A, as mentioned in the second paragraph of this section. The branches of both sub-bands should have intensities $Q_i>R_i>P_i$;[16] thus the close pairs should consist of lines of different intensity. The coefficient D will introduce a correction of significance only in the J^3 terms of the equations for the band lines, as given above, and then only for high J values. The J^2 term produces a contribution of the order of only 10^{-3} cm^{-1} for $J=70$, while the J^4 term has $(D'-D'')$ as coefficient, and this is very nearly equal to zero.

[17] Cf. R. S. Mulliken and A. Christy, Phys. Rev. **38**, 87 (1931).
[18] W. H. Schaffer, unpublished work.
[19] S. Mrozowski, private communication.

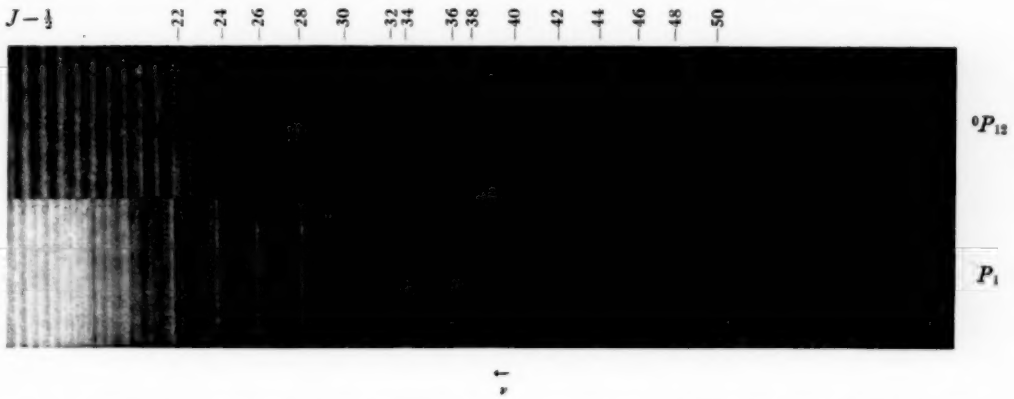

FIG. 4. Enlargement of the perturbed regions of the $^QP_{12}$ and P_1 branches (see Fig. 1 and the text), showing displacements and weakenings between $J=28\frac{1}{2}$ and $J=42\frac{1}{2}$.

Adjacent lines in a branch correspond to a difference in J of two units on account of the missing levels. If we assume[13] $B \backsimeq B_1 \backsimeq B_2$ and neglect the small constants γ and p and the terms in D, the spacing between the lines is seen to be $6B$, $2B$, $2B$, $-2B$, $-2B$, and $-6B$, respectively, in the order given above for the various branches of each sub-band.

Observed spectrum

The observed spectrum (see Fig. 1) is in agreement with these features. It consists of two well-defined sub-bands with six branches in each. The outer branches in each sub-band have fairly wide separation between lines and are free from overlapping above $J=20\frac{1}{2}$,[20] but the inner branches, which may be identified with the series of pairs mentioned previously, do not present such a simple appearance. This would be anticipated on account of their closer spacing, the small spin doubling of the $^2\Sigma^+_u$, and the presence of the low J members of the widely spaced branches, all of which effect a considerable overlapping. Indeed, the weak member of each pair is usually fused with a strong line of slightly different J. The weak branch $^QP_{21}$ is, however, well resolved from its companion Q_1 at high J values, and a few lines of R_1 begin to be resolved beyond $J=52\frac{1}{2}$.

The nearly uniform spacing of the lines in each of the various branches (aside from the perturbations discussed later) and the consequent absence of heads (see Fig. 1), at once indicates approximate equality in the rotational constants of the upper and lower states. The observed spacing is approximately three times as large for the wide branches as for the close branches, in agreement with the theoretical considerations given above.

Combination relations

After we had thus established the plausibility of a $^2\Sigma^+_u \rightarrow {}^2\Pi_g$ transition, the normal line of attack was followed to confirm the belief. The first step usually consists of getting the double-differences [see Fig. 3 and Eqs. (2)] from combination relations. Those for the lower state are

$$^2\Pi_{1/2}: \Delta_2 F''_{2e}(J) \equiv T''_{2e}(J+1) - T''_{2e}(J-1) = {}^QR_{12}(J-1) - {}^QP_{12}(J+1) \quad \text{with } (J+\tfrac{1}{2}) \text{ even,} \quad (3a)$$

$$: \Delta_2 F''_{2d}(J) \equiv T''_{2d}(J+1) - T''_{2d}(J-1) = R_2(J-1) - P_2(J+1) \quad \text{with } (J+\tfrac{1}{2}) \text{ odd,} \quad (3b)$$

$$^2\Pi_{3/2}: \Delta_2 F_1''(J) \equiv T_1''(J+1) - T_1''(J-1) = R_1(J-1) - P_1(J+1) \quad \text{with } (J+\tfrac{1}{2}) \text{ even,} \quad (3c)$$

$$: \Delta_2 F_1''(J) \equiv T_1''(J+1) - T_1''(J-1) = {}^SR_{21}(J-1) - {}^QP_{21}(J+1) \quad \text{with } (J+\tfrac{1}{2}) \text{ odd.} \quad (3d)$$

By virtue of the missing levels, each of these expressions gives only a set of alternate and not consecutive $\Delta_2 F''$'s, as shown by the designation $(J+\frac{1}{2})$ odd (or even). This means that an

[20] As usual, J is written for J''.

unambiguous selection of Δ_2F'''s cannot be made directly from them since they are all different and so cannot be used in a mutual comparison.

A more favorable situation results when the double-differences for the upper state are considered. With the combination relations

$$^2\Sigma^+_u: \Delta_2F_1'(K=J-\tfrac{1}{2}) \equiv T_1'(K+1) - T_1'(K-1) = {}^QR_{12}(J) - {}^OP_{12}(J) = R_1(J) - P_1(J) \text{ with } K \text{ even}, \quad (4a)$$

$$: \Delta_2F_2'(K=J+\tfrac{1}{2}) \equiv T_2'(K+1) - T_2'(K-1) = R_2(J) - P_2(J) = {}^SR_{21}(J) - {}^QP_{21}(J) \text{ with } K \text{ even}, \quad (4b)$$

there is the possibility of a check, as indicated. Each of the Δ_2F_1''s can be obtained in two ways, which should presumably enable one to make the correct identifications. In the actual analysis, however, many possible differences were found which agreed within the error of measurement and no final choice could be made with certainty by using Eqs. (4).

Another factor which greatly increased the difficulty of a correct determination is the following. It can be seen from Eqs. (3) and (4) that the double-differences are to be obtained by combining lines of the wide branches with lines of the *weak* component of the double branches. The latter, as already mentioned, were not readily identified initially because they are usually merged with lines of the stronger branch. Further uncertainty was at first introduced by the perturbations which affect the upper state.

TABLE II.

$J-\frac{1}{2}$	$P_1(J)$ $-{}^OP_{12}(J)$	${}^RQ_{21}(J)$ $-Q_2(J)$	Av. $\Delta(J)$	$\Delta(J+2)$ $-\Delta(J)$
20	161.16	161.21	161.18	
22	161.35	161.38	161.36	0.18
24	161.53		161.53	0.17
26	161.71		161.71	0.18
28	161.89	161.90	161.90	0.19
30	162.10	162.12	162.11	0.21
32	162.32	162.33	162.32	0.21
34	162.58	162.57	162.58	0.26
36	162.85	162.85	162.85	0.27
38	163.14	163.09	163.12	0.27
40	163.43	163.37	163.40	0.28
42	163.72	163.77	163.74	0.34
44	164.02	164.04	164.03	0.29
46	164.55	164.36	164.36	0.33
48	164.69	164.77	164.73	0.37
50	165.06	165.09	165.08	0.35
52	165.46	165.41	165.44	0.36
54	165.75	165.77	165.76	0.32
56	166.16			
58	166.56			
60	167.00			
62	167.45			
64	167.88			
66	168.38			

Identification of the lines

Fortunately, however, the perturbations observed in the ${}^OP_{12}$ and the P_1 branches (see Fig. 4) permitted an identification of lines of equal J' in these two branches, though not a determination of their absolute J numbering. The correct ordering of lines according to J was found by taking the differences [see Eqs. (1) and (2)]

$$\Delta(J) = P_1(J) - {}^OP_{12}(J) = T_{2c}''(J) - T_1''(J) = [-A + \tfrac{9}{4}B_1 - \tfrac{1}{4}B_2] - \tfrac{1}{2}p(J+\tfrac{1}{2}) + (B_2 - B_1)J(J+1) \text{ with } (J+\tfrac{1}{2}) \text{ odd} = \text{const.} + aJ + bJ^2. \quad (5a)$$

The values $\Delta(J)$ should change smoothly with J (giving constant second differences) and thus provide an identification of corresponding lines in the two branches even in the region of the perturbations, since the relations are independent of the upper state and the lower state is not perturbed. The values of $\Delta(J)$ and also of $\Delta(J+2)-\Delta(J)$ are given in Table II, which was obtained after ordering the lines so as to give Δ's varying with J in the predicted manner. Exactly the same values should, according to Fig. 3, be obtained from the combination ${}^RQ_{21}(J) - Q_2(J)$, and were actually obtained, thus providing a combination relation check. In this manner it was possible, for example, to locate the very weak and strongly displaced lines, ${}^OP_{12}(38\tfrac{1}{2})$ and $P_1(38\tfrac{1}{2})$, whose existence was not suspected from an inspection of the spectrograms (cf. Fig. 4).

Similarly, the combinations

$$\Gamma(J) = {}^SR_{21}(J) - R_2(J) = Q_1(J) - {}^PQ_{12}(J) = T_{2d}''(J) - T_1''(J) \text{ with } (J+\tfrac{1}{2}) \text{ even} \quad (5b)$$

establish a correct ordering for the lines of these four branches. Unfortunately, however, these two sets of orderings are independent of each other and do not help to determine relations between the J values of the two sets of branches.

Assignment of J values

After one had obtained the proper ordering for the lines in each of the strong branches it was

TABLE III.

$^2\Pi_{1/2}$: VALUES OF $\Delta_1F''_{2d}(J)-\Delta\nu_{dc}(J+\frac{1}{2})$				$^2\Pi_{3/2}$: VALUES OF $\Delta_1F_1''(J)$			
J	CALC.*	$^PQ_{12}(J-\frac{1}{2})$ $-{}^OP_{12}(J+\frac{1}{2})$	$R_2(J-\frac{1}{2})$ $-Q_2(J+\frac{1}{2})$	J	CALC.*	$^SR_{21}(J-\frac{1}{2})$ $-{}^RQ_{21}(J+\frac{1}{2})$	$Q_1(J-\frac{1}{2})$ $-P_1(J+\frac{1}{2})$
20	15.55	15.55	15.56	18	14.04	13.93	14.02
22	17.07	17.08	17.13	20	15.56	15.69	15.55
24	18.58	18.65	18.60	22	17.08	17.19	17.05
26	20.11	20.10	20.10	24	18.59	18.54	18.60
28	21.62	21.62	21.61	26	20.11	20.15	20.05
30	23.14	23.17	23.17	28	21.62	21.60	21.59
32	24.63	24.56	24.66	30	23.14	23.13	23.19
34	26.15	26.16	26.17	32	24.66	24.62	24.67
36	27.67	27.63	27.74	34	26.12	26.15	26.16
38	29.19		29.18	36	27.69	27.65	27.63
40	30.71	30.64	30.72	38	29.15	29.17	29.25
42	32.21	32.30	32.26	40	30.71	30.70	30.69
44	33.72	33.86	33.75	42	32.12	32.12	32.16
46	35.24	35.24	35.24	44	33.75	33.69	33.70
48	36.73	36.81	36.83	46	35.26	35.16	35.21
50		38.31	38.32	48	36.77	36.67	36.73
52		39.86	39.76	50	38.23	38.15	38.23
54		41.33	41.26	52		39.70	39.75
56		42.84	42.84	54		41.21	41.22
58		44.40	44.30	56		42.85	42.74

* This column was calculated from Mrozowski's Δ_2F'''s with the help of Eqs. (6), (7), and (8).

possible to obtain the combination differences[21]

$$
\begin{aligned}
^2\Pi_{1/2}:\ & {}^PQ_{12}(J-\tfrac{1}{2})-{}^OP_{12}(J+\tfrac{1}{2})\\
&=R_2(J-\tfrac{1}{2})-Q_2(J+\tfrac{1}{2})\\
&=T''_{2c}(J+\tfrac{1}{2})-T''_{2d}(J-\tfrac{1}{2})\\
&=\Delta_1F''_{2c}(J)-\Delta\nu_{dc}(J-\tfrac{1}{2})\\
&=\Delta_1F''_{2d}(J)-\Delta\nu_{dc}(J+\tfrac{1}{2}), \qquad (6a)\\
^2\Pi_{3/2}:\ & Q_1(J-\tfrac{1}{2})-P_1(J+\tfrac{1}{2})\\
&={}^SR_{21}(J-\tfrac{1}{2})-{}^RQ_{21}(J+\tfrac{1}{2})\\
&=T_1''(J+\tfrac{1}{2})-T_1''(J-\tfrac{1}{2})\\
&=\Delta_1F_1''(J), \text{ since } p_1=0, \qquad (6b)
\end{aligned}
$$

which seemed especially suitable for the determination of J, since in each case a combination relation check is offered and the sequence of the lines was unambiguously known from the combination relations (5). But, even so, there were several combination sets in sufficiently close agreement so that no definite selection could be made. Nevertheless, a tentative assignment of J could be made for these branches.

Fortunately, another line of inquiry was available by this time. Mrozowski,[22] working concurrently with the writer in this laboratory, as already mentioned, had been able to obtain a rotational analysis of a series of longer wavelength CO_2^+ bands previously studied by Smyth[23] and by Schmid.[24] His system of bands belongs to a $^2\Pi_u\rightarrow{}^2\Pi_g$ transition, and because he has been able to identify several members of a v' progression his Δ_2F'''s and rotational constants for the lower state ($^2\Pi_g$) are very accurate. The values he obtained[19] are: $B_1''=0.3796$ cm^{-1}, $B_2''=0.3812$ cm^{-1} and $p=+0.004$ cm^{-1} (Λ-doubling coefficient for the $^2\Pi_{1/2g}$ levels).

It was hoped that Mrozowski's lower $^2\Pi_g$ state would be the same as that for the λ2900 band. Since the double-differences [Eqs. (3)] were not reliable, no comparison with his Δ_2F'''s was possible at first. Instead, Δ_1F'''s were calculated from Mrozowski's double-differences and his B values with the help of the equations [cf. Eqs.

[21] It will be noticed that this is not the usual definition of the single-differences (i.e., $F(J+\frac{1}{2})=T(J+1)-T(J)$) in which the assignment of J is that of the lower level involved. The number J used here is the average value of the J's of the two rotational levels whose separation is given, just as in the case of the usual definition of the double-differences. This designation is preferred here by virtue of its greater consistency with that for $\Delta_2F(J)$ and the greater symmetry of the resulting equations.

[22] S. Mrozowski, Phys. Rev. **59**, 923A (1941).
[23] H. D. Smyth, Phys. Rev. **38**, 2000 (1931).
[24] R. F. Schmid, Phys. Rev. **41**, 732 (1932).

TABLE IV.

$^2\Pi_{1/2}$: VALUES OF $\Delta_2F_2''(J)$						$^2\Pi_{3/2}$: VALUES OF $\Delta_2F_1''(J)$					
$J-\frac{1}{2}$	$\Delta_2F_{2c}''(J)$*	$^QR_{12}(J-1)$ $-{}^OP_{12}(J+1)$†	$J-\frac{1}{2}$	$\Delta_2F_{2d}''(J)$*	$R_2(J-1)$ $-P_2(J-1)$†	$J-\frac{1}{2}$	$\Delta_2F_1''(J)$*	$R_1(J-1)$ $-P_1(J+1)$†	$J-\frac{1}{2}$	$\Delta_2F_1''(J)$*	$^SR_{21}(J-1)$ $-{}^QP_{21}(J+1)$†
19	30.48	30.49	22	35.08	34.99	17	27.34	27.30	22	34.92	35.06
21	33.54	33.55	24	38.13	38.14	19	30.37	30.38	24	37.94	37.95
23	36.60	36.62	26	41.18	41.07	21	33.40	33.36	26	40.98	41.07
25	39.63	39.69	28	44.22	44.15	23	36.43	36.42	28	44.01	
27	42.67	42.67	30	47.27	47.25	25	39.46	39.44	30	47.04	47.02
29	45.73	45.76	32	50.31	50.28	27	42.50		32	50.08	50.14
31	48.77	48.76	34	53.34	53.30	29	45.53		34	53.11	53.00
33	51.81		36	56.41	56.41	31	48.56		36	56.14	56.16
35	54.87		38	59.45	59.49	33	51.60	51.66	38	59.16	59.15
37	57.92		40	62.49	62.51	35	54.62		40	62.18	62.17
39	60.95		42	65.52		37	57.65	57.77	42	65.20	65.20
41	64.00	64.09	44	68.53	68.63	39	60.67	60.64	44	68.26	68.20
43	67.01	66.95	46	71.57	71.63	41	63.69	63.62	46	71.28	71.24
45	70.04	70.10	48	74.60	74.65	43	66.72	66.66	48	74.30	74.30
47	73.08	73.13	50	77.66	77.71	45	69.77	69.71	50	77.32	77.36
49	76.13	76.20	52	80.69	80.73	47	72.79	72.75			
51	79.17	79.20	54	83.73	83.75	49	75.81	75.81			
			56	86.77	86.79	51	78.84	78.83			
						53	81.86	81.85			
						55	84.88	84.87			
						57	87.91	87.97			

* Obtained from Mrozowski's analysis of his bands. Values above $J=50\frac{1}{2}$ have been extrapolated.
† Some values are missing because blends make their determination too uncertain.

(3) and (6)]

$$^2\Pi_{1/2}: \Delta_2F_{2i}''(J)=T_{2i}''(J+1)-T_{2i}''(J-1)$$
$$=4B_2(J+\tfrac{1}{2})\pm p+8DJ^2(J+\tfrac{3}{2})\cdots, \quad (7a)$$
$$: \Delta_1F_{2i}''(J)=T_{2i}''(J+\tfrac{1}{2})-T_{2i}''(J-\tfrac{1}{2})$$
$$=2B_2(J+\tfrac{1}{2})\pm p/2$$
$$+4DJ^2(J+\tfrac{3}{2})\cdots, \quad (7b)$$

where the + sign in front of p applies when i is d and the − sign applies when i is c. For $^2\Pi_{3/2}$ the subscripts 2 of F, T, and B are to be replaced by 1, and here $p=0$. Since, in general, $\Delta_2F_i(J)=\Delta_1F_i(J+\frac{1}{2})+\Delta_1F_i(J-\frac{1}{2})$, one obtains, neglecting the small quantity p,

$$\Delta_1F_i(J+\tfrac{1}{2})=\tfrac{1}{2}[\Delta_2F_i(J)]\pm B\pm 3DJ(J+1), \quad (8)$$

in which the last term may be neglected for reasons already given. The Δ_1F'''s thus calculated were corrected for the Λ-doubling, in the case of the $^2\Pi_{1/2}$, to correspond to Eq. (6a), and were used uncorrected for the $^2\Pi_{3/2}$ [cf. Eq. (6b)]. An excellent agreement was at once found for one set of combinations for each sub-band (see Table III), proving that both band systems do have the same lower $^2\Pi_g$ state, and making possible a definite assignment of J values for the λ2900 band through the use of Mrozowski's analysis of the other system.

Only alternate Δ_1F'''s are found from the combination relations (6), namely those for which J is even (see Fig. 3), a fact which proves that the upper state is a $^2\Sigma$ with missing levels.[25] A similar procedure involving Eqs. (6), (7) and (8) was now applied to the P_2, $^QR_{12}$, $^QP_{21}$ and R_1 branches. From this we obtained the Δ_1F'''s with J odd, and it was thus possible to assign correct J values for these branches, though with some uncertainty in many cases because of blends.

Having determined the position and numbering of many of the lines of the weak branches, it was then possible to get Δ_2F's for both the upper and lower states corresponding to Eqs. (4) and (3). The agreement of the latter with Mrozowski's is very good, as can be seen from Table IV, but his values for the lower state are certainly more precise because he obtained the average of several bands which are free from the serious overlapping of the present case.

Mrozowski's double-differences were also used to get more precise Δ_2F''s by employing relations

[25] That the upper level is common to both sub-bands is also shown by the identical perturbations in the $^0P_{12}$ and P_1 branches (see Fig. 4).

TABLE V.

	$^2\Sigma^+_u$: VALUES OF $\Delta_2F_1'(K)$: $J=K+\frac{3}{2}$				$^2\Sigma^+_u$: VALUES OF $\Delta_2F_2'(K)$: $J=K-\frac{3}{2}$				
K	$\Delta_2F_{2c}''(J)$ $+[{}^OP_{12}(J+1)$ $-{}^OP_{12}(J-1)]$*	$\Delta_2F_1''(J)$ $+[P_1(J+1)$ $-P_1(J-1)]$*	${}^QR_{12}(K+\frac{1}{2})$ $-{}^OP_{12}(K+\frac{1}{2})$†	$R_1(K+\frac{1}{2})$ $-P_1(K+\frac{1}{2})$†	K	$\Delta_2F_{2d}''(J)$ $+[R_2(J+1)$ $-R_2(J-1)]$*	$\Delta_2F_1''(J)$ $+[{}^SR_{21}(J+1)$ $-{}^SR_{21}(J-1)]$*	$R_2(K-\frac{1}{2})$ $-P_2(K-\frac{1}{2})$†	${}^SR_{21}(K-\frac{1}{2})$ $-{}^QP_{21}(K-\frac{1}{2})$†
20	30.75	30.81	30.76	30.76	24	36.23	36.27		
22	33.80	33.82	33.83	33.81	26	39.53	39.55	39.54	39.49
24	37.13	37.14	37.18	37.12	28	42.88	42.89	42.77	42.98
26	39.96	39.95	39.94		30	46.09	46.04	46.03	45.99
28	43.00	43.01	43.01		32	49.14	49.12	49.12	49.10
30	45.75	45.76	45.76	45.74	34	52.35	52.38	52.32	52.44
32	50.85	50.90		50.96	36	55.32	55.30	55.28	
34	51.76	51.80	51.71	51.66	38	58.38	58.44	58.35	58.45
36	56.57	56.59		56.71	40	61.48	61.48	61.52	61.45
38	58.19	58.20	58.24	58.17	42	64.50	64.48		64.46
40	61.20	61.18	61.29	61.11	44	67.53	67.55		67.50
42	64.46	64.37		64.41	46	70.53	70.56	70.63	70.50
44	67.49	67.55	67.55	67.49	48	73.56	73.60	73.62	73.56
46	70.58	70.63	70.63	70.59	50	76.62	76.63	76.67	76.63
48	73.63	73.61	73.63	73.61	52	79.60	79.69	79.65	79.73
50	76.59	76.67	76.67	76.66	54	82.66	82.69	82.70	82.64
52	79.69	79.69		79.68	56	85.64		85.66	85.76
54	82.66	82.71		82.70	58	88.61	88.53	88.63	88.64
56	85.60	85.70			60	91.65		91.72	91.73
58	88.70	88.77							
60	91.63	91.70							
62	94.50	94.53							

* The Δ_2F'''s were obtained from Mrozowski's analysis of his bands. Values above $J=50\frac{1}{2}$ have been extrapolated.
† In such a symbol as ${}^QR_{12}(K+\frac{1}{2})$, the number in parentheses of course means, as usual, the value of J'' for the line in question.
Some of the values in columns 3, 4 and 5 are missing because blends make the determination too uncertain.

of the type

$$\Delta_2F_1'(K=J-\tfrac{3}{2})=\Delta_2F_2''(J)+[{}^OP_{12}(J+1)-{}^OP_{12}(J-1)]. \quad (9)$$

(See Fig. 3.) The bracketed term is the interval between successive lines in a branch, and, since it could be very accurately determined, this set of Δ_2F''s is probably better than the one obtained directly from the combination differences (4) which depend on measurements of weak, blended lines. Both sets are given in Table V, and it may be seen that they agree well.

It was not possible to extend the analysis with certainty to lower J values than those given in the tables because of the extensive overlapping of various branches, and also because of perturbations in the branches originating from T_2' which alter their spacing and intensity below $J=27\frac{1}{2}$.

Evaluation of molecular constants

The rotational constants for the $^2\Pi_g$ state were determined from Eqs. (7) and the double-differences given by Eqs. (3). The B'' values obtained agree closely with Mrozowski's,[19] as would be expected, but certainly his are more accurate for the reasons pointed out above. Similarly, his value of p (the Λ-doubling coefficient) is more reliable than the one that could be obtained from the λ2900 band. That his p value is positive in sign and is very good is supported by the fact that it was used in Eq. (6a) as a correction of his single-differences to get the combination differences which show such an excellent agreement with those obtained directly (see Table III). Therefore, no independent evaluation of these constants need be given.

The value of the rotational constant for the $^2\Sigma^+_u$ state was found to be $B'=0.3784$ cm^{-1}, which is only slightly smaller than B''. The B value of the ground state of neutral CO_2 is[26] $B_0=0.3895$ cm^{-1}. The close similarity of all these values indicates that the σ_u electron missing in the $^2\Sigma^+_u$ state, as well as the π_g electron which is missing in the $^2\Pi_g$ state, are almost non-bonding, a rather surprising result. B' was obtained, from equations of the same type as Eq. (7), from the Δ_2F_1''s above $J=40\frac{1}{2}$ and from the Δ_2F_2''s above $J=28\frac{1}{2}$, since only for these J values is the

[26] G. Herzberg, unpublished work.

spacing of the lines fairly uniform and apparently free from perturbations.

The spin-coupling constant γ for the $^2\Sigma^+_u$ state was found to be 0.019 cm^{-1} from relations of the type

$$\Delta\nu_{12}(K)=\gamma(K+\tfrac{1}{2})$$
$$=P_{Q_{12}}(K=J-\tfrac{1}{2})-P_2(K=J-\tfrac{1}{2})$$
$$=Q_{R_{12}}(K=J+\tfrac{1}{2})-Q_2(K=J+\tfrac{1}{2}), \quad (10)$$

where, as in determining B', only the lines apparently free from perturbations were used. This value of γ, however, may not have much meaning, since it is possible that the perturbations have produced for the higher J values a permanent shift in the relative positions of T_1 and T_2.

By extrapolating the differences given by Eq. (5) to $J=0$, one gets for the spin-orbit coupling constant $A=-160.3+2B=-159.5$ cm^{-1}. The $^2\Pi_g$ is, therefore, a very good case a even to the highest J values observed since $Y=A/B=-419.5$.[27] The $^OP_{12}$ and $^SR_{21}$ branches, which would be forbidden by the selection rule $\Delta K=0, \pm1$ for case b, remain intense to very high J values, as they should in view of the good approximation of the $^2\Pi_g$ to case a.[13]

Equation (5) was also used to evaluate the difference (B_2-B_1) between the rotational constants for the $^2\Pi_{1/2}$ and $^2\Pi_{3/2}$ sub-levels. Remembering that successive intervals correspond to a change in J of two units, one gets for the difference between $\Delta(J+2)$ and $\Delta(J)$ the value $p+2(B_2-B_1)(2J+3)$, where again p may be neglected (see column 4, Table V). Taking the mean of 17 such differences, and using the average J associated with it, one finds the value of (B_2-B_1) equal to 0.0018 cm^{-1}. From the equation[27,28] $B_i=B(1\pm B/A)$, one gets $(B_2-B_1)=2B^2/A=2(0.38)^2/160=0.0018$ cm^{-1}, in perfect agreement with the experimental value. This is somewhat higher than the value $(B_2-B_1)=0.0016$ cm^{-1} obtained by Mrozowski,[19] but still the agreement is good. The present method of determining the value of the difference between the two rotational constants is very accurate since (B_2-B_1) appears directly as the coefficient of $J(J+1)$, whereas the value obtained by Mrozowski relies on the independent determination of B_2 and B_1. Using $B=\frac{1}{2}(B_1+B_2)=0.3804$ cm^{-1}, from Mrozowski's values, and $(B_2-B_1)=0.0018$ cm^{-1}, one gets the probably better values $B_1=0.3795$ cm^{-1} and $B_2=0.3813$ cm^{-1}.

Perturbations

The perturbations in the $^OP_{12}$ and P_1 branches (see Fig. 4) between the lines $J=28\frac{1}{2}$ and $J=42\frac{1}{2}$ show not only displacements but also considerable weakening of some of the lines, especially for $J=30\frac{1}{2}$, $32\frac{1}{2}$, and $38\frac{1}{2}$ of both branches, corresponding to lines originating from T_1' at $K=29$, 31, and 37 (see Fig. 3). The lines $J=25\frac{1}{2}$ and $J=41\frac{1}{2}$ of the branches $^SR_{21}$ and R_2 (originating from T_2' at $K=27$ and $K=43$), although not appreciably displaced, are also weakened. The same is true for the corresponding lines of the other branches. A few very faint extra lines appear near the weakened lines, but even the sum of intensities of the regular and extra lines is less than normal. Besides, it was not found possible to fit any of the extra lines into the perturbation, which indicates that they, just as many other additional lines which appear throughout the band, may, at least some of them, have a different origin. Further perturbations appear in the $^SR_{21}$ and R_2 branches below $J=27\frac{1}{2}$. At this point the spacing between the lines becomes smaller and their intensity is reduced, but it was difficult to carry out a detailed investigation of these perturbations, since the lines merge with the high J members of the Q branches. It seems very probable that these perturbations are caused by higher vibrational levels of the $^2\Pi_u$ state of Mrozowski's bands, since the zero vibrational level of the latter lies only about 0.8 volt below that of the $^2\Sigma^+_u$ state. Several quanta, and not all of the totally sym-

[27] E. L. Hill and J. H. Van Vleck, Phys. Rev. **32**, 250 (1923).

[28] Cf. R. S. Mulliken, Rev. Mod. Phys. **2**, 113 (1930). Carrying the expansion of Hill and Van Vleck's formula for the rotational term values of the components of doublet states (reference 27) one step farther one gets (for $|A|\gg4$)

$$B^*=B[1\pm B/A\Lambda\mp(B^3/A^3\Lambda^3)(J+\tfrac{1}{2})^2\cdots].$$

The third term then might preferably be included as a correction term for D, giving $D^*=D(1\mp B^4/A^3\Lambda^3\cdots)$. In the present case $B^4/A^3\Lambda^3=5.1\times10^{-9}$ cm^{-1}, or about 4 percent of D.

metric vibration, would be needed to give the proper perturbing $^2\Pi_u$ vibronic states.

The diminished intensity of some of the lines means, according to accepted ideas,[29] that the perturbation is accompanied by accidental predissociation. However, this does not seem possible in the present instance, since the dissociation energy of CO_2^+ is, in the most favorable case, about one volt higher than the energy (4.3 volts) of the perturbed levels. The lowest energies of dissociation would be

$$CO_2^+ \rightarrow CO + O^+ - 5.27 \text{ volts} \quad (11a)$$

$$CO_2^+ \rightarrow CO^+ + O - 5.82 \text{ volts} \quad (11b)$$

$$CO_2^+ \rightarrow C^+ + O_2 - 6.98 \text{ volts} \quad (11c)$$

$$CO_2^+ \rightarrow C + O_2^+ - 7.96 \text{ volts.} \quad (11d)$$

Equation (11b) is based on $I(CO) = 14.1$ volts (from electron impact), while (11c) and (11d) depend on $C_{solid} \rightarrow C_{gas} - 5.4$ volts. A higher heat of sublimation of carbon would give an even higher value for the heat of dissociation in (11c) and (11d). To make (11b) fit the idea of accidental predissociation would require $I(CO) = 12.6$ volts. The lowest value (11a) cannot be altered since $I(O) = 13.55$ volts and the heats of formation of CO and CO_2 are accurately known.

A possible explanation of the weakening was suggested by Professor Mulliken and Dr. H. Beutler, as follows. The perturbing $^2\Pi_u$ rotational levels may have a high probability of transition to levels of several vibrational states of the $^2\Pi_g$ electronic state with which the $^2\Sigma^+_u$ rotational levels involved cannot combine with appreciable intensity because of the Franck-Condon principle. If the radiation lifetime of the $^2\Pi_u$ levels is much shorter than that of the perturbed $^2\Sigma^+_u$ levels, as seems plausible,[30] the perturbed levels of the latter would have their population seriously depleted, and there would be a corresponding weakening of the lines originating from them.

Further study will be required before a detailed explanation of the perturbations can be given.

[29] G. P. Ittmann, Naturwiss. **22**, 118 (1934).

[30] Both on the basis of theoretical intensity calculations [cf. R. S. Mulliken, J. Chem. Phys. **3**, 720 (1935)] and in view of the fact that the total observed emission intensity of the $^2\Pi_u \rightarrow ^2\Pi_g$ system is much greater than that of the single $^2\Sigma^+_u \rightarrow ^2\Pi_g$ band.

Unexplained Features of the Band

The two strong "lines" $\nu = 34678.25$ cm^{-1} and $\nu = 34517.54$ cm^{-1} marked (a) and (b) in Fig. 1, which were assumed by Duncan[6] and by Schmid[7] to be the zero branches of the transition, are always associated with the band and are not atomic lines. They appear with the same relative intensity in all the plates taken under various conditions and may perhaps be branches of a weaker member of the same sequence as the band studied. The preponderating intensity of the band analyzed as compared with other possible bands in the same system suggests that there is very little vibration in the upper state. This may be caused by the operation of the Franck-Condon principle in the excitation process, since the B values of the CO_2 ground state and of the $^2\Sigma^+_u$ state of CO_2^+ are almost equal, and the molecule is linear in both states. From this $^2\Sigma^+_u$ state radiation is very strong only to the vibrationless $^2\Pi_g$ level, because both B values are likewise equal, and the molecule is also linear in the lower state. However, detailed attempts to account for these "lines" as, for example, Q branches, or heads of branches, have not been successful.

The heads marked (c) ($\nu = 34745.45$ cm^{-1}) and (d_1, d_2) ($\nu_1 = 34585.88$ cm^{-1} and $\nu_2 = 34585.17$ cm^{-1}) have a separation of about 160 cm^{-1}, but their structure is too weak and diffuse for precise measurements. Presumably they also represent transitions between higher vibrational levels of the same electronic states.

A similar separation of 162.14 cm^{-1} exists between (e) ($\nu = 34778.67$ cm^{-1}) and (f) ($\nu = 34616.53$ cm^{-1}), but the sharp, clear-cut appearance of the latter and its smaller intensity does not seem to justify the same correlation. The latter may be the atomic line λ2887.91 of O^+, since the wavelength from the present plate measurements is 2887.95A.

Acknowledgment

This investigation was made possible by the grant of a Latin-American Fellowship by the John Simon Guggenheim Memorial Foundation. The work was conducted under the direction of Professor R. S. Mulliken, whose continuous

encouragement and suggestions permitted a successful solution of the problem. The author is also greatly indebted to Dr. S. Mrozowski for his collaboration in the experimental work and for the use of his unpublished data, and to Dr. H. Beutler for his help and advice in various phases of the work. Thanks are also due to Professor G. R. Harrison, of the Massachusetts Institute of Technology, for the careful measurement of the plates.

OCTOBER 15, 1941 PHYSICAL REVIEW VOLUME 60

Note on the Photoelectric Threshold of Bismuth Films of Measured Thickness

ALFRED H. WEBER AND LOUIS J. EISELE, S. J.
Department of Physics, Saint Louis University, St. Louis, Missouri

(Received August 27, 1941)

The photoelectric threshold wave-length change with thickness in aged bismuth films deposited on Pyrex at room temperature in vacuum is investigated further with some important modifications in apparatus and method including measurement of the average film thickness and extension of the temperature range in which the DuBridge analysis is applied. The data show that the bismuth films are characterized by: (1), an initial value of the threshold wave-length (2497A average) fairly independent of film thickness for the first 44 atom layers; (2), a definite shift toward higher threshold wave-lengths occurring between 44 and 111 atom layers thickness; followed by (3), a steady increase of threshold wave-length with film thickness above about 111 atom layers. These results are in general agreement with the previous preliminary work but show some differences which are discussed briefly.

IN preliminary experiments[1] an increase of the photoelectric threshold wave-length with increasing film thickness was observed for aged bismuth films deposited on glass at room temperature. This note describes a further investigation of this effect with some important improvements in apparatus and method including measurement of the film thickness and extension of the temperature range in which the DuBridge[2] analysis is applied.

Apparatus. Procedure

In the first experiments[1] the photoelectric cell was constructed with a molybdenum evaporation trough containing the bismuth close to the condensation surface (inclined to the vapor stream), a design resulting in deposits of uneven thickness. The proximity of the evaporation trough to the condensation surface resulted also in undesirable heating of the lower section of the surface.

The experimental tube shown by Fig. 1 and described in the accompanying legend eliminated these defects and, following the determination of the vapor pressure of bismuth,[3] made it possible to measure the average thickness of the bismuth deposits (unknown in the earlier experiments[1]). The electrodes E, used for electrical contact with the deposited metal in these experiments, also were useful in measuring the electrical conductance of the bismuth films in a later investigation.[4] A total obstruction charcoal trap was connected between the experimental tube and the vacuum pumps and was immersed continuously in liquid air during the experiments. The experimental tube and associated glass apparatus was subjected to the usual preliminary cleaning and outgassing. The photoelectric currents were measured with a Compton electrometer and the light source was the same as that described previously.[1] The illumination of the film (dimensions between electrodes about 0.5 cm×1 cm) was confined to a central circular area of diameter about 3.35 mm.

The temperature of the bismuth films on P

[1] A. H. Weber, Phys. Rev. **53**, 895 (1938).
[2] L. A. DuBridge, Phys. Rev. **39**, 108 (1932).
[3] A. H. Weber, Phys. Rev. **57**, 1042 (1940).
[4] A. H. Weber and D. F. O'Brien, following paper.

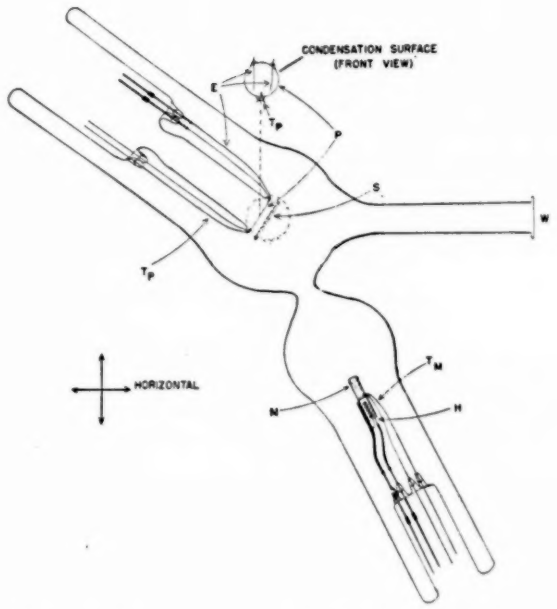

FIG. 1. Side cross-sectional view of tube. *M*, cylindrical molybdenum evaporation furnace with upper cavity filled with 99.9 percent C.P. bismuth and lower cavity containing 10-mil tungsten heater, H; T_M, tungsten-kovar thermocouple; *P*, Pyrex condensation surface (on end of reentrant tube) with tungsten-kovar thermocouple T_P and tungsten electrodes *E* sealed in *P* and ground off even with glass surface; *S*, circular nickel screen anode hinged so it could be lifted from path of bismuth vapor with an external electromagnet; *W*, polished fused quartz window joined to Pyrex cell with graded seal.

and the evaporation temperature in *M* were measured with tungsten-kovar thermocouples[5] (sealed directly into glass without the use of intermediate metals) calibrated with a" standard" Chromel-Alumel thermocouple in turn calibrated by the fixed points[6] method in conjunction with the data of Roeser and Wensel.[7] The evaporation temperature of bismuth was maintained at 603°C.

RESULTS AND DISCUSSION

The results of the experiments are shown by Figs. 2–4. Figure 2, similar to the curves of Fig. 5 of reference 1, illustrates the variation of the photoelectric current with average film thickness in atomic layers. The points plotted represent steady photoelectric currents for stable (i.e., yielding an unvarying photoelectric current) film layers; after each evaporation period (lasting from 5 to 60 minutes) an aging time, usually about two hours, was allowed before recording the photoelectric current. The deposition was interrupted also to make the photoelectric

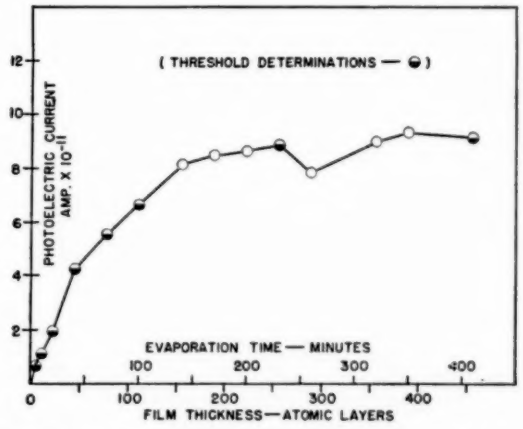

FIG. 2. Variation of photoelectric emission with bismuth film thickness. Data are for aged films condensed at room temperature. Evaporation rate 1.11 atom layers min^{-1}.

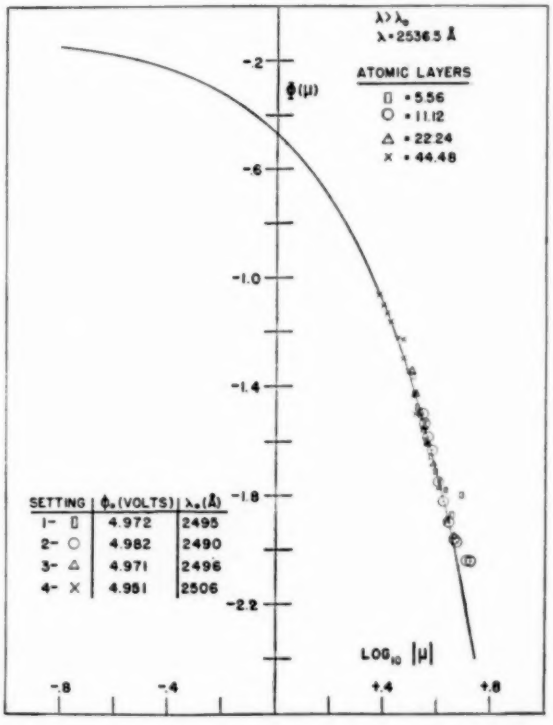

FIG. 3. Negative branch of DuBridge plot for threshold determinations made during first 40 minutes of evaporating time for bismuth film of Fig. 2. Temperature range for analysis, −78 to 22°C approximately.

[5] R. C. Mason, Rev. Sci. Inst. **8**, 265 (1937).

[6] The boiling point of liquid oxygen corrected for barometric pressure, the sublimation point of solid carbon dioxide in acetone and the melting point of mercury were the fixed points used.

[7] W. F. Roeser and H. T. Wensel, J. Research Nat. Bur. Stand. **14**, 255 (1935).

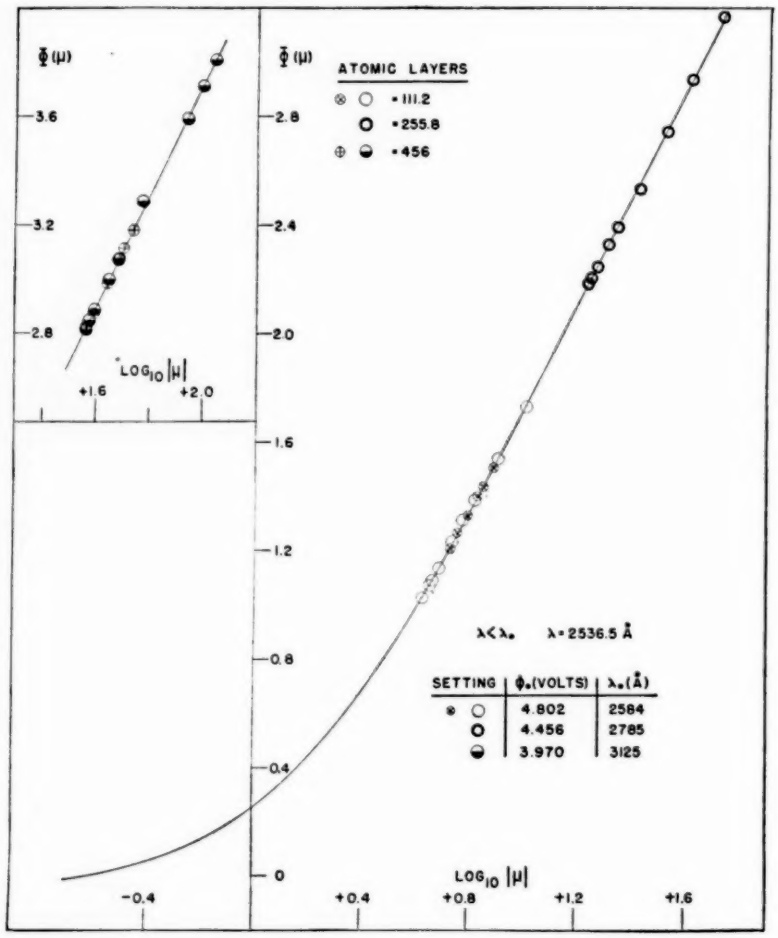

FIG. 4. Positive branch of DuBridge plot for threshold determinations made during last 310 minutes of evaporating time for bismuth film of Fig. 2. The smaller circles (⊗, ⊕) are for data obtained in the temperature range −78 to 22°C approximately, the other plotted points are for temperature range, −176 to 22°C approximately. The inset is the extension of the curve for larger coordinate values.

threshold determinations as is indicated by the half-solid circles. In all a total time of about ten days was required to obtain all the data included in Fig. 2.

It is seen that the photoelectric emission increases rapidly with film thickness and saturates beyond about 150 atom layers.

Figures 3 and 4 show the result of the DuBridge[2] isochromatic photoelectric threshold wave-length and work function determinations for the film thicknesses indicated in Fig. 2. To obtain unique fits of the experimental points on the theoretical curves (the solid lines) a scale was used such that the coordinate unit (0.4 on both abscissa and ordinate of Figs. 3 and 4) was actually 7-in. long. Two temperature ranges were employed in the threshold determinations; −176 to 22°C approximately (liquid air to room temperature) and −78 to 22°C approximately (dry ice-acetone to room temperature). The photoelectric current *versus* temperature runs were reproducible for all determinations shown in Figs. 3 and 4 and the fit of the experimental points to the theoretical curves is equally good for both temperature ranges. In the previous work[1] only the dry ice-acetone to room temperature interval was used. The present work seems to be the first reported application of the DuBridge method to temperatures as low as that of liquid air. The photoelectric current *versus* temperature data for the fifth point (film thickness, 78 atom layers) of Fig. 2 were not reproducible, probably because of instability of the film, and are not included in Figs. 3 and 4.

The data show that the bismuth films are characterized by: (1), an initial value of threshold wave-length fairly independent of film thickness (for the first 44 atom layers, Fig. 3, there is little change of threshold wave-length); (2), a marked shift of the threshold toward longer wave-lengths

accompanied by a definite increase in photoelectric emission taking place between film thicknesses of 44 and 111 atom layers approximately; followed by (3), a steady increase of threshold wave-length with film thickness above about 111 atom layers. These conclusions, stated in terms of actual film thickness, are more informative and more detailed than those of the earlier work.[1] Also, although the present and previous experiments are in general agreement, there are some differences. Thus the first films of the earlier work (described, however, as probably gas contaminated) exhibited a marked tendency to increase in threshold wave-length with increasing film thickness for all thicknesses and all films appeared to approach a limiting value of threshold wave-length. These differences in the actions of the films in the earlier and in the present work are ascribed mainly to the design of the tube used in the first experiments, which design resulted, as mentioned above, in deposits of non-uniform average thickness and probably prevented also the formation of films greater than a certain thickness because of heating of the condensation surface.

From the results of this work it is impossible to assign any fixed upper limit to the threshold wave-length of the films. In fact, the DuBridge analysis for the last point of Fig. 2 (threshold wave-length 3125A) is somewhat uncertain since the experimental points fall on a practically straight line portion of the theoretical curve as can be seen from the inset on Fig. 4. Because of lack of curvature of the theoretical curve beyond an abscissa value of about +1.6 an extension of the curve of Fig. 2 for greater film thicknesses with the corresponding threshold determinations would yield, very probably, data which could not be analyzed to obtain a unique threshold wave-length. The results of this work are of value in studying the shift of the threshold of bismuth films but not in determining the ultimate photoelectric threshold of very thick bismuth films.

It should be mentioned also that the aging of the film, though necessary for the production of stable, photoelectrically reproducible films, introduces possible complicating factors such as the gradual absorption and adsorption of gas and the formation of crystalline aggregations of the metal from mobile condensed atoms. This latter process is discussed in connection with the investigation of the photoelectric emission and electric conductance of bismuth films deposited under a variety of conditions.[4]

The senior author (A. H. W.) gratefully acknowledges the donation of some of the apparatus by Rev. T. H. Love, S. J., President of Saint Joseph's College in Philadelphia.

Electrical Conductance and Photoelectric Emission of Thin Bismuth Films

ALFRED H. WEBER AND DAVID F. O'BRIEN, S. J.
Department of Physics, Saint Louis University, St. Louis, Missouri

(Received August 27, 1941)

The electrical conductance and photoelectric emission of bismuth films on Pyrex have been simultaneously measured as functions of average film thickness. The films, evaporated always at the rate of 1.11 atom layers min.$^{-1}$ in vacuum, were condensed under three different conditions; continuously at liquid-air temperature, discontinuously at room temperature and continuously at room temperature. For all films the conductance and photoelectric emission increase abruptly and nearly together at some film thickness dependent on the temperature of condensation and aging of the film. The agglomeration of mobile condensed atoms satisfactorily explains the results but the process is complex with the condition of the backing surface a likely influencing factor. No photoconductive effect was observed for room temperature or liquid-air temperature deposited films whether aged or unaged. Various experiments on the variation of conductance *versus* temperature are in agreement with the results of Fukuroi.

PREVIOUS experiments[1,2] with aged bismuth films evaporated in high vacuum on glass at room temperature have shown that the photoelectric emission and the corresponding photoelectric threshold wave-length of these metal films increases abruptly in the region of 0–150 atom layers film thickness. The experiments described in this paper were undertaken to investigate further the properties of these bismuth films and to correlate possibly the observed changes in photoelectric emission and threshold wave-length with other electrical properties of the films.

Experiments on the electrical conductance of metallic films have been extensive. Two recent papers[3,4] in this journal give adequate discussions of and references to the pertinent literature. In the interpretation of the complex results it is helpful to consider the many experiments in three categories: (1) conductance *versus* film thickness at a fixed temperature; (2) conductance *versus* aging time at fixed temperature and film thickness; (3) conductance *versus* temperature at a fixed film thickness.

Concerning the more specific subject of the present paper, conductance and photoelectric emission of metal films, there appears to be little in the literature. Maciuc[5] finds that the logarithms of the photoelectric emission and conductance of very thin potassium films on glass both increase in proportion to the number of atoms deposited, results similar to those reported here for bismuth. Fukuroi[6] attempts to correlate his own experiments on the photoconductivity of mercury films of varying thickness deposited on glass with those of Roller, Jordan and Woodward[7] on the photoelectric emission of such films are not conclusive since the experiments were performed by different workers on films deposited under different conditions. The

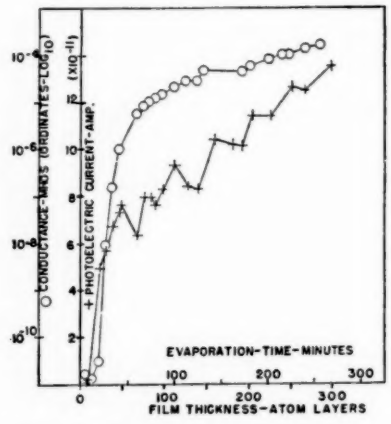

FIG. 1. Variation of electrical conductance and photoelectric emission with average film thickness during *continuous evaporation* of bismuth at 603°C and *condensed at liquid-air temperature* (measured usually as −174.6°C).

[1] A. H. Weber, Phys. Rev. **53**, 895 (1938).
[2] A. H. Weber and L. J. Eisele, this issue, preceding article.
[3] H. R. Mitchell, Phys. Rev. **53**, 250 (1938).
[4] M. G. Foster, Phys. Rev. **57**, 42 (1940).
[5] G. Maciuc, Bull. Soc. Roumaine de Phys. **40**, 3 (1939).
[6] T. Fukuroi, Sci. Pap. Institute Phys. Chem. Research **32**, 187 (1937).
[7] D. Roller, W. H. Jordan and C. S. Woodward, Phys. Rev. **38**, 396 (1931).

simultaneous measurement of electrical conductance and photoelectric emission of the same bismuth film is an important characteristic of the experiments here described.

Apparatus

The experimental tube used in this work has been described.[2] The outgassing of the tube, the maintenance of the high vacuum and the measurement of the photoelectric currents were accomplished as in the earlier investigations.[1,2] Film conductances were obtained by measuring the current through the film with a known voltage across the film. Average film thicknesses were determined by the usual effusion method following the determination of the vapor pressure of bismuth.[8]

Results and Discussion

Figures 1–3 show the results of the experiments on the electrical conductance and photoelectric

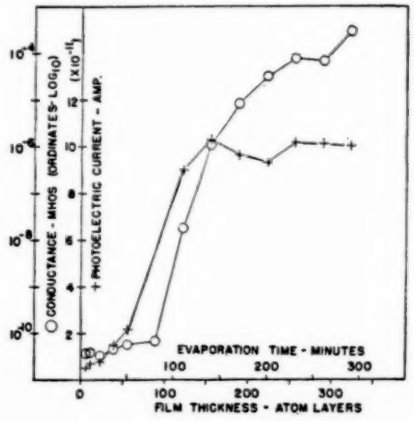
CONDUCTANCE - MHOS (ORDINATES - LOG10)
+ PHOTOELECTRIC CURRENT - AMP. (X10⁻¹¹)
EVAPORATION TIME - MINUTES
FILM THICKNESS - ATOM LAYERS

Fig. 2. Variation of electrical conductance and photoelectric emission with average film thickness for *stable* bismuth films (aged, after interrupting evaporation, for periods usually 40–60 minutes) *condensed at room temperature.* Evaporation temperature 603°C. Total time to obtain data; approximately 7 days.

emission of the bismuth films as functions of the film thickness under various conditions specified by the accompanying legends. The photoelectric currents and conductances were measured as nearly simultaneously as possible; usually about a minute separated the two readings. For all data the rate of evaporation was 1.11 atom layers min.$^{-1}$.

It is observed that abrupt increases in conductance and photoelectric emission occur, nearly together (i.e., at about the same film thickness) for each of the three films and that the thickness at which the sudden increase in the two properties takes place depends on the temperature of deposition of the film and the aging of the film. For the liquid-air temperature

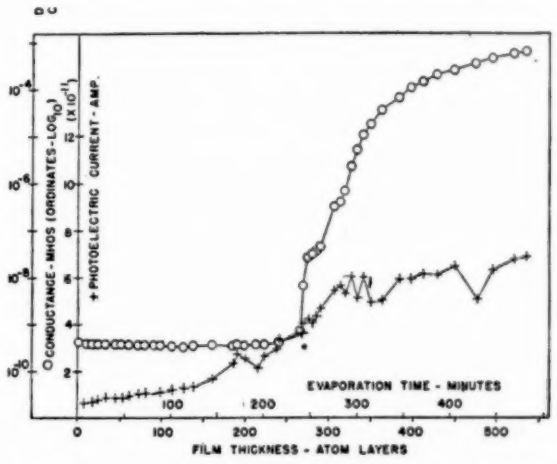
CONDUCTANCE - MHOS (ORDINATES - LOG10)
+ PHOTOELECTRIC CURRENT - AMP. (X10⁻¹¹)
EVAPORATION TIME - MINUTES
FILM THICKNESS - ATOM LAYERS

Fig. 3. Variation of electrical conductance and photoelectric emission with average film thickness during *continuous evaporation* of bismuth at 603°C and *condensed at room temperature.*

condensed film (Fig. 1) the two electrical properties show the abrupt increase at a much smaller film thickness (about 25 atom layers) than is the case for the room temperature condensed films (about 100 atom layers in Fig. 2, about 260 atom layers in Fig. 3). Also, the stable (aged) film, Fig. 2, exhibits the increase for a smaller thickness than the unstable (unaged) film, Fig. 3.

The experiments[2] on the photoelectric threshold of aged bismuth films deposited at room temperature show that a definite shift of the threshold wave-length toward the red occurs simultaneously with the increase in photoelectric current. Thus the three characteristics of the film, photoelectric threshold, photoelectric current and electrical conductance, are interrelated and dependent on the film thickness.

The essential features of Figs. 1–3 find an obvious explanation in the agglomeration and crystallization processes proposed by many workers. According to this explanation at least

[8] A. H. Weber and S. C. Kirsch, Phys. Rev. **57**, 1042 (1940).

some of the atoms condensed on the glass are mobile and tend to collect in groups unless this aggregation is inhibited by low temperature. The rate of aggregation is dependent in a complex way on many factors (temperature of condensation surface, condition of condensation surface including the extent of its outgassing, rate and temperature of evaporation of atoms, whether metal is deposited continuously or in successive aged layers, etc.). Thus Fig. 1 indicates little agglomeration because of the low temperature, hence there is little "cracking" of the film and conductance and photoelectric emission increase rapidly with the arrival of more and more atoms. From Fig. 2 it is concluded that the agglomeration process has been completed practically for each aged layer since both conductance and photoelectric current increase more gradually with film thickness than in Fig. 1.

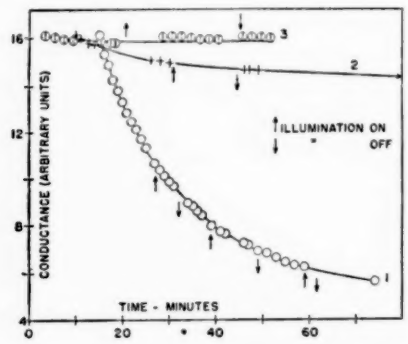

FIG. 4. Variation of electrical conductance with aging time (during which deposition is interrupted) for bismuth films of Fig. 2 with and without illumination (the 2537A mercury radiation confined to a central circular film area of about 3.35 mm diameter; dimensions of film between electrodes about 0.5 cm×1 cm). Corresponding average film thickness in atom layers for the curves: 1, 122; 2, 157; 3, 221. Zero time indicates instant of interruption of evaporation. The curves were adjusted to start at the same ordinate value. Curve 2 has an ordinate value of 13.75 at 147 min.

The fact that the aged film (Fig. 2) shows the increase in the measured properties for a thinner film than the unaged film (Fig. 3) seems anomalous at first since almost all workers report a diminution in conductance with aging time. (This tendency towards decay of conductance with aging time was observed for thinner films in the present experiments, see Fig. 4.) It is concluded, however, that the generally higher conductance and photoelectric current at a given film thickness observed in Fig. 2 in comparison with Fig. 3 are due to some complicating effect. There is evidence that the condition of the backing surface, which was subjected to repeated outgassing when removing the bismuth between experiments on different films, may have influenced the agglomeration process; for the initial conductance of Fig. 3 is about 10 times the initial conductance of Fig. 2 and it was observed in general that, though the glass backing surface was carefully and vigorously heated, the initial conductance of each successive freshly deposited film was higher than for its predecessor. It appears then that the repeated outgassing of the glass plus some possible permanent absorption of bismuth atoms by this surface gradually changes the condition of the deposition surface until there is present a substratum conduction layer existing in the backing surface under the newly condensed bismuth films. Such a backing surface would exhibit the initial conductance of Fig. 3 and could readily influence the formation of the condensing bismuth film so that it would exhibit the delayed increase in conductance and photoelectric current observed. Such an hypothesis is supported also by Fig. 5 of reference 1 which shows a gradual decrease of photoelectric emission with successive bismuth deposits on the same backing surface.

Finally, if a substratum conduction layer exists, it has more effect ultimately on the photoelectric emission than on the conductance of the film, for the conductance curves of Figs. 2 and 3, once the rapid increase has begun, have the same shape, very nearly, which means that the addition of the same number of atom layers to the thickness at which the conductance starts its rapid increase produces the same change in conductance for the two films. This is not so for the photoelectric emission. The smaller photoelectric currents of Fig. 3 may result from a process by which electrons, released photoelectrically, instead of reaching the anode of the tube merely pass from one point to another of the film and so are not registered in measuring the photoelectric current. Fukuroi[6] suggests a very similar explanation in discussing the photoconductivity of mercury films on glass.

Figure 4 shows that the conductance of room temperature deposited films decays with aging

time in general (in agreement with almost all reported work with various metal films) but that this effect diminishes rapidly with increasing film thickness. Figure 4 indicates also that the illumination used has no effect measurable with the circuit used (minimum measurable conductance change about 10^{-11} mho) on the normal rate of decay of conductance. Measurements of the dark conductance and the photoconductance of a film continuously deposited at liquid-air temperature, made with the same illumination as for the films of Fig. 4, showed no difference measurable with the circuit employed for film thicknesses between 20 and 260 atom layers.

The variation of the conductance with temperature of a bismuth film at three thicknesses is illustrated by Fig. 5. The films were deposited at liquid-air temperature and the conductance was measured as they warmed up to room temperature. Logarithmic ordinates are used to bring the three curves on a single figure. It is observed that the conductance passes through a maximum in each case, that the maximum occurs at about -25°C in each case, and that the maximum is more pronounced the thinner the film. A "transformation temperature," at which the conductance increases suddenly and irreversibly, is observed for the thinnest film and in a much less marked manner for the other two thicknesses (the conductance of the thinnest film increases about 13-fold between -124 and -83°C). The transformation temperature (as indicated very approximately by the vertical arrows under each curve) is between -125 and -75°C and appears to move closer to 0°C with increasing film thickness in agreement with Fukuroi.[9] For the thickest film the change of conductance with temperature is much more gradual so that a definite transformation temperature no longer really exists.

The solid curves of Fig. 5 are irreversible, that is they are observed only if the film is formed at low temperature and then allowed to heat up.

TABLE I. *Average temperature coefficient of resistance* α, *for film of Fig. 5.*

Curve 1, film thickness 29 atom layers, $\alpha_{20.5°C} = -0.0067$/°C
Curve 2, film thickness 61 atom layers, $\alpha_{20.4°C} = -0.0072$/°C
Curve 3, film thickness 112 atom layers, $\alpha_{20.2°C} = -0.0083$/°C

If the film is deposited at room temperature and then is cooled to liquid-air temperature a reproducible temperature-resistance effect is found as indicated in Fig. 5 by the dashed straight lines connecting the points of highest and lowest temperature on each curve. The end points of the dashed lines represent a negative temperature coefficient of resistance (see Table I) which increases slightly (in a negative sense) with increasing film thickness. Table I gives the

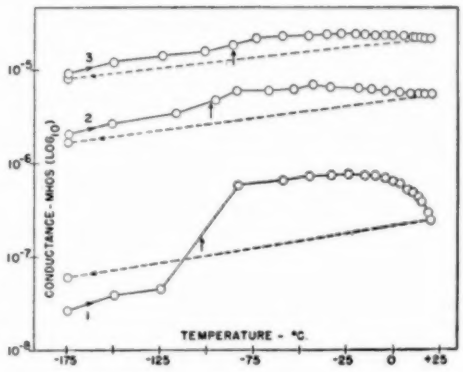

FIG. 5. Variation of electrical conductance with temperature of a liquid-air deposited film at 3 thicknesses (average thickness in atom layers for the curves: 1, 29; 2, 61; 3, 112). The order of measurement of conductances is indicated by the arrows on the curves; the point on the solid lines for the lowest temperature is for the first observation in each case.

average temperature coefficient of resistance for unaged films. The coefficient measured for a room temperature deposited aged film of 122 atom layers thickness for the same temperature range as Table I was -0.012/°C. Lane[10] reports for bismuth films an average value of -0.01/°C for $\alpha_{20°C}$ for the same temperature range as the present experiments.

The behavior exhibited by Fig. 5 may be explained by assuming that for temperatures below the transformation temperature the bismuth film is fairly continuous in structure. With rising temperature the conductance increases probably as a result of a combination of causes. Increase of mobility of the condensed atoms with increasing temperature would at the lower temperatures increase both electronic conduction, by shortening of any gaps in the metal film, and ionic conduction. At or around the trans-

[9] T. Fukuroi, Sci. Pap. Inst. Phys. Chem. Research **32**, 196 (1937).

[10] C. T. Lane, Phys. Rev. **48**, 193 (1935).

formation temperature (the experimental data are not sufficient to determine whether the transformation temperature is ever unique and critical or includes always a span of a number of degrees) a rapid increase in mobility with resultant aggregation of atoms takes place which produces a discontinuous, patch structure of the film. This film then exhibits a decrease in conductance with further temperature (and mobility) increase. The last-mentioned decrease of conductance with increasing temperature is transient; a stable (aged) film in which the agglomeration process has been completed exhibits a negative temperature coefficient of resistance as would be expected for a discontinuous structure. Fukuroi[9] gives a somewhat detailed discussion of the transformation temperature.

A few tests were made of the dependence of the conductance on the voltage applied to the film in measuring the conductance. For the thinner films an increase in conductance with applied voltage was observed in agreement with Foster's[4] results with lead films but this effect disappeared with increasing film thickness and the aged room temperature deposited film of Fig. 2 at 146 atom layers thickness showed no measurable variation of conductance with applied voltage. These results very obviously agree with the agglomeration process explanation since a discontinuous (thinner) film would be expected to exhibit a conductance which is voltage dependent because of the presence of gaps whereas a film approaching bulk metal structure (thicker film) would not.

OCTOBER 15, 1941 PHYSICAL REVIEW VOLUME 60

Exchange Forces Between Neutral Molecules and a Metal Surface*

W. G. POLLARD
University of Tennessee, Knoxville, Tennessee
(Received July 21, 1941)

A Heitler-London treatment of the exchange part of the mutual energy of a neutral atom and a metal is developed. The resulting interactions are evaluated on the basis of a simplified model of the metal and lead to a convenient and simple expression for the total exchange energy. In Section III this expression is applied to the interaction of H_2 and He with metals where it is found to represent a repulsion. By adding this exchange interaction to the attractive van der Waals interaction between the molecule and the metal, a potential curve of the usual type possessing a minimum is obtained for each system. The depths of these minima are compared with observed heats of van der Waals adsorption. A discussion is given in an appendix of the effects of some of the simplifications and approximations employed.

AT large distances from a solid surface, the mutual energy between an atom or molecule and the solid is predominantly determined by dispersion forces. These forces give rise to the usual $1/R^6$ van der Waals law for the interaction between an element of the solid and the molecule. Summation of this potential over all elements of the solid then leads to a mutual energy decreasing as the inverse third power of the normal distance between the surface and the molecule. This interaction was the subject of study in a previous paper.[1]

At closer distances the shorter range exchange interaction becomes important. For neutral molecules and rare gas atoms this represents a repulsion and its composition with the van der Waals interaction determines a minimum energy from which numerical values for the heat of physical adsorption can be inferred. This interaction is the subject of investigation here. A Heitler-London

* A preliminary report on some of the work presented here was given at the Washington Meeting, April, 1939.

[1] H. Margenau and W. G. Pollard, Phys. Rev. **60**, 128 (1941).

treatment is developed and the exchange part of the resulting expression is evaluated approximately for a simple free electron model of a metal.

The calculation of the total potential curve for a molecule near a solid surface, which is contemplated here for metals, has been performed fairly adequately in the case of adsorption on ionic crystals.[2] In such problems it is proper to express the interaction of the molecule with the whole crystal as a sum of the interactions with individual ions in it. Such individual interactions can be fairly accurately represented by simple formulae and the summation can be performed without too great difficulty in terms of the known structure of the crystal. These calculations lead to results which show excellent agreement with experimentally determined heats of adsorption at low temperatures. The procedure employed in them is, however, inappropriate for adsorption on metals since interactions with the outer shell electrons of an isolated metal atom would become radically altered when the atom became bound in the metallic state.

I. Heitler-London Treatment

The visiting atom is represented by a core of charge $+e$ above the surface at a point $\mathbf{r}_A$, and an electron with positional coordinate $\mathbf{r}_a$, spin coordinate s_a, and wave function $(c_+\alpha(s_a)+c_-\beta(s_a))\psi(\mathbf{r}_a)$. In the solid we take atomic cores of charge $Z_J e$ at points $\mathbf{r}_J$ together with electrons at points $\mathbf{r}_j$ with wave functions $u_i(\mathbf{r}_j)(i,j=1,2,\cdots N)$ and spin functions $\alpha(s_j)$ or $\beta(s_j)$. The best antisymmetric wave function of these electrons in the product of individual functions approximation is the familiar determinant

$$\Phi=\frac{1}{(N!)^{\frac{1}{2}}}\begin{vmatrix} u_1(\mathbf{r}_1)\alpha(s_1), & \cdots, & u_n(\mathbf{r}_1)\alpha(s_1), & u_{n+1}(\mathbf{r}_1)\beta(s_1), & \cdots, & u_N(\mathbf{r}_1)\beta(s_1) \\ \cdot & & \cdot & \cdot & & \cdot \\ \cdot & & \cdot & \cdot & & \cdot \\ \cdot & & \cdot & \cdot & & \cdot \\ \cdot & & \cdot & \cdot & & \cdot \\ u_1(\mathbf{r}_N)\alpha(s_N), & \cdots, & u_n(\mathbf{r}_N)\alpha(s_N), & u_{n+1}(\mathbf{r}_N)\beta(s_N), & \cdots, & u_N(\mathbf{r}_N)\beta(s_N) \end{vmatrix}. \tag{1}$$

The terms have been arranged so that the first n electrons have positive and the next $N-n$ have negative spin functions.

The system solid+atom has $N+1$ electrons which must be described as a single system by a wave function completely antisymmetric in the $N+1$ positional and spin coordinates. Since the spin function of the electron in the visiting atom is represented as a linear combination of the eigenfunctions α and β of the solid, the wave function for the whole system may be taken to be the same linear combination of the two functions

$$\Psi_1=\frac{1}{(N+1)^{\frac{1}{2}}}\begin{vmatrix} \psi(\mathbf{r}_1)\alpha(s_1), & & \\ & & \\ & \Phi & \\ & & \\ \psi(\mathbf{r}_N)\alpha(s_N), & & \\ \psi(\mathbf{r}_a)\alpha(s_a), & u_1(\mathbf{r}_a)\alpha(s_a) & \cdots \quad u_N(\mathbf{r}_a)\beta(s_a) \end{vmatrix} \tag{2}$$

and the function Ψ_2 which is obtained from Φ in the same way except that it is bordered on the right with $\psi(\mathbf{r}_i)\beta(s_i)$.

[2] J. E. Lennard-Jones and B. M. Dent, Trans. Faraday Soc. **24**, 100 (1928); F. V. Lenel, Zeits. f. physik. Chemie **B23**, 379 (1933); J. K. Roberts and W. J. C. Orr, Trans. Faraday Soc. **34**, 1346 (1938); W. J. C. Orr, Proc. Roy. Soc. **A173**, 354 (1939).

The Hamiltonian of this system is given by

$$H=-\frac{h^2}{2m}\nabla_a{}^2-\frac{h^2}{2m}\sum_i{}'\nabla_i{}^2+\tfrac{1}{2}\sum_{J,L}{}'\frac{Z_JZ_Le^2}{r_{JL}}+\sum_L\frac{e^2}{r_{AL}}-\sum_{J,k}{}'\frac{Z_Je^2}{r_{Jk}}-\sum_J\frac{Z_Je^2}{r_{Ja}}$$
$$-\sum_k{}'\frac{e^2}{r_{Ak}}-\frac{e^2}{r_{Aa}}+\tfrac{1}{2}\sum_{jk}{}'\frac{e^2}{r_{jk}}+\sum_j{}'\frac{e^2}{r_{aj}}. \quad (3)$$

The wave function for the whole system is taken to be

$$\Psi=c_+\Psi_1+c_-\Psi_2,$$

where c_+ and c_- depend on the spin function of the electron in the visiting atom. The total energy of the system is given by

$$E=\langle H\rangle_{Av}=\int\Psi^*H\Psi d\tau\Big/\int\Psi^*\Psi d\tau. \quad (4)$$

The determinant (2) was expanded by minors of the bordered row and column and substituted with (3) in Eq. (4). After summation over spins is carried out in the result it is found that the cross product terms between Ψ_1 and Ψ_2 vanish and the terms in $\Psi_1{}^*\Psi_1$ and $\Psi_2{}^*\Psi_2$ are identical except that the exchange summations in the former which ran from 1 to n are replaced in the latter by summations from $n+1$ to N. Thus the exchange terms refer only to those electrons in the solid having the same spin as that of the electron in the visiting atom. No loss in generality is involved in taking $c_+=1$, $c_-=0$ since expressions for arbitrary c_+ and c_- can always be obtained simply by replacing each

$$\sum_1^n \text{ by } |c_+|^2\sum_1^n+|c_-|^2\sum_{n+1}^N.$$

The evaluation of the total energy (3) is rather involved but quite straightforward. The results are best exhibited in terms of the following expressions

$$f(\mathbf{r}_1,\mathbf{r}_2)=\sum_{i=1}^n u_i{}^*(\mathbf{r}_2)u_i(\mathbf{r}_1), \quad (5a)$$

$$\Delta^2=\int\int\psi^*(1)\psi(2)f(1,2)d\tau_1d\tau_2, \quad (5b)$$

$$K_1=e^2\int\int\frac{\psi^*(1)\psi(2)f(1,2)}{r_{A1}}d\tau_1d\tau_2, \quad (5c)$$

$$K_2=e^2\int\int\frac{\psi^*(1)\psi(2)f(1,2)}{r_{12}}d\tau_1d\tau_2, \quad (5d)$$

$$K_3=e^2\int\int\int\frac{\psi^*(1)\psi(2)f(3,2)f(1,3)}{r_{13}}d\tau_1d\tau_2d\tau_3, \quad (5e)$$

$$G=e\int\int\psi^*(1)\psi(2)f(1,2)\phi(2)d\tau_1d\tau_2, \quad (5f)$$

where ϕ represents the electric potential of the solid

$$\phi(\mathbf{r})=\sum_J\frac{Z_Je}{|\mathbf{r}_J-\mathbf{r}|}-e\int\frac{\sum_{i=1}^N|u_i(\mathbf{r}')|^2}{|\mathbf{r}'-\mathbf{r}|}d\mathbf{r}'. \quad (6)$$

A number of other terms which are of order (surface area of crystal)$^{-1}$ compared with these appear but they were neglected.

The exchange part of the contribution to the total energy (4) representing an interaction between the visiting atom and the solid has the form

$$A(\mathbf{r}_A)=(G+K_1-K_2+K_3)/(1-\Delta^2).$$

The potential ϕ, Eq. (6), arises from the surface double layer and from the polarization of the solid by the visiting atom. In the simplified model used to evaluate this interaction in the next section, both these effects are neglected so that in this approximation the term G vanishes. From a consideration of the relative magnitudes of the various terms when such effects are included, it appears that the term is negligible compared with the others in any case. Thus we may write approximately

$$A(\mathbf{r}_A)=(K_1-K_2+K_3)/(1-\Delta^2). \tag{7}$$

For the case in which the $u_i(\mathbf{r})$ are represented by plane wave functions, the function $f(1, 2)$ defined in Eqs. (5) has been evaluated by Wigner and Seitz.[3] In this case it is a function only of the distance r_{12} between points 1 and 2 and has the form

$$f(1, 2)=3\left(\frac{n}{V}\right)\frac{\sin\xi-\xi\cos\xi}{\xi^3}, \tag{8}$$

where $\xi=k_m r_{12}=[6\pi^2(n/V)]^{\frac{1}{3}}r_{12}$. This function has the value n/V at $\xi=0$ and at large ξ falls off as $1/\xi^2$. The total number of electrons represented by the density f is $\int f(1, 2)d\tau_{12}$. This integral is unfortunately indeterminate but since the function is multiplied in all the interactions (5) by functions of exponentially decreasing character, it seems proper for the present purpose to represent this number as

$$\lim_{c\to 0}\int e^{-cr_{12}}f(1, 2)d\tau_{12}$$

which is equal to unity.

The function $f(1, 2)$ is closely connected with the function $g(1, 2)$ in the expression

$$\rho(1, 2)=\rho(1)\rho(2)[1-g(1, 2)]$$

for the density of particles 1 and 2 in terms of their individual densities. The relation between them is

$$g(1, 2)=\tfrac{1}{2}[f(1, 2)/(n/V)]^2. \tag{9}$$

The properties of this function have been extensively studied by Wigner and Seitz[3] and we may use their results to obtain an interpretation of the role of f in the exchange interactions (5). Each electron in the solid whose spin is the same as that in the visiting atom is surrounded with a "hole" in the total distribution of electrons of like spin. The exclusion of charge from this hole becomes complete as the point occupied by the electron is approached and the total charge excluded is just equal to that of the central electron. The function f represents the density of this excluded charge. The manner in which the excluded density falls off with r_{12} is, however, incorrectly given by (8) as pointed out by Bardeen.[4] In the actual case it must still be n/V for $r_{12}=0$ but should fall off much more rapidly, presumably exponentially, at large r_{12} because of the screening of the field of the central electron by the others in its neighborhood. The total number of electrons excluded must of course in any case be unity.

II. Approximate Calculation for a Metal

In this section a highly simplified and perhaps rather crude evaluation of the interactions in Eqs. (5) will be presented. The method is based on certain approximations, the first of which consists of substituting for the function $f(1, 2)$ a rectangular hole which is such that each of the n metal electrons of the same spin as the visitor is assigned a volume V/n within which the density of electrons of this spin is zero and outside of which it has its normal value n/V. In this scheme the density of the excluded electrons is given by

$$\begin{aligned} f(1, 2)&=n/V, \quad r_{12}\leqslant\rho_s,\\ &=0, \quad r_{12}>\rho_s, \end{aligned} \tag{10}$$

where $\rho_s=2^{\frac{1}{3}}r_s$ is the radius of a sphere (of volume V/n) containing one metal electron of given spin.

[3] E. Wigner and F. Seitz, Phys. Rev. **46**, 509 (1934).

[4] J. Bardeen, Phys. Rev. **58**, 727 (1940).

TABLE I. *Values and positions of the minima in the potential energy curves for the van der Waals adsorption of* He *and* H_2 *on metals having various values of* r_s.

	He				H_2			
	$-W_m$				$-W_m$			
r_s cm $\times 10^8$	Electron Volts $\times 10^3$	Calories per Mole	D_m cm $\times 10^8$	$\frac{D_m}{\rho_s}$	Electron Volts $\times 10^3$	Calories per Mole	D_m cm $\times 10^8$	$\frac{D_m}{\rho_s}$
1.0	33.0	765	1.9	1.5	38.0	865	2.3	1.8
1.5	14.0	325	2.3	1.2	32.0	730	2.7	1.4
2.0	6.1	140	3.0	1.2	16.0	375	3.3	1.3
2.5	3.0	68	3.7	1.2	8.6	200	3.8	1.2
3.0	1.6	37	4.3	1.2	4.8	110	4.6	1.2

A substitution similar to this of the rectangular for the plane wave form of "hole" has been employed with good success in discussing the cohesive energy of solids.[5] Further consideration of the effect of its use in the present problem is deferred to Section **b** of the Appendix.

The presence of the function (10) in all of the integrals of Eqs. (5) confines the variables $\mathbf{r}_1$ and $\mathbf{r}_2$ to the range $|\mathbf{r}_1-\mathbf{r}_2| \leqslant \rho_s$. When the visiting atom is far from the surface of the metal, both r_{A1} and r_{A2} will be large enough to permit the use of an approximate expansion of r_{A2} in the form

$$r_{A2}=r_{A1}-r_{12}\cos\theta, \tag{11a}$$

where θ is the angle between $\mathbf{r}_{A1}$ and $\mathbf{r}_{12}$. When this is the case it will often be possible to write the wave function of the electron in the visiting atom in the form

$$\psi(2)=\psi(1)\varphi(r_{12}), \tag{11b}$$

which will be valid in this confined region. This procedure may seem inappropriate to the present calculations because the magnitude and behavior of the exchange energy is of greatest interest close to the surface in the region where this approximation is invalid. However, as will be seen, in the case of van der Waals adsorption the minimum in the total potential energy curve will often fall at a great enough distance from the surface to make its use allowable and it is to such cases that the results obtained must be confined. The approximation is discussed further in Section **c** of the Appendix.

If one makes use of (9) and (10) the various terms in Eqs. (5) become

$$\begin{aligned}\Delta^2&=p(\rho_s)F(D),\\ K_1&=e^2p(\rho_s)G(D),\\ K_2&=e^2q(\rho_s)F(D),\\ K_3&=e^2p(\rho_s)q(\rho_s)F(D),\end{aligned} \tag{12}$$

where

$$\begin{aligned}F(D)&=\int_M|\psi(r_{A1})|^2d\tau_1,\\ G(D)&=\int_M|\psi(r_{A1})|^2d\tau_1/r_{A1},\\ p(\rho_s)&=(n/V)\int_s\varphi(r_{12})d\tau_{12},\\ q(\rho_s)&=(n/V)\int_s\varphi(r_{12})d\tau_{12}/r_{12},\end{aligned} \tag{13}$$

and the regions of integration denoted by M and s are defined as follows: The region s is the sphere of radius ρ_s about the point $\mathbf{r}_1$ as center within which the function $f(1, 2)$ defined by Eq. (10) has non-zero values. The region M is the region occupied by the metal and is taken of infinite extent in the x and y directions and extending in the z direction from $z=D$ to $z=\infty$. Substituting the expressions (12) in Eq. (7) we obtain for the total exchange interaction

$$\begin{aligned}A(\rho_s, D)&=e^2[p(\rho_s)G(D)\\ &+q(\rho_s)(p(\rho_s)-1)F(D)]/[1-p(\rho_s)F(D)].\end{aligned} \tag{14}$$

In case the wave function in the visiting atom can be represented by a 1*s* function of the form

[5] J. C. Slater, Rev. Mod. Phys. **6**, 209 (1934).

$\psi=[1/(\pi a^3)^{\frac{1}{2}}]e^{-r/a}$, the use of Eq. (11a) leads to

$$\psi(r_{A2})=[1/(\pi a^3)^{\frac{1}{2}}]e^{-(r_{A1}-r_{12}\cos\theta)/a},$$

so that, comparing with Eq. (11b), we have

$$\varphi(r_{12})=e^{(r_{12}/a)\cos\theta}.$$

If these functions are substituted into Eqs. (13) the resulting integrals are easily evaluated and lead to the results

$$\begin{aligned}
&F(D)=\tfrac{1}{2}(1+D/a)e^{-2D/a},\\
&G(D)=(1/2a)e^{-2D/a},\\
&p(\rho_s)=3[(\rho_s/a)\cosh(\rho_s/a)-\sinh(\rho_s/a)]/(\rho_s/a)^3,\\
&q(\rho_s)=(3/a)[\cosh(\rho_s/a)-1]/(\rho_s/a)^3.
\end{aligned}\tag{15}$$

III. Adsorption of He and H_2 on Metals

The total exchange interaction of both electrons in He and in H_2 will be twice that for one of them when the metal contains equal numbers of both spin varieties and when the distance from the metal is large enough to make the double exchange integrals negligible. In the van der Waals case, and particularly in all cases to which the approximation (11) is applicable, the latter condition is fulfilled. For both gases single particle $1s$ functions are used here to describe each of the two electrons. The parameter a in this function may be chosen either from an examination of more elaborate variational wave functions for these systems or from their diamagnetic susceptibilities χ and atomic polarizabilities α calculated on the assumption of $1s$ functions. From the latter method we obtain

$$a\leqq[-mc^2\chi/N_0e^2]^{\frac{1}{3}}\leqq[\hbar^2\alpha/8me^2]^{\frac{1}{3}}.\tag{16}$$

For He the form of the variational wave function gives $a=0.59a_0$ while from Eq. (16) we get $a=0.64a_0$. In these calculations the value $a=0.62a_0$ was used for He. In the case of H_2, the wave function around each nucleus is best approximated by a $1s$ function with $a=0.84a_0$. But since the nuclei are $1.4a_0$ apart, the resulting configuration is more or less that of a spheroid with major and minor semi-axes $1.54a_0$ and $0.84a_0$. If a is determined from the radius of a sphere whose volume is equal to that of this spheroid, it should be $1.03a_0$. From Eq. (16) we get $a=0.91a_0$. The value $a=0.95a_0$ was used in these calculations for H_2.

In order to obtain the total potential energy of the system in the field of the metal surface, the potential of the attractive forces must be added to the exchange term. These forces are, of course, of the van der Waals type and so occur only in second order. The validity of adding first-order exchange forces to second-order dispersion forces has been investigated by Margenau[6] who finds for the He−He potential that no great error is involved because the contribution from exchange in second order is negligible in the neighborhood of the minimum. Presumably it would also be small in this case and well within the limits of accuracy of Eqs. (14) and (15). The particular form of van der Waals potential used in these calculations was that obtained by Margenau and Pollard.[1]

On adding the exchange potential $A(\rho_s, D)$ of Eq. (14) computed with the functions of Eqs. (15) to the van der Waals potential $W(r_s, D)$ of reference 1, curves possessing minima of the usual type are obtained. In Table I the depths of these minima, W_m, and the corresponding distances D_m at which they occur are shown for He and H_2 at various values of r_s. The ratio D_m/ρ_s of this equilibrium distance to the radius of the sphere in the metal to which the vector r_{12} is confined is also shown. In order for the approximation of Eq. (11) to be valid, this ratio should be large; a condition which unfortunately is not very well fulfilled. This situation will be discussed further in the appendix where it will be shown that the results in Table I are somewhat more reliable for small r_s than this indicates.

The minimum energies expressed in calories per mole are also tabulated in Table I and may be compared roughly with observed heats of adsorption at low temperatures. Such a comparison neglects the vibrational energy of the adsorbed molecule but this will be smaller than the limits of accuracy of the present treatment. Very little experimental data relevant for this comparison is available. Since a large number of investigations of the adsorption of gases on metals have been made (most of them concerning "activated" adsorption or chemisorption), this

[6] H. Margenau, Phys. Rev. **56**, 1000 (1939).

situation suggests that the binding forces in van der Waals adsorption of H_2 and He on metals are very weak; a condition reflected by the results in Table I. Only one case suitable for comparison with the present results has been found. This is a measurement of the heat of adsorption of H_2 on Ni at 20°K by Eucken and Hunsman.[7] They obtain values of 1200 cal./mole in the initial stages of adsorption which decrease to 400 in the final stages. They give 800 cal./mole as a mean value. With $r_s=1.38$ for Ni, a potential curve for H_2 having a minimum of 0.032 electron volts per molecule corresponding to a heat of adsorption of 795 cal./mole is obtained.

It is of interest to note here the order of magnitude of the heats of van der Waals adsorption of He and H_2 on non-metals. For H_2 it is 1100 cal./mole on Acheson graphite[8] and varies from 1300 to 1700 cal./mole on various charcoals.[9] For He a value of about 140 cal./mole is given by Stout and Giauque[10] for the heat of adsorption on $NiSO_4\cdot 7H_2O$ at 4°K. These values are comparable with those in Table I for metals.

In conclusion I wish to express my gratitude to Professor Henry Margenau for his continued interest in this work and for a very helpful criticism of the manuscript.

Appendix

The evaluation of the exchange integrals (5) which is performed in Section II is based on several approximations and simplifications which are in need of some justification.

Table II. *Values of the coefficients $M(\rho_s)$ and $N(\rho_s)$ in Eq. (21) showing the effect of the modification (a) on the exchange interaction.*

ρ_s/a	$f(1,2)$ FROM EQ. (10) $M(\rho_s)$	$N(\rho_s)$	$f(1,2)$ FROM EQ. (20) $M(\rho_s)$	$N(\rho_s)$
1.5	0.34	0.065	0.088	−0.021
3.0	0.17	0.062	0.011	−0.0023
6.0	0.12	0.090	0.00027	−0.000039
12.0	1.34	1.35	0.000011	−0.000001

Some of the aspects of the problem which seem to require the most attention may be listed as follows: (a) The metal wave functions $u_i(r)$ obey boundary conditions at the surface so that all electronic densities are much smaller near the surface than in the body of the metal; (b) The use of the rectangular form, Eq. (10), of the function $f(1,2)$ may introduce considerable error when used in integration with an increasing function of r_{12}; (c) The approximation represented by Eq. (11) is valid only for reasonably large values of the ratio D_m/ρ_s. We consider these aspects separately.

a. Effect of boundary conditions on metal wave functions

This effect may be roughly accounted for by choosing the wave functions $u_i(r)$ for a region of constant potential within the metal bounded somewhat beyond its surface by a barrier of infinite height. If the z axis is chosen, as before, normal to the surface and the barrier is taken at $z=0$, the wave functions are given by

$$u_i(r)=(2/V)^{\frac{1}{2}}\sin kz e^{i(k_x x+k_y y)}, \tag{17}$$

where $k_x=2\pi\nu_x/L$, $k_y=2\pi\nu_y/L$, and $k=2\pi\nu/L$ with ν_x, ν_y taking all integral values and ν positive half integral values. If the positive ions in the metal are replaced by a uniform charge distribution of constant density extending from z_0 to infinity, the metal can be made electrically neutral by choosing $z_0=3\pi/8k_m$ where k_m is the maximum wave number in the Fermi distribution.[11] This gives rise to a surface double layer which produces a potential $\phi(z)$, Eq. (6). The resulting exchange interaction G, Eq. (5f), is, however, negligible compared with the others.

The density $f(1,2)$ computed with the wave functions (17) when there are equal numbers of both spins in the metal is given by [cf. Eq. (5a)]

$$\begin{aligned} f(1,2)&=\sum_{i=1}^{n} u_i^*(2)u_i(1)\\ &=[2V/(2\pi)^3]\int_0^{k_m}dk\int_0^{(k_m^2-k^2)^{\frac{1}{2}}}\kappa d\kappa\int_{-\pi}^{\pi}u_i^*(2)u_i(1)d\theta\\ &=(z_1^{\frac{1}{2}}z_2^{\frac{1}{2}}/2\pi\rho_{12})\int_0^{k_m}J_1[(k_m^2-k^2)^{\frac{1}{2}}\rho_{12}]\\ &\qquad\times J_{\frac{1}{2}}(kz_1)J_{\frac{1}{2}}(kz_2)(k_m^2-k^2)^{\frac{1}{2}}kdk \end{aligned}$$

with $\rho_{12}=[(x_1-x_2)^2+(y_1-y_2)^2]^{\frac{1}{2}}$. This integral may be evaluated[12] through the substitution $k=k_m\cos\theta$ with the result

$$f(1,2)=3\frac{n}{V}\left[\frac{\sin\xi-\xi\cos\xi}{\xi^3}-\frac{\sin\eta-\eta\cos\eta}{\eta^3}\right], \tag{18}$$

where $\xi=k_m r_{12}$ has the same meaning as before and $\eta=k_m[\rho_{12}^2+(z_1+z_2)^2]^{\frac{1}{2}}$. At $r_{12}=0$ the function is still equal to the density at the point r_1 but this is no longer n/V; it is replaced by

$$f(1,2)=3\frac{n}{V}\left[1-\frac{\sin 2k_m z_1-2k_m z_1\cos 2k_m z_1}{(2k_m z_1)^3}\right].$$

The density (18) integrates to a total excluded charge of

$$\int f(1,2)d\tau_{12}=(2/\pi)Si(k_m z_1), \tag{19}$$

where $Si(x)=\int_0^x \sin x dx/x$ denotes the integral sine function.

[7] A. Eucken and W. Hunsman, Zeits. f. physik. Chemie, **B44**, 163 (1939).
[8] R. M. Barrer, Proc. Roy. Soc. **A161**, 476 (1937).
[9] R. M. Barrer and E. K. Rideal, Proc. Roy. Soc. **A149**, 231 (1935).
[10] J. W. Stout and W. F. Giauque, J. Am. Chem. Soc. **60**, 393 (1938).
[11] J. Bardeen, Phys. Rev. **49**, 653 (1936).
[12] G. N. Watson, *Theory of Bessel Functions* (Cambridge, 1922), p. 377.

An indication of the effect of this form for $f(1, 2)$ on the results of the present calculation may be obtained by employing an approximation similar to (10) as follows:

$$f(1, 2) = (n/V)(2/\pi)Si(k_m z_1)h(z_1/\rho_s), \quad r_{12} \leqslant \rho_s$$
$$= 0, \quad r_{12} > \rho_s \tag{20}$$

where

$$h(z_1/\rho_s) = 4/[2+3(z_1/\rho_s)-(z_1/\rho_s)^3], \quad z_1 \leqslant \rho_s$$
$$= 1. \quad z_1 \geqslant \rho_s$$

The sphere of radius ρ_s about the point z_1 does not extend beyond the barrier and the purpose of the function $h(z_1/\rho_s)$ is to correct for that part of it which is cut off.

Equation (20) has been used in place of Eq. (10) to evaluate the interactions (5). In either case the total exchange energy (7) can be written as

$$A(\rho_s, D) = [M(\rho_s)+(D/a)N(\rho_s)]\exp[-(2D-\rho_s)/a]. \tag{21}$$

The coefficients M and N have been evaluated for several values of the quantity ρ_s/a with both forms of $f(1, 2)$ by numerical integration in this case and the results are given in Table II. It is clear that the introduction of metal wave functions obeying boundary conditions at the surface has a profound effect on the exchange interaction. If this effect were the only one operative, it would completely invalidate the results of Section III but as we shall see in what follows another equally strong effect is present which very nearly counteracts it.

b. Exponential form of $f(1, 2)$

As pointed out at the end of Section I in this paper and in reference 4, the correct form of $f(1, 2)$ should show an exponential decrease with r_{12} at large values. Deep in the body of the metal both of the plane wave forms of this function, Eqs. (8) and (18), are equivalent. In this region a simple function showing the same behavior as these for small r_{12} and representing the same total excluded charge but exhibiting the desired behavior at large r_{12} is given by

$$f(1, 2) = (n/V)[e^{-6.4r_{12}/\rho_s}+(6.4r_{12}/\rho_s)e^{-3.2r_{12}/\rho_s}]. \tag{22}$$

In any scheme employing the approximation of Eqs. (11), this function cannot be used for values of $\rho_s > 3$. The functions $p(\rho_s)$ and $q(\rho_s)$ as defined in Eqs. (13) on the basis of $f(1, 2)$ being given by Eq. (10) may be written for use with Eq. (22)

$$p(\rho_s) = \int \varphi(r_{12})f(1, 2)d\tau_{12}, \quad q(\rho_s) = \int \varphi(r_{12})f(1, 2)d\tau_{12}/r_{12},$$

where the integration now extends throughout space. These integrals are easily evaluated with the form $\varphi(r_{12}) = \exp[(r_{12}/a)\cos\theta]$. If it is assumed that the ratio of values so obtained to those given by Eqs. (15) may be used throughout the metal, including regions near the surface, these new functions may be used in the calculations performed in (a) above to give a new set of exchange interactions. The exchange energy so obtained represents in a rough way the combined effect on the original results of both the modification introduced in (a) and the present one. The coefficients in Eq. (21) obtained in this way are compared in Table III with the original ones. It is evident that the use of Eq. (22) in this way almost cancels the effect of (a) shown in Table II.

TABLE III. *Values of the coefficients $M(\rho_s)$ and $N(\rho_s)$ of Eq. (21) showing the combined effect of modifications (a) and (b) on the exchange interactions.*

	$f(1, 2)$ FROM EQ. (10)		$f(1, 2)$ FROM EQ. (20) WITH p AND q FROM EQ. (22)	
ρ_s/a	M	N	M	N
1.0	0.47	0.062	0.34	0.003
1.5	0.34	0.065	0.25	0.032
2.0	0.26	0.065	0.26	0.058
2.5	0.21	0.062	0.57	0.162

c. The approximation of Eqs. (11)

It was pointed out in the discussion of the results of Table I that the smallness of the ratio D_m/ρ_s made the use of the approximation (11) questionable. However, if one takes the refinement introduced in (a) above into account, the situation is somewhat improved. As a result of the behavior of the density $f(1, 2)$ in Eq. (20), the main contribution to the exchange interaction does not come from a sphere centered at the surface and extending beyond it, as in the simple theory, but from a sphere centered within the metal at a depth of order $1/k_m$ and cut off at the surface. This effect adds about 0.4 to the ratios D_m/ρ_s given in Table I so that the use of the approximation seems somewhat better justified.

It is to be noted that all of the difficulties discussed in this appendix are least important at small ρ_s. Thus it appears that the simple theory developed in the body of the paper represents the limiting case of metals with high electronic density fairly reliably but should be used with caution in the case of metals having large values of ρ_s.

A Determination of the Atomic Field of Bromine from Electron Scattering

WILLIAM E. FRYE
Ryerson Physical Laboratory, University of Chicago, Chicago, Illinois
(Received September 2, 1941)

The experimental curves for the scattering of electrons by bromine have been analyzed to determine the phase shifts as functions of the energy. The method of phase shift analysis is described in detail. The atomic field of bromine is calculated from the phase shifts by a method involving the WKB approximation to the phase shifts.

THE angular distribution of electrons elastically scattered in bromine gas has been determined experimentally for several energies by Arnot.[1] Various attempts have been made to fit these experimental curves by calculation of the scattering intensity with phase shifts derived either from an estimate of the atomic field of bromine[2] for which the Hartree field has not yet been calculated, or by extrapolation of the phase shifts for the neighboring atom, krypton.[3]

In the present paper the above procedure is reversed. The experimental scattering curves are analyzed by a method developed by Voss[4] to determine the phase shifts. The atomic field of bromine is then calculated from these empirical phases by an approximate method due to Hoyt and Frye.[5]

PHASE SHIFT ANALYSIS BY THE METHOD OF VOSS

A brief account of the method of Voss[4] is given below. The intensity of scattering (cross section per unit solid angle) can be represented in terms of phase shifts K_l, that are functions only of the energy of the incident electrons, by the familiar expression

$$I(\theta)=\frac{C}{4k^2}\left|\sum_{l=0}^{\infty}(2l+1)(\exp 2iK_l-1)P_l(\cos\theta)\right|^2, \quad (1)$$

where k is the de Broglie wave number of the electrons, and a constant C, which is independent of the energy, has been included because only measurements of relative intensities are available. Given $I(\theta)$, one cannot calculate directly the phase shifts from Eq. (1). However, if only a finite number n of the phase shifts are assumed to be of importance, then the best approximation to the scattering intensity is obtained if

$$\int_{-1}^{+1}\left[I(\theta)-\frac{C}{4k^2}\left|\sum_{l=0}^{n}(2l+1)(\exp 2iK_l-1)P_l(\cos\theta)\right|^2\right]^2 dx=\text{minimum}, \quad (2)$$

where $x=\cos\theta$. The measured intensity $I(\theta)$ can be expanded in a series of zonal harmonics,

$$I(\theta)=\sum_\nu B_\nu P_\nu(\cos\theta), \quad (3)$$

where the B_ν are constant coefficients which can be calculated from $I(\theta)$ by a method due to Gauss.[6] We, using the formula for the expansion of the product of two zonal harmonics,[7] can also write

$$\frac{C}{4k^2}\left|\sum_{l=0}^{n}(2l+1)(\exp 2iK_l-1)P_l(\cos\theta)\right|^2 = \sum_{\lambda=0}^{2n}A_\lambda(K_0, K_1, \cdots K_n; C)P_\lambda(\cos\theta). \quad (4)$$

The substitution of Eqs. (3) and (4) into Eq. (2) and the use of the orthogonality and normalization properties of the $P_l(\cos\theta)$ give the condition

$$\sum_{\nu=0}^{2n}\frac{(B_\nu-A_\nu)^2}{2\nu+1}=\text{minimum}.$$

If the constant C is assumed to be known, this condition can be expressed in the form of the

[1] F. L. Arnot, Proc. Roy. Soc. **A144**, 360 (1934).
[2] F. L. Arnot and J. C. McLauchlan, Proc. Roy. Soc. **A146**, 662 (1934).
[3] C. H. Shaw and T. M. Snyder, Phys. Rev. **58**, 600 (1940).
[4] W. Voss, Zeits. f. Physik **83**, 581 (1933).
[5] F. C. Hoyt and W. E. Frye, Phys. Rev. **58**, 784 (1940).
[6] E. W. Hobson, *Theory of Spherical and Ellipsoidal Harmonics* (Cambridge, 1931), p. 81.
[7] Reference 6, p. 86.

system of equations,

$$\sum_{\nu=0}^{2n} \frac{B_\nu}{2\nu+1}\frac{\partial A_\nu}{\partial K_l}=\sum_{\nu=0}^{2n}\frac{A_\nu}{2\nu+1}\frac{\partial A_\nu}{\partial K_l}, \quad l=0,1,\cdots n. \quad (5)$$

Adding $\sum_{\nu=0}^{2n} -(A_\nu^0/2\nu+1)(\partial A_\nu/\partial K_l)$ to both sides of each of Eqs. (5), where

$$A_\nu^0=A_\nu(K_0^0, K_1^0, \cdots K_n^0),$$

and the K_l^0 are zero order approximations to the phase shifts, replacing $\partial A_\nu/\partial K_l$ by $\partial A_\nu^0/\partial K_l^0$ and expanding $(A_\nu-A_\nu^0)$ in a Taylor's series keeping only first-order terms one obtains

$$\sum_{\lambda=0}^{n}\Delta_\lambda C_{\lambda l}=C_l, \quad l=0,1,\cdots n, \quad (6)$$

where

$$\Delta_\lambda=K_\lambda-K_\lambda^0,$$

$$C_{\lambda l}=C_{l\lambda}=\sum_{\nu=0}^{2n}\frac{1}{2\nu+1}\frac{\partial A_\nu^0}{\partial K_\lambda^0}\frac{\partial A_\nu^0}{\partial K_l^0},$$

$$C_l=\sum_{\nu=0}^{2n}\frac{B_\nu-A_\nu^0}{2\nu+1}\frac{\partial A_\nu^0}{\partial K_l^0}.$$

Equations (6) form a system of linear equations to be solved for the corrections Δ_λ to the phase shifts K_l.

The procedure can be repeated as many times as desired, in each case the A_ν^0 and $\partial A_\nu^0/\partial K_l^0$ calculated from the phase shifts obtained from the previous application of the method is used. The corrections in general become successively smaller so that satisfactory convergence is usually obtained after four or five applications of the method.

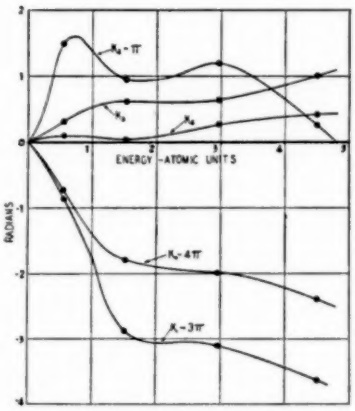

FIG. 1. Phase shifts for bromine deduced from the observed scattering of electrons.

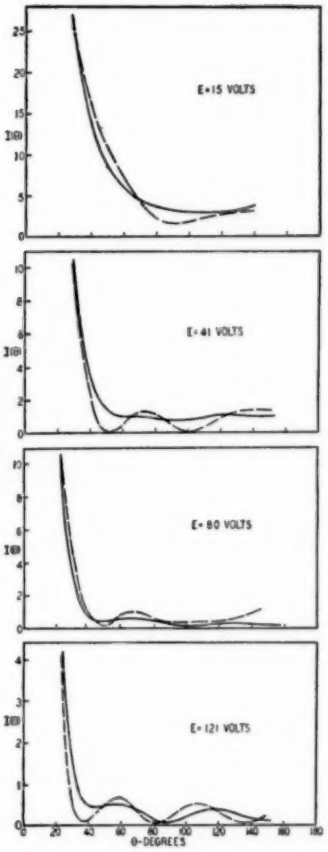

FIG. 2. Broken curves represent intensity against scattering angle θ calculated from the phase shifts of Fig. 1. Solid curves represent the experimental data of Arnot. All intensities are measured in atomic units.

The constant C can be included as an additional unknown in the above procedure, and an additional equation obtained in (6). Since C is independent of the energy, it need be determined only at one value of the energy. Calculation of C at the two energies, 15 ev and 41 ev, showed good agreement.

Phase shifts for bromine up to order five inclusive were calculated by the above method of Voss, with the phase shifts of Shaw and Snyder[3] as zeroth-order approximations. It was found that from four to six successive applications of the method were required to reduce the corrections Δ_λ below 0.2 radian. The calculated phase shifts are shown in Fig. 1 where the phase shifts in radians are plotted against energy in Hartree atomic units. K_5 is not included because it was very small and varied irregularly about zero.

In Fig. 2 the scattering intensities in atomic units, calculated from the phase shifts of Fig. 1, are plotted in broken lines for the four energies, 15, 41, 80 and 121 ev. The experimental curves of Arnot, with the scattering intensities reduced to

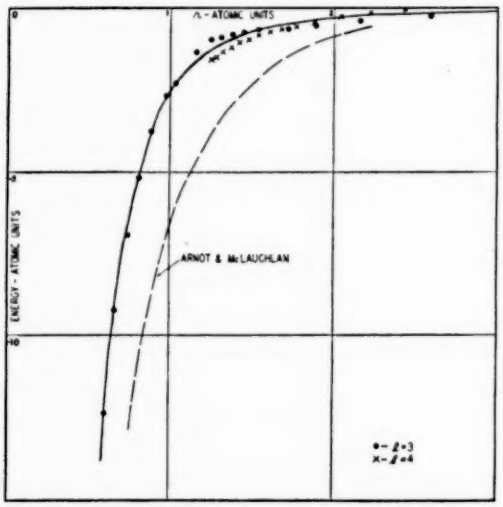

FIG. 3. The solid line represents the atomic field deduced from the observed scattering of electrons by bromine. Points are calculated from the phase shifts K_3 and K_4 of Fig. 1. For $l<3$ the barrier is not removed, and the method of calculation is not applicable. The broken curve is the field extrapolated by Arnot and McLauchlan from the Hartree field of krypton.

atomic units by use of the calculated value of the constant C of Eq. (1) ($C=19.48$), are shown in solid lines. The high value of K_2 at 15 volts (15 ev$=0.55$ atomic units of energy) seems to have physical significance, for a lower value gives poorer agreement of the scattering intensity with the experimental values.

Determination of the Field from the Phase Shifts

The potential field has been calculated directly from the phase shifts by a method[5] involving the WKB approximation to the phase shifts. The method is applicable only if the effective field (actual field plus centrifugal term) contains no barrier. Calculation of points for the field of bromine, in which were used the phase shifts of order less than three, gave anomalous results, which were interpreted as due to the presence of a barrier in the effective potential for these low angular momenta. Points calculated from third- and fourth-order phase shifts (the barrier is removed for $l\geq 3$) are shown in Fig. 3, where the potential in atomic units of energy is plotted against radial distance in atomic units. The broken curve represents the field estimated by Arnot and McLauchlan[2] by extrapolation from the Hartree field of krypton.

Points obtained from phase shifts of one order are calculated quite independently of those from another order. The points in Fig. 3 which are derived from K_3 show good agreement with those from K_4, and both sets of points lie on a smooth curve.

The calculated field in Fig. 3 is that field which acts on an electron at a distance r from the center of the atom, and hence it includes the polarization energy of the scattering atom due to the presence of the scattered electron. A discussion of this polarization correction has been given by Shaw and Snyder.[3]

Discussion

Several limitations and sources of error have influenced the calculations here described. The scattering has been measured experimentally for only a few energies and over a limited angular range. Such factors as finite resolving power, space charge, etc., may have given rise to experimental errors. The methods of phase shift analysis and calculation of the field from the phase shifts are approximate in nature. Only a finite number of phase shifts have been assumed to be of importance. This assumption is valid for low energies, but higher order phase shifts may become important at higher energies. The distortion of the field due to the binding of the bromine atoms in the molecule has been neglected but may be expected to be small. Exchange effects, which may be important at low energies, have not been considered.

An attempt was made to calculate the fine structure of the x-ray absorption edge for bromine[8] with the phase shifts calculated here. However, it was found that the shape of the curve was very sensitive to small variations in the lower order phase shifts at low energies, and good agreement with experiment was not obtained in that region. At higher energies somewhat better agreement than that of Snyder and Shaw was found.

The author wishes to express his deep appreciation to Professor Hoyt who suggested the problem and under whose guidance the calculations were carried out.

[8] T. M. Snyder and C. H. Shaw, Phys. Rev. **57**, 881 (1940).

Special Relativity in Refracting Media

WALTER C. MICHELS AND A. L. PATTERSON
Department of Physics, Bryn Mawr College, Bryn Mawr, Pennsylvania

(Received August 25, 1941)

A reformulation of the Lorentz transformations for an observer in a refracting but non-dispersive medium is suggested. In this statement of the transformations, the speed ($\mathbf{c}=c/n$) of light signals in the medium replaces the free space speed (c) which appears in the usual form. It is shown that the Fresnel drag coefficient takes the same form in the new formulation that it did in the old. Other consequences of this assumption are discussed and, in particular, the mechanics of the photon are shown to lead to correct expressions for Snell's law and for the pressure of radiation at the boundary of the medium.

IN spite of the successes of special relativity in dealing with the problems of the velocity of light, such as the Michelson-Morley experiment, the Fresnel-Fizeau drag coefficient, and the results of Airy on aberration, the more recent attempts to base the treatment of optics on the theory have not been very successful. These attempts have followed two distinct lines. In the first, various workers[1] have developed a relativistic electrodynamics. While this work is of interest in the interpretation of many effects, it is admittedly incomplete and has led to few new optical predictions. Working along a second line, several authors[2] have attempted to deduce the laws of geometrical optics from a photon hypothesis. In general, it has been necessary in such attempts to introduce some *ad hoc* assumptions regarding the velocity or the momentum of the photon. The difficulties which have arisen seem to make it desirable to attempt another approach to the subject, in the hope that this may lead to suggestions for the development of a more complete electrodynamic theory.

In the present treatment, we shall assume that the discrete distribution of matter which comprises a medium may be replaced, to a first approximation, by a continuum characterized by phenomenological constants, such as a dielectric constant, a refractive index, etc. Under this assumption, a treatment of such optical phenomena as diffraction and scattering would be impossible. It should, however, be quite adequate for the treatment of geometrical optics and the optics of the photon. We shall further assume that the medium is refractive but non-dispersive.

Since there are no sufficiently precise experiments which involve an observer embedded in a refracting medium, we cannot say whether such an observer could detect, by *optical* experiments not involving the boundaries of the medium, his motion through the medium. It is certainly true, however, that an observer at rest with respect to the medium could not detect any absolute motion in space, since this would be a violation of the relativity postulate. Were he able to detect such motion, an observer outside the medium could also detect such motion by exchange of signals with him.

If we consider the role of the speed c in the mechanics of special relativity, we find that it acquires its special importance simply because it is the signal speed in free space, and as such it must be used in making the measurements of length and time necessary for the discussion of a mechanics. In a medium of constant refractive index n, the signal speed is $\mathbf{c}=c/n$, and it is not unreasonable to suppose that it is this speed which must replace the c of free space in the discussion of mechanics in the medium.[3] In studying the consequence of such an assumption, it will be necessary for us to refer to six different observers. Two observers, O and O', move freely

[1] For example see W. Pauli, Enc. der Math. Wiss. **5**, Part 2, 539 (1922); H. Bateman, Bull. Nat. Res. Council **4**, Part 6, 96 (1922); W. Gordon, Ann. d. Physik **72**, 421 (1923).

[2] L. Brillouin, Comptes rendus **178**, 1696 (1924); S. Serghiesco, Comptes rendus **202**, 1563 and 1761 (1936).

[3] H. Weyl has considered the possibility of this assumption, but has discarded it because of the success of the conventional theory in the deduction of the Fresnel drag coefficient [*Raum, Zeit, Materie*, fifth edition, Springer, Berlin, 1923, pp. 180–181]. We shall see later that the present assumption gives rise to the same expression for the drag coefficient.

in free space, while a third O_0 makes his measurements in free space, but is at rest with respect to the medium. Within the medium, the two observers **O** and **O′** are free to move, while the third $\mathbf{O}_0$ is fixed with respect to the medium. In discussing transformations connecting the observations of these various observers, we shall use boldface type for observations made within the medium, and italic type for those made in free space. The diacritical marking of the symbols used for the observed quantities will correspond to that of the symbols used for the observers. The complete notation, together with a statement of the relative velocities of the various observers is given in Table I. For simplicity, we shall take all velocities as parallel.

If now the velocity of the observer O' with respect to O is U, the velocity addition theorem will take the usual form:

$$v'=(v-U)/(1-Uv/c^2). \tag{1}$$

The corresponding theorem for any two observers **O** and **O′** within the medium will then be

$$\mathbf{v}'=(\mathbf{v}-\mathbf{U})/(1-\mathbf{U}\mathbf{v}/\mathbf{c}^2). \tag{1′}$$

There is one very important consequence of this formula. If **O** observes a signal of velocity $\mathbf{v}=\mathbf{c}=c/n$, then **O′** will observe the same velocity, i.e., $\mathbf{v}'=\mathbf{c}=c/n$. This indicates that an observer in a continuous medium cannot, by measurements of the velocity of light alone, determine his velocity with respect to the medium. It, of course, follows *a fortiori* that an observer in the medium will be unable to observe any absolute motion in space.

At first glance, it would seem that Eq. (1′) was in contradiction with the experimental results on the Fresnel drag coefficient, but it is to be noted that in every experiment which verifies this coefficient, the observer is located *outside* the medium. In order to discuss experiments of this kind, we must therefore obtain transformations connecting the results of observers in two different media. So far, however, we have made no assumption connecting observations within the medium with those made outside. The simplest assumption of this nature which we can make is that measuring rods and clocks are unaffected by transfer between two observers O_0 and $\mathbf{O}_0$, both of whom are at rest with respect to the medium. Thus the kinematic observations of these two observers will be identical and we shall have $x_0=\mathbf{x}_0$, $t_0=\mathbf{t}_0$, and $v_0=\mathbf{v}_0$. We must now establish the velocity addition theorem for the two observers O and **O**. To do this we make use of the proper observers O_0 and $\mathbf{O}_0$.

TABLE I. *Notation. Observers O_0 and $\mathbf{O}_0$ are at rest with respect to the medium.*

	In Free Space				In Medium	
Observer	O'	O	O_0	$\mathbf{O}_0$	**O**	**O′**
Speed of Light		c			$\mathbf{c}=c/n$	
x coordinate	x'	x	x_0 =	$\mathbf{x}_0$	$\mathbf{x}$	$\mathbf{x}'$
t coordinate	t'	t	t_0 =	$\mathbf{t}_0$	$\mathbf{t}$	$\mathbf{t}'$
Velocity	v'	v	v_0 =	$\mathbf{v}_0$	$\mathbf{v}$	$\mathbf{v}'$
Velocity of O'	0	U	—	—	—	—
" " O	$-U$	0	U_0	—	$\mathbf{V}$	—
" " O_0	—	$-U_0$	0	0	—	—
" " $\mathbf{O}_0$	—	—	0	0	$-\mathbf{U}_0$	—
" " **O**	—	V	—	$\mathbf{U}_0$	0	$-\mathbf{U}$
" " **O′**	—	—	—	—	$\mathbf{U}$	0

If the observer **O** observes a particle of velocity **v**, the observer $\mathbf{O}_0$ will observe a velocity $\mathbf{v}_0$ given by

$$\mathbf{v}_0=(\mathbf{v}+\mathbf{U}_0)/(1+\mathbf{v}\mathbf{U}_0/\mathbf{c}^2),$$

in which $\mathbf{U}_0$ is the velocity of **O** with respect to the medium. In accordance with the above assumption, however, $\mathbf{v}_0=v_0$ and we can find, for the velocity v observed by an observer O, the formula:

$$v=\frac{\mathbf{v}(1-U_0\mathbf{U}_0/\mathbf{c}^2)+(\mathbf{U}_0-U_0)}{(1-U_0\mathbf{U}_0/c^2)+\mathbf{v}(\mathbf{U}_0/\mathbf{c}^2-U_0/c^2)}, \tag{2}$$

in which U_0 is the velocity of O with respect to the medium. Similarly, by interchanging boldface and italic type, it follows from symmetry that

$$\mathbf{v}=\frac{v(1-U_0\mathbf{U}_0/c^2)+(U_0-\mathbf{U}_0)}{(1-U_0\mathbf{U}_0/\mathbf{c}^2)+v(U_0/c^2-\mathbf{U}_0/\mathbf{c}^2)}. \tag{2′}$$

From these formulae, we can obtain directly the observed relative velocities of the two systems. The observer O finds for the velocity of the system **O** a value V given by

$$V=(\mathbf{U}_0-U_0)/(1-U_0\mathbf{U}_0/c^2), \tag{3}$$

and with an interchange of observers we find

$$\mathbf{V}=(U_0-\mathbf{U}_0)/(1-U_0\mathbf{U}_0/\mathbf{c}^2). \tag{3′}$$

There is thus no simple way of expressing the formulae (2) and (2′) in terms of the observed relative velocities of the two systems.

If now the observer **O** observes a light pulse of velocity $\mathbf{c}=c/n$, then the velocity v of this pulse with respect to O will be obtained by making the substitution $\mathbf{v}=\mathbf{c}$ in Eq. (2). We then obtain

$$v=(\mathbf{c}-U_0)/(1-\mathbf{c}U_0/c^2),$$

which may be rewritten in the form

$$v=(c/n-U_0)/(1-U_0/nc)$$
$$=c/n-U_0(1-1/n^2)+\cdots. \quad (4)$$

to give the usual form for the Fresnel drag coefficient in special relativity for a medium whose velocity is $-U_0$ with respect to the observer.

It is interesting to note here that there should be an inverse drag effect on light traveling in free space as seen by an observer moving in the medium. An observer **O** should find a velocity **v** for a light signal in vacuum [cf. Eq. (2′)] given by

$$\mathbf{v}=(c-\mathbf{U}_0)/(1-c\mathbf{U}_0/\mathbf{c}^2),$$

which may be rewritten in the form

$$\mathbf{v}=(c-\mathbf{U}_0)/(1-n^2\mathbf{U}_0/c)$$
$$=c-\mathbf{U}_0(1-n^2)+\cdots. \quad (4')$$

We notice that this velocity depends only on the velocity of **O** with respect to the medium, just as, in the previous case, the observed velocity depended only on the velocity of the free space observer with respect to the medium.

If $U_0=\mathbf{U}_0$, the velocities of the observers O and **O** with respect to the medium are the same, and the transformation (2) takes the form:

$$v=\mathbf{v}(1-U_0^2/\mathbf{c}^2)/[(1-U_0^2/c^2)$$
$$+U_0\mathbf{v}(c^{-2}-\mathbf{c}^{-2})], \quad (5)$$

with an inverse transformation obtained by an interchange of type face. We notice that in the present case $V=\mathbf{V}=0$, i.e., both observers agree that they are at rest with respect to one another.

From now on we shall be concerned only with the observations of the proper observers O_0 and $\mathbf{O}_0$. We shall therefore drop the use of the subscript zero, except as it is required in the normal usage for the rest mass and rest energy, and in the labeling of the observers.

We shall be particularly interested in the expressions for the energy and momentum of a particle as observed within the medium. These follow from an argument exactly analogous to that used in the conventional treatment.[4] For the proper observer $\mathbf{O}_0$ we then find that

$$\mathbf{E}=\mathbf{m}c^2=\mathbf{m}_0c^2/(1-\mathbf{v}^2/\mathbf{c}^2)^{\frac{1}{2}} \quad (6)$$

and

$$\mathbf{p}=\mathbf{m}\mathbf{v}=\mathbf{m}_0\mathbf{v}/(1-\mathbf{v}^2/\mathbf{c}^2)^{\frac{1}{2}}. \quad (7)$$

We thus obtain, for the ratio of energy to momentum in the medium, the expression

$$\mathbf{E}/\mathbf{p}=\mathbf{c}^2/\mathbf{v}. \quad (8)$$

If we expand the expressions (6) and (7) in terms of the proper rest mass $\mathbf{m}_0$, we find that

$$\mathbf{E}=\mathbf{m}_0c^2+\tfrac{1}{2}\mathbf{m}_0\mathbf{v}^2+3\mathbf{m}_0\mathbf{v}^4/8\mathbf{c}^2+\cdots, \quad (6')$$

and that

$$\mathbf{p}=\mathbf{m}_0\mathbf{v}+\tfrac{1}{2}\mathbf{m}_0\mathbf{v}^3/\mathbf{c}^2+\cdots. \quad (7')$$

Thus the Newtonian terms are left unaffected by the proposed assumption. The most serious difference between the present and the conventional treatment is that the rest energy in the medium is now $\mathbf{E}_0=\mathbf{m}_0c^2=\mathbf{m}_0c^2/n^2$. At first glance this result may seem strange, as it indicates that a particle passing from one medium to another must change either its rest mass or its energy. If we remember, however, that the energy necessary to build up an electric charge configuration is inversely proportional to the dielectric constant of the medium surrounding it (i.e., in this case to n^2), the new result seems in complete agreement with classical electromagnetic theory.

We now have the necessary equations for the consideration of geometrical optics. It is commonly recognized that the result of a measurement of the velocity of light yields the group velocity, but there remains the question of whether this quantity is identical with the velocity of the photon in a refractive medium. If we limit ourselves to true velocity determinations, such as those of Fizeau, Foucault, and Michelson, rather than interference experiments, there seems to be no doubt that the measured velocity in a non-dispersive medium is that of the photon, since the detecting device in

[4] See for example: R. C. Tolman, *Relativity, Thermodynamics, and Cosmology* (Oxford, 1934), Chapter III.

the measurement is one which responds to photon energy. Consequently, we shall suppose that the photon velocity in a refractive medium is given by $\mathbf{c}=c/n$. Substitution of this value into Eqs. (6) and (7) shows that the rest mass of the photon must be zero for a proper observer in the medium. Equation (8) then becomes, for the photon:

$$\mathbf{E}/\mathbf{p}=\mathbf{c}=c/n. \tag{9}$$

When a photon passes from one medium to another, it is almost certain that its energy remains unchanged. We may reach this conclusion either from the consideration of the constancy of frequency of a wave in passing from one medium to another, or from the photoelectric effect. In the former case the energy must remain constant if the Einstein frequency relation is to hold. In the latter case, the actual absorption of the photon takes place within the medium, and it is very hard to see how the Einstein photoelectric equation could hold if the photon energy changed at the boundary. Consequently, for a given photon in vacuum, we have

$$E/p=c;$$

and for the same photon in the medium, we have

$$\mathbf{E}/\mathbf{p}=\mathbf{c}=c/n;$$

with the condition that $E=\mathbf{E}$. It then follows that

$$\mathbf{p}=np. \tag{10}$$

This equation indicates that the momentum of the photon increases as it passes from free space into the refractive medium. If we suppose that the change of momentum is normal to the surface, as is indicated by the lack of a tangential light pressure; and if we let I and R, respectively, be the angles of incidence and refraction; we then have

$$\mathbf{p}/p=n=\sin I/\sin R,$$

so that Snell's law follows directly from the photon mechanics.

Use of the component of the momentum perpendicular to the surface enables us to calculate the radiation pressure on the interface. If N photons per second pass unit area of the surface, and none are reflected, the pressure will be

$$P=(Nh\nu/c)(\cos I-n\cos R),$$

which reduces for normal incidence to

$$P=(Nh\nu/c)(1-n).$$

While Eq. (10) eliminates the difficulty which has been present in earlier particle treatments of optics, namely that the momentum must increase when a photon passes into a more refractive medium, it seems strange that it ascribes to the photon a momentum which is inversely proportional to its velocity. This, of course, follows only because of the constancy of the energy, which requires that the effective mass of the photon increase by a factor n^2 in passing the boundary.

If the usual de Broglie relationships are derived for an observer in the medium, the relation between the velocity of a particle $\mathbf{G}$ and the phase velocity of the associated wave $\mathbf{W}$ becomes

$$\mathbf{G}\mathbf{W}=\mathbf{c}^2=c^2/n^2. \tag{11}$$

In the case of the non-dispersive medium this equation reduces to a trivial identity for the photon and the electromagnetic wave.

The treatment of dispersive media would be of considerable interest, but it presents many difficulties. It seems clear, however, that the mechanics of an observer embedded in a dispersive medium may depend on the exact nature of the signal which he uses in making his observations and in synchronizing his clocks.

We present this paper, with an alternative formulation of the special relativity postulates, with considerable hesitation. The difficulties of performing direct experiments to test its validity seem insurmountable, since such experiments would involve precise measurements with the apparatus moving in a refracting medium. The only justification for the proposed system seems to be the experimental determination of the ratio $\mathbf{p}/p$ given by the interpretation of Snell's law on a photon hypothesis.

Theory of the Optical and Magnetic Properties of Ferromagnetic Suspensions

W. C. ELMORE
Department of Physics, Swarthmore College, Swarthmore, Pennsylvania
(Received August 8, 1941)

The theory of the optical transparency of ferromagnetic suspensions, as modified by magnetic fields, is developed along lines suggested by C. W. Heaps. It is proposed to determine the average "shape" of the particles by measuring the transmission of a suspension in various directions while the particles are magnetically aligned parallel to one another. From this information, the complete magneto-optic behavior of the suspension can be deduced; comparison between experimental and theoretical curves gives a value of the (average) magnetic moment of the particles. In addition, theory for two new magneto-optic experiments is developed, one which will give directly the intensity of magnetization of the particles, the other which will give directly the volume of the particles. In the first experiment changes in transparency are used to indicate when the particles have been rotated magnetically through a definite angle; the second experiment is based on the changes in transparency accompanying the return to random particle orientation following the removal of an applied magnetic field. It is shown that suspensions should have a transmission of $(1/e)$ to give a maximal magneto-optic effect.

A CELL containing a suspension of particles of magnetite acts in a limited way as a magnetically controlled light shutter. This effect, discovered nearly a century ago by W. R. Grove,[1] recently has been rediscovered and studied by C. W. Heaps.[2] The latter made measurements of cell transmission with respect to magnetic field intensity, and attempted to account for the variation in transmission on the following basis. (1) The magnetite particles possess permanent magnetic moments. (2) Magnetically linked groups of particles are responsible for the effect and they cast shadows characteristic of a cylinder. (3) The particle groups behave as a classical paramagnetic gas. From these assumptions Heaps deduced that the cell transmission should approach a limiting value proportional to H^{-1}; his experimental findings, however, failed to agree with this deduction. In a short note[3] the writer showed that by assuming spheroidal rather than cylindrical particle groups the transmission should vary as H^{-1} for intense fields, and that Heaps' data are in fair accord with this prediction, the computed value of μ being 1.4×10^{-12} e.m.u. This value would seem to indicate that the particle groups, estimated by Heaps to average 5 microns in diameter, have a very small intensity of magnetization. The conclusion is of interest, for it appears likely that much smaller particles of magnetite exist as single ferromagnetic domains.[4]

Since the light shutter action of ferromagnetic suspensions affords a simple method of studying the remanent magnetization of small ferromagnetic particles, it appears worth while to reconsider the theory of the phenomenon, and to carry out experiments with a variety of ferromagnetic suspensions and colloids. The present paper, therefore, will be devoted to modifying and to extending Heaps' theory, particularly in the direction of devising new experiments which will give additional information concerning the magnetization of ferromagnetic particles. A second paper is planned which will be devoted to new experimental results.

Variation in Transparency with Magnetic Field Intensity

A small particle in a beam of light removes light by scattering and by absorption, thereby possessing a certain effective cross section Q which is defined as the ratio of the total energy per second removed by the particle from the light beam to the intensity of the beam. For a particle of a given size, shape and orientation the value of Q may depend on the wave-length of light, on the optical properties of the material constituting the particle, and on the refractive

[1] See discussion by L. W. McKeehan, Phys. Rev. **57**, 1177 (1940).
[2] C. W. Heaps, Phys. Rev. **57**, 528 (1940).
[3] W. C. Elmore, Phys. Rev. **57**, 842 (1940).
[4] W. C. Elmore, Phys. Rev. **54**, 1092 (1938).

index of the medium in which the particle is immersed. In general, Q will differ from the geometrical cross section of the particle even though the particle be opaque. In view of the dependence of Q on wave-length, the following theory will hold strictly only for the transmission of monochromatic light through a ferromagnetic suspension or colloid. However, the theory may be applied safely to measurements made with white light, provided that the light is not colored appreciably by the suspension.

Let n be the number of particles per unit volume in the suspension, and let Q be their average effective cross section. The fraction of light removed by a layer of the suspension of thickness dx is $dl/l=-nQdx$, so that the transmission t of a cell of length L is

$$t=e^{-nLQ}, \tag{1}$$

which is, of course, Beer's law.[5] Since the particles are permanently magnetized, and since they are not in general perfect spheres (a "particle" may be a magnetically linked group of the ultimate particles of the suspension), the value of Q, and hence that of t, will depend on the direction and magnitude of an applied magnetic field. Let $Q_{||}$ be the average value of Q when all particle moments are lined up parallel to the optic axis of the cell, and let us define the average relative cross section $q\equiv Q/Q_{||}$, thus referring all cross sections to $Q_{||}$. Experimental values of q may be computed from measured transmissions by the relation

$$q=\log t/\log t_{||}, \tag{2}$$

which follows immediately from Eq. (1). Since it will be found convenient to make all comparisons between theory and experiment by means of curves of relative cross section, all derivations regarding transparency of suspensions will be left as formula for q, Eq. (2) being implied.

Let us denote by $q_\infty(\psi)$ the relation connecting the average relative cross section for completely aligned particles with the angle ψ between the aligning field and the cell axis. Then the value of q for any field H making an angle α with the cell axis can be determined by the extension of Langevin's theory of a paramagnetic gas suggested by Heaps. For this calculation it is convenient to use spherical coordinates, with the polar axis in the direction of the magnetic field, and let the angle between the particle moments and the field be specified by the polar angle θ and the azimuth ϕ. In these coordinates the light axis can be specified by $\theta=\alpha$, $\phi=0$, so that the value of ψ in $q_\infty(\psi)$ is related to θ and ϕ by $\cos\psi=\sin\alpha\,\sin\theta\,\cos\phi+\cos\alpha\,\cos\theta$. Hence the dependence of q on $a\equiv\mu H/kT$ and on α is given by

$$q(a,\alpha)=\frac{\int_0^{2\pi}\int_0^{\pi} q_\infty(\psi)e^{a\cos\theta}\sin\theta d\theta d\phi}{\int_0^{2\pi}\int_0^{\pi} e^{a\cos\theta}\sin\theta d\theta d\phi}. \tag{3}$$

Before proceeding further, it is necessary to have an expression for $q_\infty(\psi)$. Instead of assuming that the form of the average particle cross section is similar to that of a cylinder or of a spheroid, it is more satisfactory to determine its form by measuring cell transmission as a function of ψ. By symmetry one expects that the experimental data can be expressed by the series

$$q_\infty(\psi)=1+q_1\sin^2\psi+q_2\sin^4\psi+\cdots \tag{4}$$

where q_1, q_2, $\cdots$ are constants. Now it will be shown in a subsequent paper that in many cases only two constants, q_1 and q_2, are required to fit Eq. (4) to the measured curve of $q_\infty(\psi)$. Hence all calculations based on (4) will be carried only through the term containing q_2. On substituting (4) in (3) and performing the integration, one obtains an expression governing the response of the light cell to a magnetic field of arbitrary magnitude and direction. Only the results for $\alpha=0$ and for $\alpha=\pi/2$ will be given here, since they possess the greatest experimental interest. By writing $L(a)\equiv\coth a-1/a$, the two results become, respectively,

$$q(a,0)=1+q_1(2/a)L(a)+q_2\{8/a^2-(24/a^3)L(a)\}, \tag{5}$$

and

$$q(a,\pi/2)=1+q_1\{1-(1/a)L(a)\}+q_2\{1-(2/a)L(a)+(3/a^2)[1-(3/a)L(a)]\}. \tag{6}$$

In the foregoing theory, all quantities except μ can be determined experimentally. To test the

[5] In his theory Heaps assumed that $t=1-nLQ$. This is not a good approximation to Beer's law for transmissions differing appreciably from unity.

theory plots of Eqs. (5) and (6) can be compared with the experimental curves of relative cross sections against magnetic field intensity. Provided that the distribution in particle moments is not too broad, the two sets of curves should coincide when the value of μ is correctly chosen.

To obtain the intensity of magnetization of the particles from the value of μ it is necessary to know the particle volume. Now the microscope will give only a rough estimate of this volume if the particle diameter is less than one micron. The sedimentation method based on Stokes law cannot be used, for, on standing, the particles in the suspension tend to form larger and larger magnetically linked groups. For the same reason the method based on counting particles in a suspension of known concentration is unsatisfactory. It is possible, however, to perform other experiments with the light cell which will give, independently, the intensity of particle magnetization, and the volume of the particles. These two results can then be compared with the value of the particle magnetic moment obtained in the first experiment.

Variation in Transparency with Time Following a Change in Field Direction

Let r be the mean particle radius and η the coefficient of viscosity of the suspending liquid. Then, according to Stokes law for rotation, the torque required to turn a particle at constant angular velocity $d\psi/dt$ is $8\pi r^3\eta d\psi/dt$. Consider the case where the suspended particles are magnetically aligned in some particular direction. If, now, the direction of the field is suddenly shifted, the torque acting on any one particle is $\mu H \sin\psi$ where ψ is the angle between μ and H. Hence we must have $8\pi r^3\eta d\psi/dt = \mu H \sin\psi$ since the inertial term is negligible. Let us integrate this equation for a change in field direction of $\frac{1}{2}\pi$, thus obtaining

$$\tau = \frac{8\pi r^3\eta}{\mu H}\int_{\frac{1}{2}\pi}^{\theta}\frac{d\psi}{\sin\psi} = \frac{8\pi r^3\eta}{\mu H}\ln|\tan(\theta/2)|, \quad (7)$$

which gives the time τ required for the particles to turn through an angle $\frac{1}{2}\pi-\theta$. If we write $\mu=(4\pi/3)r^3I$, where I is the intensity of magnetization of the particles, we obtain from Eq. (7)

$$I = (6\eta/\tau H)\ln|\tan(\theta/2)|, \quad (8)$$

a result *independent of the size of the particles*. By suspending the particles in an aqueous glycerol solution, a wide range of values of η are available. Values of τ for various field strengths can be obtained by measuring the time required for the particles to rotate through a particular angle as indicated by the change in transparency of the suspension. Hence we have a simple method for determining directly the average intensity of magnetization of the particles.

Variation in Transparency During Relaxation

Einstein has shown[6] that rotational Brownian motion obeys the diffusion equation with the coefficient of rotational diffusion given by

$$D = kT/4\pi r^3\eta. \quad (9)$$

Let us apply this concept to determine the changes in transparency following the removal of a magnetic field applied parallel to the cell axis. When the field is present, the distribution of particle moments is given by $\nu = \text{Const. } e^{a\cos\theta}$ where ν is the number of particle moments per unit solid angle making an angle θ with the magnetic field. To obtain an expression governing the relaxation of this distribution to a random one, we must solve the diffusion equation

$$\frac{\partial\nu}{\partial t} = \frac{D}{\sin\theta}\frac{\partial}{\partial\theta}\left(\sin\theta\frac{\partial\nu}{\partial\theta}\right), \quad (10)$$

subject to the boundary conditions that at $t=0$, $\nu=\text{Const. } e^{a\cos\theta}$ and at $t=\infty$, $\nu=\text{Const.}$ Now the elementary solutions of (10) have the form

$$e^{-n(n+1)Dt}P_n(\cos\theta),$$

where $n=0, 1, 2, \cdots$ and $P_n(\cos\theta)$ is a Legendre polynomial. By means of the integral

$$\int_{-1}^{+1} e^{az}P_n(x)dx = (2\pi/a)^{\frac{1}{2}}I_{n+\frac{1}{2}}(a),$$

where $I_{n+\frac{1}{2}}(a)$ is a modified Bessel function, it is easy to obtain the expansion

$$e^{a\cos\theta} = (\pi/2a)^{\frac{1}{2}}\sum_0^\infty (2n+1)I_{n+\frac{1}{2}}(a)P_n(\cos\theta),$$

[6] See, for instance, R. H. Fowler, *Statistical Mechanics* (Cambridge, 1936) p. 774.

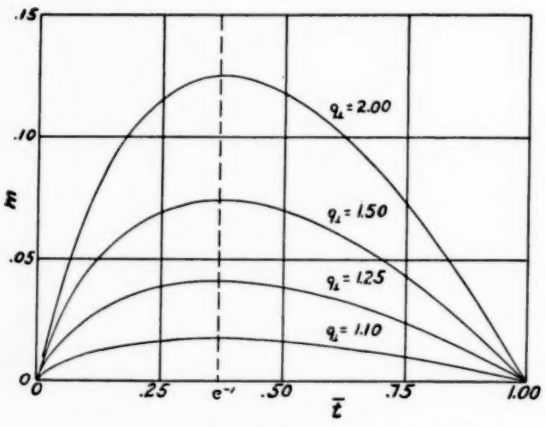

FIG. 1. Illustrating the dependence of modulation on transmission for several shapes of particles.

so that the solution of (10) which satisfies the required boundary conditions is

$$\nu(\theta,t)=\text{Const.}(\pi/2a)^{\frac{1}{2}}\sum_0^\infty (2n+1)I_{n+\frac{1}{2}}(a) \times P_n(\cos\theta)e^{-n(n+1)Dt}. \quad (11)$$

Finally, the time variation in the average relative cross section during relaxation will be given by a calculation similar to Eq. (3),

$$q(t)=\frac{\int_0^\pi q_x(\theta)\nu(\theta,t)\sin\theta d\theta}{\int_0^\pi \nu(\theta,t)\sin\theta d\theta}, \quad (12)$$

where $q_x(\theta)$ is given by Eq. (4) with $\psi=\theta$.

To evaluate Eq. (12) it is convenient to rewrite Eq. (4) in the form

$$q_x(\theta)=c_0+c_2P_2(\cos\theta)+c_4P_4(\cos\theta)+\cdots, \quad (13)$$

where the new constants c_i are related to the old constants q_i as follows:

$$\left.\begin{aligned} c_0&=1+(2/3)q_1+(8/15)q_2+\cdots\\ c_2&=-(2/3)q_1-(16/21)q_2+\cdots\\ c_4&=(8/35)q_2+\cdots\\ &\cdots\cdots\cdots\end{aligned}\right\}. \quad (14)$$

Hence Eq. (12) becomes, on integrating,

$$q(t)=[1/I_{\frac{1}{2}}(a)]\sum c_nI_{n+\frac{1}{2}}(a)e^{-n(n+1)Dt}, \quad (15)$$

where the summation is to be taken for $n=0, 2, 4, \cdots$, the number of terms depending on the number of constants in Eq. (13) [or in Eq. (4)] required to represent the experimental of curve of $q_x(\theta)$. For purposes of computation Eq. (15) may be written in terms of hyperbolic functions by means of the well-known formulae for modified Bessel functions of half-integral order. A case interesting from the experimental standpoint arises when a is very large, i.e., when initially all particles are aligned parallel to the cell axis. Since for large a, $I_{n+\frac{1}{2}}(a)\rightarrow(1/2\pi a)^{\frac{1}{2}}e^a$, Eq. (15) becomes

$$q(t)=c_0+c_2e^{-6Dt}+c_4e^{-20Dt}+\cdots. \quad (16)$$

By comparing the observed changes in transparency during relaxation with those predicted from Eq. (15) or (16) it is possible to obtain a value of the rotational diffusion constant D. By means of Eq. (9) the volume (average) of the particles may then be computed.

BEST VALUE OF TRANSMISSION FOR EXPERIMENTAL STUDIES

It is helpful to know what transmission suspensions should have to be best suited for experimental study. Let us define the average transmission of a cell by $\bar{t}=\frac{1}{2}(t_{||}+t_\perp)$ and the modulation (maximum) of the cell by $m=\frac{1}{2}(t_{||}-t_\perp)$, where the subscripts refer to the direction of the magnetic field with respect to the cell axis. On using (1) and (2), and maximizing m with respect to nL, it is found that

$$\left.\begin{aligned} \bar{t}&=\tfrac{1}{2}(q_\perp+1)q_\perp^{-q_\perp/(q_\perp-1)}\doteq(1/2e)(q_\perp+1),\\ m&=\tfrac{1}{2}(q_\perp-1)q_\perp^{-q_\perp/(q_\perp-1)}\doteq(1/2e)(q_\perp-1),\end{aligned}\right. \quad (17)$$

where $q_\perp\equiv\log t_\perp/\log t_{||}$, and where the approximate expressions hold for values of $q_\perp$ not differing much from unity, a situation which is (unfortunately!) always true. Hence it is concluded that the greatest changes in transmission are produced by a magnetic field when the cell transmits about $(1/e)$ of the light which it would transmit if it contained pure liquid. In Fig. 1 is illustrated the dependence of modulation on transmission for several values of $q_\perp$.

The Thermal Expansion of Pure Metals: Copper, Gold, Aluminum, Nickel, and Iron

F. C. NIX AND D. MACNAIR
Bell Telephone Laboratories, New York, New York

(Received August 8, 1941)

Extremely accurate determinations of the linear thermal expansions have been made interferometrically from −196°C to temperatures about +400°C for Al and +700°C for Fe, Ni, Cu and Au. The relationship between true thermal coefficient of expansion and temperature conforms very well to the Grueneisen-Debye theory when values are chosen for the Debye characteristic temperatures which turn out to agree well with those chosen to achieve agreement with the Debye theory of specific heats. Our values for these characteristic temperatures are: 410°K for Ni, 420°K for Fe, 400°K for Al, 325°K for Cu, and 190°K for Au. The magnetic Curie temperature for Ni is found to be 352°C. In plotting true coefficient of thermal expansion *versus* temperature Simon and Bergmann found a horizontal plateau at about 175° to 235°K for Ni and Fe; but we do not confirm this.

IN view of the discrepancies in the recorded values of true coefficients of thermal expansion for pure metals over a rather wide range of temperatures, we thought it worth while to reinvestigate a series of very pure metals from the temperature of liquid nitrogen up to about 700°C, by means of an interferometer dilatometer with photographic recording recently developed in these Laboratories. Another important purpose was to test the validity of the Grueneisen theory[1] of thermal expansion over a similarly wide temperature range.

The Grueneisen theory presents the following expression for the true linear coefficient of thermal expansion as a function of the specific heat and two constants, Q_0 and $\frac{1}{6}(m+n+3)$:

$$\beta = C_v \Big/ 3Q_0\left[1-\frac{m+n+3}{6}\frac{E}{Q_0}\right]^2, \qquad (1)$$

where β is the true linear coefficient of thermal expansion, C_v the specific heat at constant volume; $E=\int_0^T C_v dT$; m and n are the exponents in the attractive and repulsive terms, respectively, in the Mie equation relating the potential energy to the distance between vibrating atoms in a monatomic solid. The constant Q_0 is defined in terms of specific heat and coefficient of thermal expansion, or in terms of atomic volume, Grueneisen's constant γ, and compressibility K_0, as follows:

$$Q_0=\frac{(C_P)}{[(1/V)(\partial V/\partial T)]}=\frac{V_0}{\gamma K_0}. \qquad (2)$$

The constants necessary to evaluate β as a function of temperature are Q_0, m, n, and the Debye constant θ which determines C_v and E; one can, in principle, get their values from measurements of specific heats and compressibility. The constant γ, commonly known as "Grueneisen's constant," can be obtained either from the Grueneisen relation

$$\gamma=\frac{\text{(thermal expansion) (volume)}}{\text{(specific heat at const. vol.) (compressibility)}}, \qquad (3)$$

or, as Slater[2] has recently shown, from the constants used in Bridgman's expression relating change in volume to pressure. Slater has shown that values of γ thus obtained are in good agreement with those obtained from the Grueneisen relationship. Grueneisen further showed that γ is related to the exponent n in the repulsion term in the following manner

$$\gamma=\tfrac{1}{6}(n+2). \qquad (4)$$

In the applications of Eq. (1) it has been customary to assume the exponent m of the attractive term to be equal to 3.

The characteristic Debye temperatures θ used to obtain C_v and E in Eq. (1) are taken from experimental specific heat values.

In actual practice one must fit the constants

[1] E. Grueneisen, *Handbuch der Physik* (1926), Vol. 10, p. 1.

[2] J. C. Slater, Phys. Rev. **57**, 744 (1940).

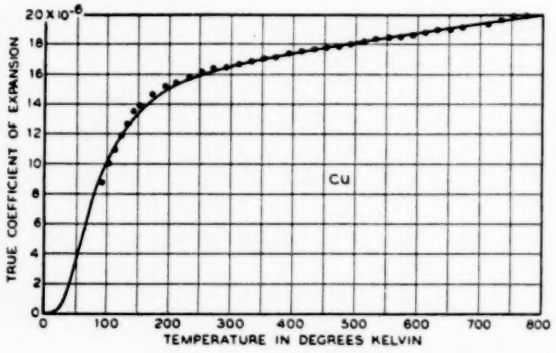

FIG. 1. True coefficient of thermal expansion *vs.* temperature for Cu. The dots are experimentally derived coefficients. The solid curve is the Grueneisen plot with $\theta=325$, $\frac{1}{6}(m+n+3)=2.8$, $Q_0=120\times10^3$ cal.

$\frac{1}{6}(m+n+3)$ and Q_0 to at least one point of the experimental data, and in some cases two points, in order to obtain a good fit between the Grueneisen curve and the experimental points. In some cases it was necessary to make slight adjustments in the value of θ in order to obtain a satisfactory fit. In the captions of the figures given below we give the values of θ, Q_0, and $\frac{1}{6}(m+n+3)$ used in order to obtain the agreement between the experimental data and the Grueneisen curve of the respective figures.

Method of Measurements

The measurements were made with an interferometric dilatometer previously described by us,[3] involving photographic recording; it permits slow rates of heating and cooling, so that sufficient time can be allowed for the specimens to come to thermal equilibrium with the refraction thermometer. The specimens were about 6 mm in length. All specimens were sealed in evacuated Pyrex glass tubing and subjected to a prolonged annealing to remove the effects of cold working. The low temperature portion of each test was made at a cooling rate of 20°C per hour from room temperature, with system containing the gas at a pressure of 3 mm of Hg. The fringe systems were photographed at intervals of about 30 seconds, thereby yielding a quasi-continuous record of both expansion and thermometer fringes. The complete unison of motion of the two sets of fringes assured thermal equilibrium of the specimens and refraction thermometer. The temperature was held constant at the lowest temperature obtainable for a period of two hours, in order to obtain a further check on assuring thermal equilibrium. In the temperature region above room temperature, the gas at a pressure of 3 mm of Hg was used in order to facilitate the establishment of thermal equilibrium up to +150°C at a heating rate of 15°C per hour at which point the system was held at a constant temperature while it was evacuated to a pressure of 10^{-5} mm of Hg. At higher temperatures the heating rate was increased to 20°C per hour.

[3] F. C. Nix and D. MacNair, Rev. Sci. Inst. **12**, 66 (1941).

TABLE I. *Thermal expansion of copper.*

T °C	$\Delta l/l_0\times10^4$	T °C	$\Delta l/l_0\times10^4$	T °C	$\Delta l/l_0\times10^4$
−185.5	−25.956	−8.0	−1.285	173.4	29.653
−179.0	−25.443	−4.5	− .7710	178.0	30.607
−173.0	−24.903	−1.5	− .2570	183.1	31.560
−168.5	−24.415	0	0	189.0	32.514
−164.5	−23.926	1.5	.2570	193.8	33.468
−159.5	−23.387	4.2	.7710	199.8	34.422
−154.0	−22.924	7.5	1.285	204.0	35.376
−152.0	−22.410	11.0	1.799	209.8	36.330
−147.0	−21.840	13.4	2.313	215.4	37.280
−142.5	−21.382	16.0	2.827	220.8	38.238
−137.5	−20.817	19.2	3.341	226.2	39.192
−134.0	−20.303	22.1	3.855	232.6	40.146
−131.2	−19.789	25.0	4.326	243.5	42.054
−123.0	−18.761	28.5	4.807	249.0	43.007
−119.2	−18.247	31.7	5.288	259.0	44.915
−116.0	−17.810	37.0	6.249	263.2	45.869
−112.0	−17.219	42.3	7.211	268.1	46.823
−108.0	−16.705	47.1	8.172	273.5	47.777
−104.5	−16.216	54.0	9.133	279.0	48.732
−100.5	−15.677	59.6	10.095	283.8	49.685
− 97.2	−15.163	65.5	11.056	288.8	50.639
− 93.5	−14.649	71.0	12.018	293.0	51.593
− 90.5	−14.160	77.0	12.979	298.8	52.547
− 86.1	−13.621	83.0	13.941	303.7	53.501
− 83.2	−13.107	89.0	14.902	311.9	54.931
− 80.2	−12.644	92.0	15.383	314.0	55.408
− 77.0	−12.130	94.5	15.863	318.8	56.362
− 73.2	−11.565	100.7	17.252	323.7	57.316
− 70.0	−11.051	104.0	17.729	328.8	58.270
− 66.2	−10.537	107.0	18.206	338.2	60.178
− 62.0	−10.023	108.9	18.583	343.9	61.132
− 60.2	− 9.535	112.0	19.159	353.2	63.040
− 56.6	− 8.995	114.6	19.636	362.6	64.948
− 53.0	− 8.481	117.0	20.113	372.1	66.855
− 49.0	− 7.967	120.5	20.590	384.0	68.763
− 46.5	− 7.543	122.6	21.067	394.1	70.671
− 44.1	− 6.965	126.0	21.544	403.8	72.579
− 39.5	− 6.425	128.8	22.021	412.8	74.487
− 36.1	− 5.911	132.0	22.498	422.0	76.395
− 33.1	− 5.397	134.7	22.975	432.5	78.303
− 29.6	− 4.883	138.0	23.452	442.0	80.210
− 27.0	− 4.369	140.1	23.929	452.1	82.142
− 23.2	− 3.855	146.0	24.883	462.0	84.026
− 20.3	− 3.341	151.4	25.837	471.2	85.934
− 17.3	− 2.827	157.8	26.791	481.0	87.842
− 14.5	− 2.313	162.5	27.745	489.7	89.750
− 11.0	− 1.799	168.0	28.699	500.1	91.657

TABLE II. *Thermal expansion of gold.*

T °C	$\Delta l/l_0\times10^4$	T °C	$\Delta l/l_0\times10^4$	T °C	$\Delta l/l_0\times10^4$	T °C	$\Delta l/l_0\times10^4$	T °C	$\Delta l/l_0\times10^4$	T °C	$\Delta l/l_0\times10^4$
−187.0	−24.481	−15.0	−2.134	124.8	17.549	276.1	40.028	417.0	62.477	603.0	93.525
−185.0	−24.049	−11.0	−1.586	129.5	18.213	279.6	40.633	420.5	63.054	606.0	94.101
−179.0	−23.473	− 6.1	− .9805	133.0	18.675	283.8	41.210	424.0	63.630	609.8	94.677
−175.0	−22.897	− 2.7	− .4037	137.6	19.336	287.0	41.786	428.0	64.207	613.8	95.311
−170.0	−22.318	0	0	141.0	19.883	290.8	42.334	431.6	64.783	616.5	95.888
−164.5	−21.741	2.0	.1730	145.0	20.459	294.0	42.939	435.3	65.359	619.8	96.406
−160.0	−21.165	4.10	.5189	149.5	21.036	297.7	43.515	439.7	65.936	623.7	97.040
−154.7	−20.589	10.0	1.327	152.9	21.556	301.4	44.092	443.0	66.570	628.0	97.559
−150.0	−20.013	14.0	1.903	156.5	22.132	305.1	44.668	446.0	67.088	630.0	98.135
−145.0	−19.436	18.0	2.480	161.0	22.767	308.0	45.215	449.8	67.665	633.0	98.712
−140.5	−18.857	22.0	3.088	164.0	23.285	311.6	45.763	453.7	68.241	636.8	99.288
−137.0	−18.310	25.0	3.490	168.1	23.890	315.6	46.368	457.0	68.817	640.5	99.951
−131.1	−17.734	25.0	3.489	172.5	24.467	318.8	46.916	460.8	69.394	644.0	100.49
−126.5	−17.128	29.7	4.181	175.2	25.014	322.2	47.521	463.8	69.970	647.0	101.02
−122.5	−16.552	34.0	4.758	180.0	25.590	326.0	48.068	467.6	70.546	650.5	101.59
−117.3	−15.973	38.0	5.334	183.2	26.166	330.0	48.674	471.6	71.123	654.0	102.17
−112.7	−15.397	42.6	5.911	188.2	26.772	333.9	49.221	475.1	71.699	657.5	102.75
−108.0	−14.821	45.8	6.488	191.0	27.318	337.4	49.798	478.9	72.276	661.0	103.32
−104.0	−14.244	50.1	7.093	195.6	27.924	341.0	50.403	489.0	74.005	663.0	103.90
− 99.5	−13.668	54.0	7.641	199.0	28.471	344.8	50.950	492.0	74.581	668.0	104.48
− 95.0	−13.092	58.5	8.247	203.0	29.047	347.8	51.527	506.2	76.829	672.0	105.11
− 90.5	−12.516	62.0	8.795	206.8	29.653	351.3	52.103	510.5	77.578	675.0	105.63
− 86.2	−11.939	66.0	9.371	211.0	30.229	354.8	52.679	514.8	78.183	677.0	106.20
− 82.0	−11.360	70.0	9.948	215.0	30.864	358.2	53.256	517.3	78.673	681.0	106.78
− 78.5	−10.784	74.2	10.525	218.2	31.355	362.5	53.832	529.8	80.748	684.8	107.36
− 73.8	−10.208	78.8	11.101	222.4	31.931	366.0	54.408	557.0	85.744	688.0	107.93
− 69.0	− 9.629	83.0	11.707	226.3	32.508	368.8	54.985	559.0	86.032	691.0	108.51
− 65.0	− 9.055	87.0	12.255	230.8	33.140	373.0	55.561	568.0	87.588	694.5	109.14
− 60.2	− 8.479	91.0	12.832	234.6	33.716	377.0	56.137	569.1	87.819	697.6	109.66
− 56.5	− 7.900	94.0	13.293	238.5	34.236	380.3	56.714	572.7	88.337	701.0	110.30
− 52.0	− 7.324		12.832	243.2	34.868	384.4	57.290	575.0	88.798	705.0	110.90
− 48.2	− 6.747		12.255	246.2	35.389	387.1	57.867	576.0	88.914	708.2	111.39
− 44.6	− 6.171		11.678	249.8	35.965	391.2	58.443	579.0	89.490	711.0	111.97
− 40.0	− 5.595	100.0	14.12	254.0	36.541	395.1	59.019	583.1	90.153	714.0	112.54
− 36.0	− 5.045	104.2	14.638	257.6	37.118	398.8	59.596	586.0	90.700	717.0	113.18
− 31.2	− 4.439	108.5	15.215	261.3	37.694	403.1	60.172	589.0	91.219	720.5	113.70
− 27.0	− 3.863	112.3	15.791	264.9	38.270	405.9	60.748	592.3	91.795	723.8	114.27
− 23.0	− 3.287	117.0	16.370	268.8	38.847	409.9	61.325	596.0	92.429	726.0	114.85
− 19.0	− 2.711	121.0	16.946	272.7	39.423	413.0	61.901	599.0	92.948	729.8	115.43

EXPERIMENTAL RESULTS

Copper

The copper used in these experiments was taken from rods produced by Adam Hilger for use as spectroscopic standards which, according to their analysis, possess a copper content of 99.979 percent and oxygen of 0.02 percent. We give in Table I the data obtained, the first column containing the temperature in degrees centigrade and the second column the thermal expansivity, $(\Delta l/l_0)\times10^4$, where l_0 is the length of specimens at 0°C and Δl is the change in length. In Fig. 1 is plotted the true coefficient of thermal expansion, $(1/l_0)(dl/dT)$, as a function of temperature in degrees Kelvin; the curve is graphically obtained from the plot of data of Table I. The dots represent the experimental points; the solid curve is the Grueneisen curve obtained with a characteristic Debye temperature of 325, 2.8 for $\frac{1}{6}(m+n+3)$ and 120×10^3 cal. for Q_0.

The temperature region from room temperature to 800°K has been previously studied by Eucken and Dannoehl;[4] Rosenbohm;[5] Henning;[6] and Uffelman.[7] The low temperature region has been previously investigated by Adenstedt;[8] Buffington and Latimer;[9] Henning;[6] Dorsey;[10] Keesom, van Agt and Jansen;[11] Borelius and

[4] A. Eucken and W. Dannoehl, Zeits. f. Elektrochemie **40**, 814 (1934).
[5] E. Rosenbohm, Physica **5**, 385 (1938).
[6] F. Henning, Ann. d. Physik **22**, 631 (1907).
[7] F. L. Uffelman, Phil. Mag. **10**, 633 (1930).
[8] H. Adenstedt, Ann. d. Physik **26**, 69 (1936).
[9] R. M. Buffington and W. M. Latimer, J. Am. Chem. Soc. **48**, 2305 (1926).
[10] H. G. Dorsey, Phys. Rev. **25**, 88 (1907).
[11] W. H. Keesom, F. P.G.A.J. van Agt, and A. F. J. Jansen Proc. k. Acad. Amst. **29**, 786 (1926).

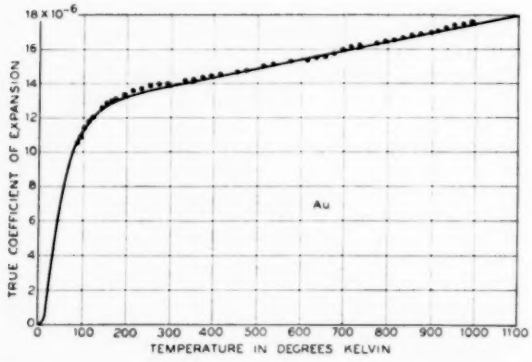

FIG. 2. True coefficient of thermal expansion *vs.* temperature for Au. The dots are experimentally derived coefficients. The solid curve is the Grueneisen plot with $\theta=190$, $\frac{1}{6}(m+n+3)=3.4$, $Q_0=148.8\times10^3$ cal.

Johansson;[12] Simon and Bergmann;[13] and Aoyama and Ito.[14] We are in quite good agreement with the work of Adenstedt; Buffington and Latimer; and Dorsey. The values reported by Simon and Bergmann are much too high near room temperature and too low near 95°K. We are in excellent agreement with the values of Q_0 and $\frac{1}{6}(m+n+3)$ obtained by Adenstedt, but we obtain a value of 325 for θ somewhat higher than Adenstedt's value of 315.

Gold

The gold used in these expansion experiments was obtained from Handy and Harmon as a spectroscopic standard, containing 99.99+ percent Au, the impurities being traces of Ag, Cu, and Pd. The data are presented in Table II with the temperatures given in degrees centigrade and expansivity as $(\Delta l/l_0)\times10^4$. The true coefficient of thermal expansions, obtained graphically from a plot of the data given in Table II, is given by the dots as a function of temperature in degrees Kelvin in Fig. 2. The solid line is the Grueneisen curve obtained by using a characteristic Debye temperature of 190, a value of 3.4 for $\frac{1}{6}(m+n+3)$, and 148.8×10^3 cal for Q_0.

Our results are in good agreement with recent studies of Austin[15] and of Esser and Eusterbrock,[16] in the region from room temperature to 1000°K. The low temperature region has been previously studied by Ebert;[17] Dorsey;[10,18] and Grueneisen.[19]

Aluminum

The specimens were cut from a block of high purity aluminum containing 99.997 percent Al.

TABLE III. *Thermal expansion of aluminum.*

T °C	$\Delta l/l_0\times10^4$	T °C	$\Delta l/l_0\times10^4$	T °C	$\Delta l/l_0\times10^4$
−191.0	−34.358	43.0	10.273	233.2	57.073
−184.5	−33.891	47.5	11.209	237.1	58.009
−176.5	−32.932	50.7	12.145	240.2	58.945
−169.5	−31.996	55.0	13.104	244.1	59.881
−161.5	−31.061	59.0	14.017	247.9	60.817
−156.0	−30.125	62.8	14.953	251.0	61.753
−148.0	−29.189	67.0	15.889	254.7	62.889
−142.7	−28.277	70.3	16.825	258.0	63.625
−137.0	−27.342	75.9	17.761	261.1	64.561
−130.5	−26.406	79.0	18.697	264.6	65.497
−126.0	−25.517	82.8	19.633	268.0	66.433
−120.0	−24.512	87.0	20.615	271.0	67.369
−115.0	−23.576	91.0	21.505	275.0	68.305
−109.0	−22.664	95.0	22.441	277.9	69.241
−104.0	−21.775	97.6	23.377	281.0	70.177
− 99.5	−20.816	102.8	24.359	284.5	71.113
− 93.6	−19.834	106.4	25.272	287.5	72.049
− 89.0	−18.898	110.5	26.231	291.0	72.985
− 84.0	−17.963	114.0	27.121	294.0	73.921
− 79.5	−17.027	117.8	28.057	297.1	74.857
− 75.3	−16.092	122.5	29.086	300.6	75.793
− 70.5	−15.156	126.0	29.929	303.7	76.729
− 66.0	−14.225	130.0	30.888	307.0	77.665
− 61.3	−13.285	134.4	31.801	310.0	78.601
− 56.5	−12.349	138.0	32.760	313.0	79.537
− 52.5	−11.413	142.0	33.673	316.0	80.473
− 48.0	−10.478	145.1	34.632	319.7	81.409
− 43.5	− 9.543	149.0	35.545	322.8	82.345
− 37.5	− 8.607	153.0	36.481	326.1	83.281
− 34.6	− 7.672	157.0	37.417	329.2	84.217
− 30.1	− 6.736	160.0	38.353	333.0	85.153
− 26.0	− 5.800	162.5	38.938	336.0	86.089
− 22.0	− 4.865	163.0	39.289	339.0	87.025
− 17.0	− 3.929	167.2	40.225	341.9	87.961
− 13.2	− 2.994	171.0	41.161	345.0	88.897
− 9.0	− 2.058	175.0	42.097	348.0	89.833
− 5.0	− 1.123	178.6	43.033	351.0	90.815
0	0	182.0	43.969	354.1	91.705
3.5	.7484	185.9	44.905	357.0	92.641
7.6	1.684	189.9	45.841	360.0	93.577
11.0	2.620	193.0	46.777	363.0	94.513
15.1	3.555	196.7	47.713	366.1	95.449
19.2	4.491	200.8	48.649	369.4	96.385
21.0	4.958	204.0	49.585	372.8	97.321
23.0	5.426	208.0	50.521	375.5	98.280
25.0	5.894	211.5	51.457	379.0	99.193
28.0	6.646	215.0	52.393	381.6	100.13
29.0	6.997	218.9	53.329	384.7	101.06
31.0	7.465	222.5	54.265	387.5	102.00
35.0	8.401	226.0	55.201	391.0	102.96
39.0	9.337	229.7	56.137	393.8	103.87

[12] G. Borelius and C. H. Johansson, Ann. d. Physik **75**, 23 (1924).
[13] F. Simon and R. Bergmann, Zeits. f. physik. Chemie **B8**, 255 (1930).
[14] S. Aoyama and T. Ito, Tohoku Imp. Univ. Sci. Rep. **27**, 348 (1939).
[15] J. B. Austin, Physics **3**, 240 (1932).
[16] H. Esser and H. Eusterbrock, Arch. f. Eisenhüttenwesen **14**, 341 (1941).
[17] H. Ebert, Zeits. f. Physik **47**, 712 (1928).
[18] H. G. Dorsey, Phys. Rev. **27**, 1 (1908).
[19] E. Grueneisen, Ann. d. Physik **33**, 33 (1910).

The heating rate from room temperature to 500°C was 30° per hour. The cooling rate from room temperature to −191°C was 20°C per hour. Helium gas at a pressure of 3 mm of Hg was used in low temperature test, and also in the high temperature test up to +170°C, at which point the system was evacuated to a pressure of 10^{-5} mm of Hg for the remainder of the high temperature test. Table III contains the data tabulated as before. There is a small amount of scattering from 160 to 300°C caused by the lack of thermal equilibrium between specimens and refraction thermometer on evacuation of the gas. A plot of the true linear coefficient of thermal expansion *versus* temperature in degrees Kelvin is given in Fig. 3. The dots represent the data with the solid line giving the Grueneisen plot. This excellent fit between the Grueneisen equation and the experimental data was obtained using a characteristic Debye temperature of 400, a value of 2.7 for $\frac{1}{6}(m+n+3)$, and a value of 83.6×10^3 cal for Q_0.

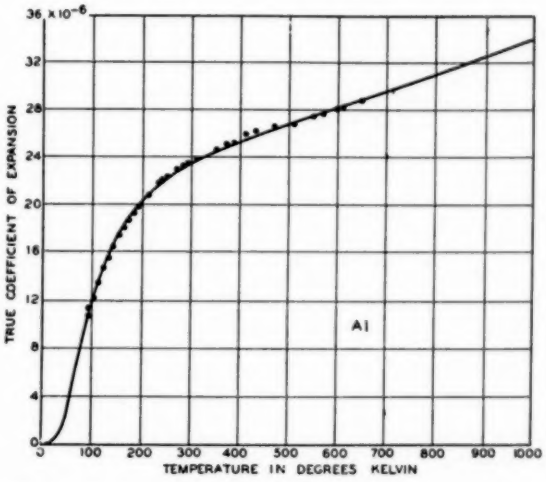

FIG. 3. True coefficient of thermal expansion *vs.* temperature for Al. The dots are experimentally derived coefficients. The solid curve is the Grueneisen plot with $\theta=400$, $\frac{1}{6}(m+n+3)=2.7$, $Q_0=83.6\times10^3$ cal.

Previous measurements in the temperature region from room temperature to 700°K have been made by Hidnert;[20] Uffelman;[7] Henning;[6] and by Taylor, Willey, Smith and Edwards.[21] The low temperature region from room temperature to −191°C has been studied by Buffington and Latimer;[9] Henning;[6] and Ebert.[17] A comparison of our values of mean coefficient of thermal expansion with values reported by Hidnert; and Taylor, Willey, Smith, and Edwards is fairly good. We are also in fairly good agreement in the low temperature region with the results of Buffington and Latimer.

Nickel

The nickel used for the specimens, obtained from the International Nickel Company, contained 99.90 percent Ni, the impurities consisting of 0.03 percent Fe, 0.0035 percent Mg, 0.0005 percent Cu, 0.05 percent C, <0.001 percent Mn, 0.0043 percent Al, 0.011 percent SiO_2. Table IV contains the experimental data tabulated as before. The true coefficient of thermal expansion *versus* temperature in degrees Kelvin is given in Fig. 4. The dots again represent the experimentally derived coefficients with the theoretical Grueneisen plot given by the full drawn curve. The Grueneisen curve was obtained by using a characteristic Debye temperature θ, of 410, the value of 4 for $\frac{1}{6}(m+n+3)$, and the value of 151.5×10^3 cal for Q_0. In the case of nickel, in contrast to the metals Au, Cu, and Al, the behavior of the thermal coefficient of expansion is obscured by the presence of a volume change accompanying the vanishing of ferromagnetism. The peak in the β *vs.* T plot occurs at 635°K, which is the Curie point. In view of the excellent agreement between experiment and theory for the cases of Cu, Au, and Al, we feel that the Grueneisen curve of Fig. 4 represents the course of β *vs.* T insofar as controlled by thermal vibrations, while the deviation beginning at about 320°K is due to the volume change of magnetic origin. It is also of interest to note that the experimental points do not again coincide with the theoretical curve until a temperature of about 780°K is reached, which is some 145° above the Curie point, the peak in the β *vs.* T plot.

A detailed plot of temperature coefficient of electrical resistivity *vs.* temperature of nickel of the same purity, from unpublished data, shows a peak in the identical position on the temperature scale. The temperature coefficient of resistivity does not again become constant at higher temperatures until a temperature of about 800°K,

[20] P. Hidnert, Sci. Pap. Bur. Stand. **19**, 697 (1924).
[21] C. S. Taylor, L. A. Willey, D. W. Smith, and J. D. Edwards, Metals and Alloys **9**, 189 (1938).

TABLE IV. *Thermal expansion of nickel.*

T °C	$\Delta l/l_0 \times 10^4$	T °C	$\Delta l/l_0 \times 10^4$	T °C	$\Delta l/l_0 \times 10^4$
−192.0	−18.830	99.0	12.930	308.0	44.528
−191.0	−18.579	101.0	13.243	311.6	45.018
−184.5	−18.127	104.0	13.684	314.0	45.507
−174.0	−17.575	107.0	14.174	317.0	45.997
−165.5	−17.072	111.1	14.663	320.2	46.487
−158.2	−16.570	115.5	15.202	322.8	47.001
−152.0	−16.068	118.3	15.642	326.0	47.515
−145.0	−15.616	122.6	16.156	329.0	47.980
−139.8	−15.139	125.1	16.622	331.8	48.494
−133.1	−14.562	129.6	17.136	334.8	49.008
−128.0	−14.060	133.8	17.650	337.1	49.473
−122.5	−13.558	137.0	18.090	340.5	49.963
−117.5	−13.080	140.5	18.604	343.0	50.403
−112.0	−12.553	144.0	19.143	344.7	50.648
−107.0	−12.126	147.5	19.559	346.0	50.893
−101.0	−11.549	151.0	20.073	347.5	51.138
− 96.0	−11.047	154.0	20.538	348.1	51.382
− 92.0	−10.545	157.8	21.101	349.6	51.627
− 87.0	−10.043	160.1	21.566	350.9	51.872
− 82.2	− 9.591	163.5	22.007	352.8	52.192
− 78.0	− 9.089	167.0	22.546	354.0	52.362
− 74.0	− 8.536	170.0	22.986	355.0	52.606
− 69.0	− 8.034	173.4	23.476	357.0	52.900
− 64.6	− 7.582	176.2	23.990	358.1	53.096
− 60.0	− 7.030	180.0	24.480	359.5	53.390
− 55.6	− 6.528	182.8	24.945	360.8	53.586
− 51.2	− 6.026	186.0	25.483	362.0	53.830
− 47.0	− 5.574	189.1	25.924	363.4	54.075
− 42.3	− 5.021	192.6	26.462	364.0	54.320
− 38.2	− 4.569	196.2	26.927	366.2	54.565
− 33.3	− 4.017	199.4	27.393	367.8	54.834
− 29.7	− 3.540	203.0	27.931	369.0	55.054
− 25.4	− 3.013	206.0	28.372	370.6	55.299
− 21.1	− 2.460	209.2	28.886	372.4	55.617
− 17.0	− 2.009	213.0	29.424	373.7	55.813
− 13.0	− 1.506	216.0	29.914	375.0	56.034
− 9.0	− 1.004	219.0	30.330	376.7	56.278
− 4.5	− .502	222.7	30.869	378.0	56.572
0	0	226.5	31.383	379.1	56.768
2.0	.351	229.6	31.823	381.2	57.013
8.1	1.004	233.3	32.362	382.5	57.282
12.0	1.506	236.0	32.803	385.3	57.747
15.1	2.009	239.0	33.292	388.0	58.237
20.1	2.511	243.0	33.806	391.6	58.726
23.2	3.013	246.0	34.271	394.6	59.216
28.0	3.590	249.0	34.785	397.8	59.706
31.2	4.017	252.1	35.299	400.8	60.195
36.0	4.519	255.0	36.009	404.5	60.734
39.4	5.021	258.3	36.205	407.0	61.223
43.0	5.523	261.3	36.768	409.0	61.664
47.0	6.026	264.5	37.184	413.0	62.153
51.0	6.528	268.0	37.723	415.5	62.668
55.0	7.030	270.3	38.164	418.5	63.133
58.8	7.532	273.6	38.678	422.0	63.647
62.2	8.034	279.2	39.657	424.0	64.112
66.0	8.536	282.3	40.146	427.1	64.601
69.8	9.038	285.0	40.611	430.0	65.140
74.0	9.540	288.8	41.126	434.0	65.630
77.7	10.043	291.2	41.591	442.7	67.049
81.5	10.545	294.0	42.080	454.0	69.008
85.4	11.047	297.0	42.643	467.2	70.966
89.1	11.549	299.0	43.108	477.5	72.924
93.4	12.051	303.0	43.574	486.2	74.491
97.1	12.553	305.7	44.039	488.5	74.883

a behavior very like that of the expansion coefficient. Mott and Potter explain such "tails" extending over a rather wide range by the assumption that at the Curie point the large Weiss domains break up, leaving something of the nature of short range order to vanish gradually as T is further increased.

The Heisenberg theory of ferromagnetism, as pointed out by Fowler and Kapitza[22] and later demonstrated by Powell,[23] can account in a rough quantitative way for the change in volume which ferromagnetic substances undergo as the ferromagnetism vanishes on heating. The first careful experimental attempt to obtain the ferromagnetic change in length was made by Williams[24] on quite pure nickel. In order to obtain the area under the Curie peak Williams used as a base line his own data at temperatures from room temperature to about 300°C and those of Hidnert[25] for temperatures considerably above the Curie point. We feel in view of the excellent agreement obtained between theory and experiment for Cu, Au, and Al that a theoretical Grueneisen curve which fits the experimental points at temperatures around room temperature and below would serve as a much more accurate base line than the experimental curve used by Williams. The increase in volume due to the vanishing of ferromagnetism begins as low as 325°K in Fig. 4 whereas in Fig. 5 of Williams' paper it is not perceptible until about 525°K is attained.

A careful measurement of the area between the Grueneisen and the experimental curves gives the value 3.65×10^{-4} for the ferromagnetic change in length per unit length, compared with Williams' value of 0.92×10^{-4} for nickel of comparable purity.

We are in quite good agreement with the previous experimental values of Williams.[24] Other work at temperatures above room temperature includes the studies of Hidnert;[25] Henning;[6] Disch;[26] Uffelman;[7] Eucken and Dannoehl;[4] Rosenbohm;[5] Colby,[27] and x-ray studies at high

[22] R. H. Fowler and P. Kapitza, Proc. Roy. Soc. **124**, 1 (1929).
[23] F. C. Powell, Proc. Phys. Soc. London **42**, 390 (1930).
[24] C. Williams, Phys. Rev. **46**, 1011 (1934).
[25] P. Hidnert, J. Research Nat. Bur. Stand. **5**, 1305 (1930).
[26] J. Disch, Zeits. f. Physik **5**, 173 (1921).
[27] W. F. Colby, Phys. Rev. **30**, 506 (1910).

temperatures by Owen and Yates[28] and also by Jesse.[29] We are in good agreement with recent low temperature work of Adenstedt.[8] Other low temperature work includes that of Henning;[6] Disch;[26] Aoyama and Ito,[14] and also of Simon and Bergmann.[13] We do not confirm the existence of a flat plateau in the β *vs.* T plot for the temperature region from 175 to 235°K reported by Simon and Bergmann, nor do we agree with the value of β at any temperature.

Iron

The iron used in this investigation was kindly furnished by Dr. J. G. Thompson of the United States Bureau of Standards. He reports the impurities to be

Cu—<0.002 percent	P —0.0005 percent
Si—0.001 percent	O_2—0.0003 percent
Be—<0.001 percent	N_2—0.0002 percent
Al—Nil	H_2—0.0002 percent
C—0.001 percent	Fe—99.992 (by difference)
S—0.0023 percent	

The iron specimens were heated in He gas at a pressure of 3 mm of Hg up to 100°C at a rate of 10°C per hour, then in a vacuum of 10^{-5} mm of Hg up to 800°C. The low temperature test was made in an atmosphere of He at 3 mm of Hg at a cooling rate of 20°C per hour. Table V contains data on the expansion at different temperatures. The dots in Fig. 5 again give the graphically derived true coefficients of thermal expansion as a function of temperature in degrees Kelvin, with the solid curve giving the Grueneisen plot. We note that the fit is much worse than in the case of Ni and we are forced to the conclusion that deviations from the Grueneisen curve at temperatures above 200°K are to be attributed to disturbances arising from the slow disappearance of ferromagnetism with increasing temperature. The Grueneisen curve was obtained with the characteristic Debye temperature of 420, the value of 3.7 for $\frac{1}{6}(m+n+3)$, and the Q_0 value of 166.67×10^3 cal.

In the temperature region above room temperature we find ourselves in rather good qualitative agreement with the results of Austin and

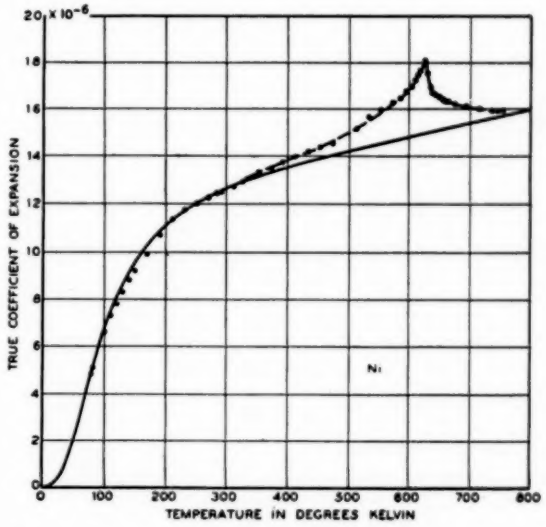

FIG. 4. True coefficient of thermal expansion *vs.* temperature for Ni. The dots are experimentally derived coefficients. The solid curve is the Grueneisen plot with $\theta=410$, $\frac{1}{6}(m+n+3)=4.0$, $Q_0=151.5\times10^3$ cal.

Pierce,[30] and with those of Esser and Eusterbrock.[16] The variations from sample to sample are quite considerable in the region above room temperature where presumably the effects of extremely small amounts of impurities can materially affect the ferromagnetic change in length. In the low temperature region we are in rather good agreement with the results of Adenstedt[8] and somewhat in poorer agreement with the results of Dorsey[10] and of Ebert.[17] Again, as in the case of Ni we fail to find any evidence of the flat plateau extending from 195 to 235°K as reported by Simon and Bergmann. Furthermore we fail to agree with them as to values of the coefficient throughout the region.

Discussion of Results

The agreement between our experimental results and the Grueneisen theory is excellent in the cases of the metals Cu, Au and Al, i.e., in metals free of complications arising from volume changes due to slow disappearance of ferromagnetism with increasing temperature. In the case of Ni the fit is good below 325°K which indicates that the thermal expansion is to be attributed solely to the normal lattice vibrations

[28] E. A. Owen and E. L. Yates, Phil. Mag. **21**, 809 (1936).
[29] W. P. Jesse, Physics **5**, 147 (1934).
[30] J. B. Austin and R. H. H. Pierce, Jr., Physics **4**, 409 (1933).

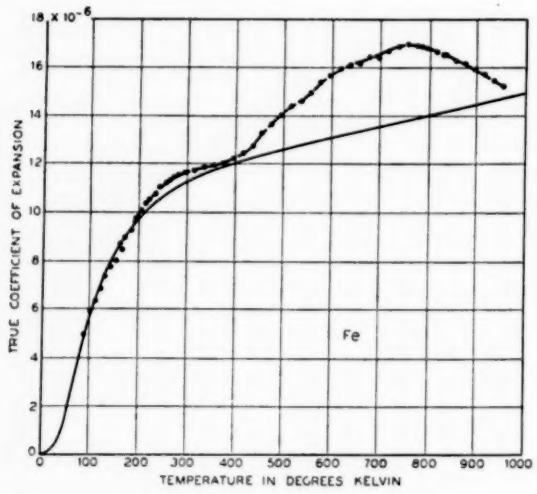

FIG. 5. True coefficient of thermal expansion *vs.* temperature for Fe. The dots are experimentally derived coefficients. The solid curve is the Grueneisen plot with $\theta=420$, $\frac{1}{6}(m+n+3)=3.7$, $Q_0=166.67\times10^3$ cal.

considered in the Grueneisen theory. Above this temperature, where the disappearance of ferromagnetism produces an increase in volume, the total thermal expansion is much greater up to a temperature some 135° above the peak or Curie point. Since such considerations are not involved in the basis of the Grueneisen theory, we should not expect the latter to agree with the experimental results. For the same reasons we should also expect no agreement between theory and experiment for the case of Fe.

The theoretically expected values for $\frac{1}{6}(m+n+3)$,—obtained by assuming $m=3$ along with values of n taken from the Grueneisen constant γ with the aid of Eq. (4)—are 2.68, 3.70, 2.83, 2.55, and 2.26 for Cu, Au, Al, Ni, and Fe, respectively. These values are in moderately good agreement with the values used in order to obtain a good fit between the theoretical Grueneisen curve and the data of 2.8, 3.4, 2.7, 3.7 and 4.0, respectively.

It is of interest to note that small amounts of impurities appear to play only a minor role in the thermal expansion of non-ferromagnetic metals, and also a vanishingly small role in the ferromagnetic metals at temperatures sufficiently low for the temperature dependence of the ferromagnetism to play a small part in the thermal expansion. The good agreement obtained between our results and those of Taylor, Willey, Smith, and Edwards[21] on the very pure Al at high temperatures compared with results obtained by Hidnert[20] using Al of a substantially less degree of purity indicate that the small amounts of impurities do not play a very important role. The same can be said for the agreement between our results on Al at low temperatures and those of Buffington and Latimer[9] obtained with rather impure material.

TABLE V. *Thermal expansion of iron.*

T °C	$\Delta l/l_0\times10^4$	T °C	$\Delta l/l_0\times10^4$	T °C	$\Delta l/l_0\times10^4$
−181.5	−16.607	81.0	9.710	385.1	53.830
−176.0	−16.109	85.2	10.210	392.0	54.806
−166.0	−15.241	90.0	10.711	398.5	55.757
−159.0	−14.740	93.0	11.211	405.2	56.808
−148.0	−14.240	97.1	11.712	410.7	57.759
−142.0	−13.739	102.9	12.262	417.1	58.760
−134.0	−13.289	106.2	12.713	423.2	59.761
−127.0	−12.738	111.6	13.213	430.0	60.837
−121.0	−12.237	115.2	13.714	435.3	61.788
−114.5	−11.737	119.9	14.265	441.3	62.764
−109.5	−11.236	123.0	14.715	447.0	63.765
−103.5	−10.786	127.9	15.241	453.0	64.766
− 98.0	−10.235	132.0	15.716	459.0	65.767
− 92.5	− 9.735	136.0	16.267	465.0	66.768
− 87.0	− 9.234	141.0	16.767	471.0	67.769
− 81.2	− 8.734	144.0	17.218	477.0	68.770
− 77.0	− 8.233	147.2	17.768	483.5	69.771
− 73.0	− 7.783	151.0	18.219	488.8	70.772
− 67.1	− 7.232	155.1	18.769	495.0	71.773
− 62.8	− 6.732	161.6	19.720	501.0	72.774
− 57.8	− 6.231	169.2	20.721	507.0	73.775
− 53.3	− 5.806	176.5	21.797	513.0	74.776
− 48.0	− 5.230	183.0	22.723	519.0	75.777
− 42.2	− 4.730	190.0	23.724	525.0	76.778
− 38.0	− 4.229	197.0	24.800	531.5	77.779
− 33.2	− 3.729	205.0	25.726	537.0	78.780
− 29.0	− 3.228	212.0	26.802	543.0	79.781
− 25.0	− 2.728	218.1	27.728	549.0	80.882
− 20.5	− 2.227	226.1	28.804	555.2	81.883
− 16.0	− 1.727	232.3	29.730	561.0	82.784
− 11.0	− 1.226	239.6	30.731	567.0	83.785
− 6.7	− .7257	246.2	31.732	573.0	84.786
− 2.7	− .2252	252.9	32.733	579.0	85.787
0	0	260.0	33.734	582.8	86.438
2.5	.3504	266.0	34.735	584.2	86.788
5.8	.7758	272.7	35.736	590.5	87.789
10.5	1.276	279.0	36.737	597.9	88.841
14.0	1.777	285.2	37.738	602.8	89.842
18.0	2.277	292.1	38.739	609.0	90.793
22.0	2.778	298.1	39.740	615.8	91.844
28.0	3.304	304.5	40.742	622.1	92.795
32.5	3.454	310.8	41.793	627.5	93.796
36.0	4.204	317.0	42.794	635.2	94.797
40.3	4.705	323.8	43.770	641.2	95.798
45.1	5.205	329.8	44.796	648.5	96.899
48.8	5.706	336.0	45.822	655.0	97.900
53.0	6.206	342.0	46.748	660.1	98.801
57.0	6.707	348.0	47.774	667.0	99.802
61.5	7.207	354.1	48.800	674.3	100.90
65.0	7.708	360.5	49.801	678.0	101.30
68.9	8.208	362.2	50.752	681.0	101.91
73.0	8.709	373.0	51.753	684.8	102.90
77.8	9.209	379.8	52.804		

In ferromagnetic metals such as Ni and Fe, on the other hand, the presence of small amounts of impurities can play a dominating role in determining the total thermal expansion for certain temperature regions. This is clearly indicated for the case of Fe by a comparison of our results with those of Austin and Pierce[30] and of Esser and Eusterbrock,[16] as well as results obtained by these workers on irons of slightly different purity. For the temperature region between room temperature and the temperature of liquid nitrogen the role played by small amounts of impurities in Fe is much smaller than in the high temperature region, as evidenced by the rather good agreement between our results and those of Adenstedt[8] and also the older results of Dorsey.[10] Williams[24] demonstrated rather clearly the influence of small amounts of impurities on the thermal expansion for the case of nickel near the Curie temperature.

ACKNOWLEDGMENT

We wish to thank Dr. L. A. MacColl for many helpful discussions of the Grueneisen theory and Dr. K. K. Darrow for his comments in the preparation of the manuscript.

OCTOBER 15, 1941 PHYSICAL REVIEW VOLUME 60

Rigidity Modulus of Beta-Brass Single Crystals

WALTER A. GOOD
Department of Physics, State University of Iowa, Iowa City, Iowa
(Received August 5, 1941)

The rigidity modulus of ten beta-brass single crystals has been measured as a function of crystal orientation and of temperature from 25° to 500°C by the method of the composite piezoelectric oscillator. The reciprocal of the rigidity modulus, $1/G'$, is linearly related to the orientation function. When these data are combined with Rinehart's previous measurements of Young's modulus, the principal elastic parameters are found to be 3.88, -1.52 and 0.578×10^{-12} cm²/dyne, respectively, at room temperature. Curves and tables give them as functions of temperature up to and slightly beyond the critical temperature for order-disorder. At room temperature, the rigidity modulus is a maximum in the [100] direction, $G'_{[100]}=17.3\times10^{11}$ dyne/cm², and a minimum in the [111] direction, $G'[111]=1.35\times10^{11}$ dyne/cm², and at the critical temperature, $G'[100]=13.5\times10^{11}$ dyne/cm² and $G'[111]=1.06\times10^{11}$ dyne/cm². The elastic anisotropy as given by $G'[100]/G'[111]$ is 12.8 at room temperature, decreases to 12.3 at 250°C and has a value of 13.0 at the critical temperature. The bending-torsion effect was found to be large and in agreement with theory.

INTRODUCTION

THE transition from "order" to "disorder" in certain binary alloys has been studied in terms of changes in various physical properties during this transition.[1] The study of the elasticity of single crystals has been particularly interesting, although a complete theoretical treatment has not been given. Siegel[2] has determined all the principal elastic constants (and corresponding elastic parameters) for Cu_3Au single crystals, from room temperature up to and beyond the critical temperature for order-disorder. Both Webb[3] and Rinehart[4] have worked with single crystals of beta-brass. The former's work included a preliminary study of Young's modulus at room temperature and as a function of the orientation of the crystals. A static method was used. Rinehart, using a more accurate dynamic method extended the work on Young's modulus from about $-80°$ to 500°C (about 30° above the critical temperature). The dependence on orientation was very precisely determined. Rinehart's data established, throughout the temperature range, the elastic parameter, s_{11}, and a

[1] F. Nix and W. Shockley, Rev. Mod. Phys. **10**, 1 (1938).
[2] S. Siegel, Phys. Rev. **57**, 537 (1940).
[3] W. Webb, Phys. Rev. **55**, 297 (1939).
[4] J. Rinehart, Phys. Rev. **58**, 385 (1940) and **59**, 308 (1941).

relation between the other two, s_{12} and s_{44}. The parameters s_{12} and s_{44} cannot be determined separately from Young's modulus alone. In order to get these, some other type of elastic measurement must be made. For the present investigation the measurement of rigidity modulus was chosen. It was measured for a set of ten crystals of various orientations and in a temperature interval from 25° to 500°C. When these data are combined with Rinehart's, there results a complete determination of the three principal elastic parameters throughout the temperature interval.

Whether ordered or disordered the beta-brass[5] crystal structure is body-centered cubic. In the ordered state the copper atoms occupy the corners of the cubes and the zinc atoms the centers. In the disordered state the copper and zinc atoms have equal probabilities of appearing in either the corner or center lattice positions as evidenced by x-ray experiments.[6]

Preparation of Crystals

The crystal specimens were prepared from some of the same material[7] which was used by Rinehart. The crystal growing procedure differed from Rinehart's in two details. Dental casting investment[8] was used instead of Insalute cement to form the mold, and a steel tube leading to the top of the mold allowed the introduction of air or nitrogen under pressure. This prevented pits from forming in the freezing crystal. The crystals produced in this way were smooth and uniform. The rate of lowering of the specimen through the furnace was 3.5 cm/hr. and the temperature gradient was about 20°C/cm. The crystals were four mm in diameter and were grown up to lengths of six cm.

The orientation function, $F(l, m, n)$, of the single crystal specimen is:

$$F(l, m, n) = l^2m^2 + m^2n^2 + n^2l^2, \qquad (1)$$

in which l, m and n are the direction cosines of the specimen length with respect to the three crystallographic axes. These direction cosines were determined as described by Webb[3] and Rinehart.[4] The orientation function may have a value from zero to one-third. The zero value corresponds to a direction along a crystal cube edge, and the one-third value, along a cube diagonal. The direction of the face diagonal has the function equal to one-fourth, but certain other directions also have this value.

Measurement of Rigidity Modulus

The rigidity modulus was measured by the dynamic method of the composite piezoelectric oscillator as used by Siegel[2] and others.[9] The cylindrical brass specimen was cemented to a quartz cylinder of the same diameter. The axis of the latter cylinder coincided with the quartz x axis. Torsional oscillations were excited by applying alternating potentials to four suitably placed electrodes on the quartz crystal. The method finally allows the determination of certain resonance frequencies of the specimen.

The rigidity modulus, G^*, of the specimen at temperature T is given by the formula,[5,10]

$$G^* = 4\rho_{25}L^2{}_{25}f^2(L_{25}/L_T), \qquad (2)$$

in which ρ_{25} is the density at 25°C, L_T the length at T°C, and f is the fundamental resonance frequency of the specimen. The thermal expansion factor L_{25}/L_T, has a value near unity and is calculated from the data of Merica and Schad.[11] Rinehart's value of the density, 8.35 g per cm^3 was used.

The application of an external twisting moment to a crystalline specimen of arbitrary orientation causes bending moments in it.[12] The specific twist (twist per unit length) is different depending on whether flexure is free to occur or is prevented. Thus, in the torsion of a crystal there may exist two measured or effective rigidity moduli. One modulus ($G^* = G'$) results when both twisting and bending are allowed. The other modulus ($G^* = G$) occurs when the bending is prevented. In the case of the cubic crystal the

[5] Approximately one-half copper and one-half zinc.
[6] F. Jones and C. Sykes, Proc. Roy. Soc. **161**, 440 (1937).
[7] Kindly supplied by the American Brass Company, Waterbury, Connecticut. Composition was 52.8 and 47.2 atomic percents copper and zinc, respectively.
[8] Ransom and Randolph Gray Casting Investment.
[9] J. Zacharias, Phys. Rev. **44**, 116 (1933); L. Balamuth, Phys. Rev. **45**, 715 (1934); F. Rose, Phys. Rev. **49**, 50 (1936).
[10] This is taken as the definition of G^*. It is, under certain circumstances (see later), either one or the other of two otherwise defined rigidity moduli. Naturally for an isotropic material, G^* is the single rigidity modulus.
[11] P. Merica and L. Schad, Bull. Bur. Stand. **14**, 571 (1918).
[12] W. F. Brown, Phys. Rev. **58**, 998 (1940).

first modulus G', is related rather simply to the principal elastic parameters (s_{11}, s_{12}, s_{44}) and F, the orientation function:

$$\frac{1}{G'}=s_{44}+4sF, \tag{3}$$

where

$$s=s_{11}-s_{12}-\tfrac{1}{2}s_{44}.$$

A less simple formula holds for the other modulus, G:

$$\frac{1}{G}=s_{44}+4sF-\frac{2s^2[F-4F^2+3\chi]}{s_{11}-2sF}, \tag{4}$$

where

$$\chi=l^2m^2n^2.$$

Formula (4) is seen to be the same as (3) except for its last term, the so-called bending-torsion correction.[13] A combination of (3) and (4) gives:

$$\frac{1}{G'}=\frac{1}{G}+\frac{2s^2[F-4F^2+3\chi]}{s_{11}-2sF}, \tag{5}$$

which shows that $1/G'$ is $1/G$ plus the bending-torsion correction. The bending-torsion correction vanishes for certain directions, [100], [110] and [111] in the crystal and hence in these directions G and G' are identical. Some previous work[14] has been done with specimens of only these orientations. The interpretation of such data does not involve the bending-torsion effect.

Measurements have been made, in this and previous investigations[2,15] on crystals of other than these special orientations. The question has naturally arisen whether G, G', or perhaps neither, has actually been measured. It has been found previously, and here also, that assuming that G is measured gives more consistent and satisfying results. Recently Brown[12] in a theoretical treatment, has given the explanation. According to him, it is possible to get either G or G' or something which is neither one. To obtain physically significant values of G, one must use a long enough specimen and avoid conditions for which torsional and flexural resonances, when considered separately, occur at the same frequency. Because of the coupling between these two types of oscillations, there results a perturbation in both the torsional and flexural frequencies, necessitating a further correction. As far as possible crystals having these troublesome lengths were not used. In actual practice many resonance responses are found and one of the major experimental difficulties lies in identifying the desired torsional one.

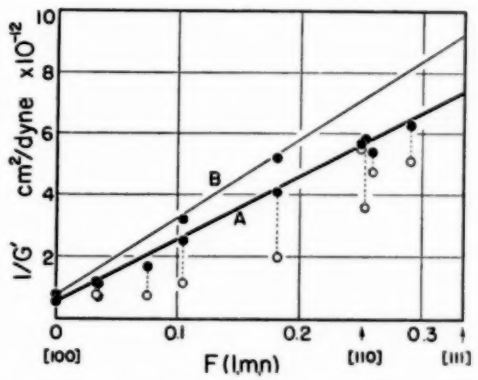

FIG. 1. Reciprocal rigidity modulus against orientation. Curve A, at room temperature. $1/G$, open circles ○. $1/G'$ closed circles ●. Dotted line, bending-torsion correction. Curve B at 466°C, just below critical temperature.

Rigidity modulus measurements were made at room temperature on ten crystals having orientation functions: 0.0017, 0.034, 0.035, 0.075, 0.107, 0.180, 0.248, 0.254, 0.258, 0.290. The modulus of three crystals was found as a function of temperature from 25° to 500°C. The electrical apparatus, the furnace and the procedure for carrying out temperature measurements were substantially the same as used by Rinehart.[4]

RESULTS

Figure 1 shows $1/G$ and $1/G'$ plotted against F (l, m, n) for the ten crystals. Curve A represents data at room temperature. The open circles are measured values of $1/G$ [$G=G^*$, Eq. (2)]. The closed circles show the values of $1/G'$ as calculated from Eq. (5). The length of the dotted connecting line between each pair of points represents the value of the bending-torsion correction. As may be easily seen this term is surprisingly large for some of the crystals. In view of this, the curve A (also B, see later) was not drawn, as it might have been, so as to give the best fit with the points (solid circles, ●), but its

[13] If one defines G' as the "true" rigidity modulus then the word "correction" is fitting; if not, perhaps "bending-torsion difference" would be suitable.

[14] F. Rose, Phys. Rev. **49**, 50 (1936); M. Durand, Phys. Rev. **50**, 449 (1936).

[15] S. L. Quimby and S. Siegel, Phys. Rev. **54**, 293 (1938).

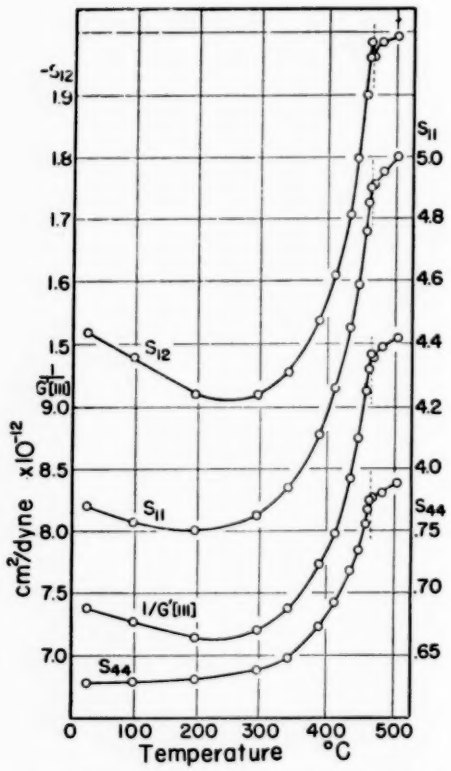

FIG. 2. The values of $1/G'$ [111] and the principal elastic parameters, s_{11}, s_{12} and s_{44} against temperature.

position is partially based on Rinehart's data as follows. He measured the Young's modulus, E, as a function of orientation, F, and plotted the relation:

$$\frac{1}{E} = s_{11} - 2sF, \tag{6}$$

which is similar in form to Eq. (3). Both (3) and (6) yield independent determinations of s, i.e., the slope of (6) is $-2s$ while the slope of (3) is $+4s$. However, since Rinehart's value of s is determined without the introduction of the bending-torsion term, it is believed to be more accurate than one that might be taken from these data. Thus curve A has been drawn through the almost zero correction crystal ($F=0.0017$) with twice the slope determined by Rinehart. The other crystal ($F=0.248$) with a small correction lies practically on the line so drawn. The remaining points, considering again how much they have been "corrected," lie surprisingly near the curve and seem to give good justification both for the experimental method used and its interpretation. It should be emphasized that the calculation of the bending-torsion correction is not proportional to, or simply dependent on, the orientation function, F, but depends in a rather complicated way on the direction cosines, l, m and n. Two crystals may have the same orientation function, F, but differ widely in the correction (see Fig. 1, $F=0.25$). Moreover the accuracy of determining the correction from the measured l, m and n is not as high as the determination of F from the same data. Curve B, Fig. 1, shows the modulus, $1/G'$, at 466°C, which is just below the critical temperature (468°C) for order-disorder. This curve was drawn in the same fashion as curve A, i.e., through the point for $F=0.0017$ and with the slope based similarly on Rinehart's data at that temperature.

The value of $1/G'$ for the crystal, $F=0.0017$, is practically s_{44} [Eq. (3), $F \doteq 0$]. Thus the reciprocal modulus of that crystal as a function of temperature is also the value of s_{44} as a function of temperature. The temperature dependence of s_{44} is shown graphically in Fig. 2. Also shown are s_{11} (Rinehart's determination); and s_{12} which is calculated from s_{11}, s_{44}, and s. The s_{44} varies little up to 300°C where the slope starts to increase rapidly, due to the rapid disordering, becoming very large as the critical temperature (468°C, indicated by dotted line) is reached. The critical temperature is well marked by the definite discontinuity in the slope. This is supposed to be the final and complete disappearance of order. Although similar in shape to s_{11}, the s_{44} does not have the unusual negative slope exhibited by s_{11} at room temperature. The s_{12} curve, however, does show this negative slope characteristic, as does $1/G'$ [111]. This contrasts markedly with the fact that Siegel's s_{11}, s_{12} and s_{44} for Cu_3Au

TABLE I. *Principal elastic parameters of beta-brass at various temperatures.*

	Elastic Parameters (10^{-12} cm²/dyne)		
T°C	s_{11}	$-s_{12}$	s_{44}
24	3.88	1.52	0.578
195	3.61	1.42	0.580
293	3.87	1.42	0.588
389	4.15	1.53	0.624
448	4.64	1.80	0.685
466	4.96	1.98	0.725
468Tc	4.97	1.96	0.727
506	5.06	1.99	0.739

all slope positively at room temperature. The variation of these beta-brass parameters seems to be in general agreement with other order-dependent quantities such as specific heat,[16] resistivity[3] and the determination of Young's modulus[17] for polycrystalline beta-brass. Values of s_{11}, s_{12} and s_{44} are given at selected temperatures in Table I.

Knowledge of the temperature-dependence of the three elastic parameters s_{11}, s_{12} and s_{44} allows the calculation of the behavior of the elasticity in any direction at any temperature. The value of $1/G'[111]$ (reciprocal of the rigidity modulus in the [111] direction) has been calculated from these data and is shown in Fig. 2. It again shows the initial negative slope before much disorder sets in.

The ratio of maximum to minimum modulus in the [100] and [111] directions is taken, as was done by Webb[3] and Rinehart,[4] as a measure of the elastic anisotropy. Figure 1, curve *B* shows greater anisotropy at the higher temperature than curve *A* at room temperature, although both anisotropies are large. The dependence of anisotropy on temperature is shown in Fig. 3, curve *A*. The anisotropy in the rigidity modulus agrees well in shape with the similar Young's modulus anisotropy, but has a larger absolute value (12.8 compared to 8.2 at room temperature).

The compressibility, k, may be found from

$$k=3(s_{11}+2s_{12}). \tag{7}$$

It[18] was computed as a function of the temperature and plotted in Fig. 3 curve *B*. Unfortunately the quantity k, depends upon the difference between two almost equal quantities, thus making it very sensitive to slight changes in s_{11} and s_{12}. Therefore the accuracy of the compressibility curve is not great, but probably sufficient to show the general trend. The compressibility increases with temperature almost to the critical temperature where it suffers a rather rapid decrease, to rise again just beyond the critical temperature. It would be interesting to check the genuineness of this dip by a direct measurement of compressibility as a function of temperature.

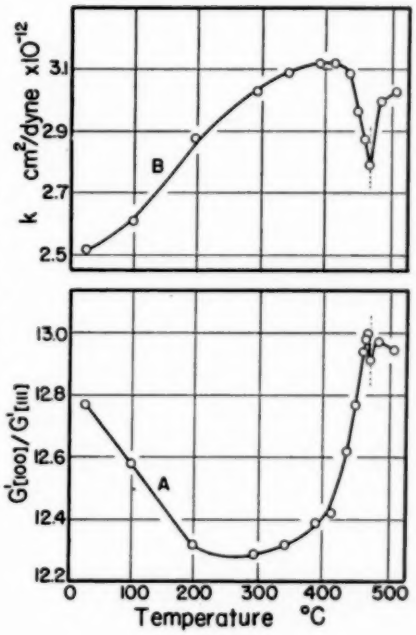

FIG. 3. Curve *A*, anisotropy, $G'[100]/G'[111]$, in rigidity modulus against temperature. Curve *B*, computed compressibility against temperature.

Perhaps this change may be correlated with the thermal volume expansion[11] which also undergoes a discontinuity at the critical temperature.

In conclusion, the writer gratefully acknowledges his indebtedness to Professor E. P. T. Tyndall for much helpful advice and many valuable suggestions; to the Physics Department of the State University of Iowa for the facilities generously placed at his disposal; and to others who assisted him in this work.

[16] H. Moser, Physik. Zeits. **37**, 737 (1936).
[17] W. Köster, discussion of paper by G. Borelius, Zeits. f. Elektrochemie **45**, 16 (1938).
[18] S. Lussana, Nuovo Cimento **19** (1910), gives a value 1.62×10^{-12} cm²/dyne for this composition of brass at room temperature. However, his values of k for copper and zinc do not agree with Bridgman's; so there exists some doubt about Lussana's value for beta-brass.

Mesotron Variation with Upper Air Temperatures

V. F. Hess and F. A. Benedetto
Department of Physics, Fordham University, New York, New York
(Received September 3, 1941)

A TWIN, large area cosmic-ray telescope, after the design of W. F. G. Swann and to be described in a later article, is in operation at Fordham University and is being used in connection with studies of the time variation of the mesotron component and of the temperature coefficient of the mesotron.

Duperier[1] has made a careful investigation of seasonal temperature and cosmic-ray variations. Our investigation has so far been concerned with variations of daily 12-hr. means (6 P.M.–6 A.M.) of mesotron intensity at ground level with upper air temperature data as reported by sounding balloons at Lakehurst, New Jersey, daily from 4–6 A.M. Correlations were made for ground mesotron intensity, reduced for barometer changes,[2] and "spacial average" temperatures up to 16 km. Correlations between ground mesotron intensity and temperatures *at* given levels of 3, 6, 9, and 12 km were also made and are given by the dashed portion of Fig. 1.

Average temperatures up to other levels were not computed because from the trend of our correlation data for temperatures prevailing *at* given levels, Fig. 1, we were led to a new method of taking mean temperatures. The former method, a spacial average, was to integrate the temperature *vs.* height curve and divide by height. The new method we have adopted is to integrate the pressure *vs.* temperature curve and divide by pressure. This is in keeping with the air mass effect noted by Loughridge and Gast.[3] Accordingly, we have indicated by the solid portion of Fig. 1 the temperature coefficient as calculated by our revised method for taking mean temperatures of different air masses.

As is seen from the figure, there is a continually decreasing temperature coefficient as one correlates ground mesotron intensity with temperature values *at* the indicated heights. This itself seems to indicate that air mass is more fundamental in these investigations and hence by taking average temperatures by the spacial average method the temperature at the higher atmospheric levels plays undue influence. On the other hand, if one follows the newer method proposed above, elements of equal mass play equal roles in obtaining mean temperatures. We designate these latter as *mean mass temperatures* or *mass temperatures*.

A comparison between the two methods shows that during the period from March 23 until August 21 the mean spacial temperatures from 0–16 km varied between −36.5°C and −18.4°C whereas the mean mass temperatures for the same air column varied between −28.3°C and +4.0°C. Since the latter range is greater one obtains a smaller temperature coefficient $(1/I)\times(dI/dT)$ by this method than by the former. With the former method the coefficient may be made to increase continually if one takes tem-

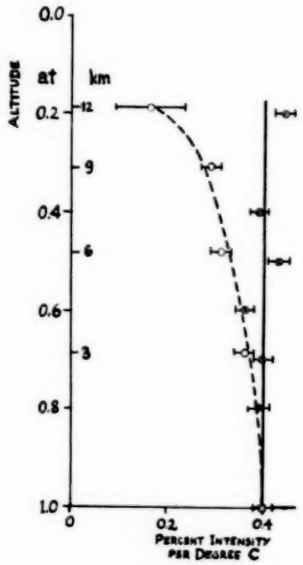

FIG. 1. Dashed curve: temperature coefficient as function of mesotron intensity at ground and temperatures prevailing *at* the level indicated by position of circle. Solid curve: temperature coefficient as function of mesotron intensity at ground and *mean mass temperature* between ground and levels corresponding to indicated fractions of *standard* atmosphere.

[1] A. Duperier, Proc. Roy. Soc. **A177**, 204 (1941).
[2] A. H. Compton and R. N. Turner, Phys. Rev. **52**, 799 (1937).
[3] D. H. Loughridge and P. F. Gast, Phys. Rev. **56**, 1169 (1939).

perature averages progressively higher into the stratosphere.

The seeming constancy of the temperature coefficient for mass temperatures taken for various fractions of the atmospheric mass seems to indicate a fundamental significance of the new method. Data for solid portion of Fig. 1 are taken for given fractions of a *standard* atmosphere. The original data are now being correlated with mass temperatures of given fractions of the actually prevailing *daily* atmosphere, and also with the change in height of the center of gravity of the daily atmosphere, to attempt to determine whether deviations from the straight line occur and whether possibly a peak occurs for some particular fraction of atmospheric mass. For these determinations 24-hr. mean values for mesotron intensity, 6 P.M.–6 P.M., are now being used as closer correlation is obtained thereby. Analysis of data showed that one telescope (upper) ceased to give reliable counts around the beginning of June. Data from lower telescope were accordingly used in our determinations.

The high value for the temperature coefficient of the mesotron component, -0.40 ± 0.02 (percent/°C), is interpreted on the basis that our measurements are essentially of only the mesotron component since vertical screening of 22 cm Pb is used between the counter trays, and side showers are screened by 4 in. Fe. Previous values for the temperature coefficient, obtained with ionization chambers, range between -0.1 percent and -0.25 percent. Hess[4] and collaborators reported at greater altitudes in the Tyrol values of α for shielded chambers 0.09 percent, and for unshielded chambers even much smaller values were found due to the increased number of electrons measured.

According to Blackett[5] the temperature coefficient is

$$\alpha=(1/L)(dz/dT)=(1/N)(dN/dT.$$

If we resolve the cosmic-ray intensity N into mesotron (M) and soft (S) components we may write

$$\alpha_1=[1/(M+S)][d(M+S)/dT]$$

and

$$\alpha_2=(1/M)(dM/dT).$$

Since it may be safely assumed that $dS/dT=0$ it is obvious that $\alpha_1<\alpha_2$, namely, $\alpha_1=\alpha_2 M/(M+S)$. Considering that at sea level about 80 percent of observed cosmic-ray intensity is due to the mesotron component this would account for an actual ratio $\alpha_1/\alpha_2=3/4$ which is almost the ratio actually obtained if one assumes with Gill that the correct value of α obtained with the Model C meter above the geomagnetic knee is $\backsimeq 0.25$ percent. This seems to indicate that in broad outlines the above interpretation is correct. Inserting our value for $\alpha=-0.4$ percent and taking Blackett's $dz/dT=0.05$ km/°C we obtain for the "life range" L of the mesotron $L=0.05/0.004=12.5$ km. Using Blackett's estimate of the total mass (40 times the mesotron rest mass) we obtain the lifetime of the mesotron at rest $\tau_0\backsimeq 1\times10^{-6}$ sec. for the more energetic part of the mesotron spectrum (3.7 Bev). The value $\alpha=-0.4$ percent at present is taken as tentative only and will be checked over a period of at least six more months.

We wish to make acknowledgment of financial aid for this research to the American Philosophical Society and to the Carnegie Institution of Washington. We are especially indebted to Professor W. F. G. Swann for his interest in this project and for allowing the construction of the counters in the shops of the Bartol Foundation. We wish also to thank Mr. Holzman of the La Guardia Airport Weather Bureau and Mr. J. H. Kimball and Mr. D. R. Morris of the Weather Bureaus in New York for furnishing necessary meteorological data.

[4] V. F. Hess, Phys. Rev. **57**, 781 (1940).
[5] P. M. S. Blackett, Phys. Rev. **54**, 973 (1938).

Meson Lifetime and Radioactive β-Decay

S. ROZENTAL
Institute of Theoretical Physics, University of Copenhagen, Copenhagen, Denmark
(Received September 15, 1941)

IN tracing the connection between β-ray decay and the lifetime of free mesons indicated by Yukawa's ingenious theory we meet, as pointed out by Nordheim,[1] with a serious difficulty, since the meson lifetime estimated from cosmic-ray experiments in the well-known way is about 100–1000 times as large as that deduced from the rate of decay of radioactive nuclei. In a theory based on the representation of the meson field by a vector function this discrepancy can only be avoided by assuming the existence of strong direct couplings between the nucleons and the light particles (electrons, neutrinos), an assumption inconsistent with Yukawa's original idea. During the subsequent development of the meson theory the lifetime difficulty has been much discussed, and it was early suggested[2] that a clue to its removal may be found in the fact that the different kinds of meson fields introduced in the theory of nuclear forces correspond to different states of mesons with different decay constants and that, therefore, the available experiments on cosmic rays did not tell the whole story of the meson decay. Still, at that time the appearance of a great number of independent constants in the theory was a hindrance for any more definite conclusions.

In the meantime arguments regarding the unambiguous description of the nuclear forces have been developed[3] leading to a reduction of the number of constants, and especially it has been pointed out by Møller[4] that this number may be further reduced by the suggestive condition of invariance with respect to five-dimensional transformations. In a general treatment of the β-decay problem recently attempted by the writer[5] it appeared impossible on such a basis to avoid the discrepancy as regards the meson lifetime. A renewed examination, however, shows, that this is the case only, if the two universal constants which so far remained unfixed are taken to be of the same order of magnitude, and that the situation is entirely changed if in the set of constants entering in the interaction between mesons and light particles one is taken to be much smaller than the other.

In fact, for the decay constants λ_v and λ_{PS} of the two kinds of meson states involved in the theory and represented by vector and pseudoscalar field functions, we have the following expressions deduced by Yukawa *et al.*[6] and Chang,[7] respectively:

$$\lambda_v=\frac{\mu c^2}{4\pi h}\frac{1}{hc}\left(\frac{2}{3}\gamma_1^2+\frac{1}{3}\gamma_2^2\right), \tag{1}$$

$$\lambda_{PS}=\frac{\mu c^2}{4\pi h}\frac{1}{hc}\left(\gamma_1-\frac{m}{\mu}\gamma_2\right)^2. \tag{2}$$

Here, m is the mass of the electron and μ that of the meson; γ_1 and γ_2 are the two universal constants in question, which in the five-dimensional formulation are the same for the vector and the pseudoscalar meson state. While λ_v and λ_{PS} are comparable in size, if γ_2 is of the same order of magnitude or smaller than γ_1, the ratio between λ_v and λ_{PS} will obviously be very large, if γ_1 is assumed to be small compared with γ_2,

[1] L. Nordheim, Phys. Rev. **55**, 506 (1939).
[2] C. Møller, L. Rosenfeld, S. Rozental, Nature **144**, 629 (1939). In a note which has just reached this country [Phys. Rev. **59**, 1043 (1941)] Snyder has arrived at similar conclusions on the basis of newer experiments.
[3] C. Møller and L. Rosenfeld, D. Kgl. Danske Vidensk. Selskab. Math.-fys. Medd. (Math.-phys. Comm. Acad. Sci. Copenhagen) **17**, 8 (1940).
[4] C. Møller, D. Kgl. Danske Vidensk. Selskab. Math.-fys. Medd. (Math.-phys. Comm. Acad. Sci. Copenhagen) **18**, 6 (1941). (See also A. Pais, *Projective Theory of Meson Fields and Electromagnetic Properties of Atomic Nuclei* (Proefschrift, Amsterdam, 1941).
[5] S. Rozental, D. Kgl. Danske Vidensk. Selskab. Math.-fys. Medd. (Math.-phys. Comm. Acad. Sci. Copenhagen) **18**, 7 (1941).
[6] H. Yukawa, S. Sakata and M. Taketani, Proc. Phys. Math. Soc. Japan **20**, 319 (1938); H. Yukawa, S. Sakata, M. Kobayashi and M. Taketani, Proc. Phys.-Math. Soc. Japan **20**, 726 (1938); see also H. A. Bethe and L. W. Nordheim, Phys. Rev. **57**, 998 (1940).
[7] T. S. Chang, D. Kgl. Danske Vidensk. Selskab. Math.-fys. Medd., in print. In the citation of this formula in reference 5 the sign of the constant f_2 is unfortunately reversed.

and in the extreme case $\gamma_1=0$ it will attain the value $\frac{1}{3}(\mu/m)^2\sim 10^4$.

Under this assumption, the theory of β-decay becomes also much simpler. In fact, for the probability $P(E)$ of emission per unit time of an electron with the energy E in a radioactive process, where the total energy W is released, we obtain the formula[8]

$$P(E)=\frac{4}{\pi^3}\left(\frac{m}{\mu}\right)^4\left(\frac{mc^2}{\hbar}\right)E(E^2-1)^{\frac{1}{2}}(W-E)^2\frac{f_2^2\gamma_2^2}{(\hbar c)^2}|G|^2, \quad (3)$$

where the energies are expressed in units mc^2, G is a matrix element depending on the spins of the two nuclear states concerned, and f_2 is one of the constants responsible for the magnitude of nuclear forces. This formula gives essentially the same energy distribution as Fermi's original theory, and the matrix element is just of the type which, according to Gamow and Teller,[9] is necessary to account for the selection rules in β-transitions. The value of the decay constant, obtained by integrating $P(E)$ from $E=1$ to $E=W$, is of the same order of magnitude as that which would result from a simple vector representation of the meson field. For any reasonable estimate of f_2 and G and for a value of the ratio γ_1/γ_2 about $(1/20)$–$(1/50)$ it gives a value for λ_{PS} quite comparable with the observed decay constant of free mesons in cosmic radiation, while the value for λ_v becomes, of course, far greater.

The identification of the decay constant of mesons in cosmic rays with that of mesons represented by a pseudoscalar wave function does in no way infer that all meson fields are of this type. On the contrary, we may in the present state of the meson theory expect that not only the meson fields in atomic nuclei but also the fields representing the free mesons liberated in violent nuclear collisions are represented by a superposition of vector and pseudoscalar wave functions. Since, however, according to the theory there will be no transitions between states of free mesons, corresponding to the one or the other of these functions, the liberated mesons will behave as a mixture of two ordinary radioactive substances with very different lifetimes. Thus a fraction of the free mesons liberated in the upper part of the atmosphere will disintegrate very quickly with the great decay constant λ_v and escape detection, while the other fraction will disintegrate with the smaller decay constant λ_{PS} and in considerable number be available for observations at lower altitudes. Such mesons should, therefore, in all respects behave like particles with spin 0, represented by a pseudoscalar wave function, a conclusion which is in agreement with recent investigations on meson produced bursts.[10]

The writer wishes to express his sincere thanks to Professor Niels Bohr and Dr. C. Møller for many helpful discussions.

[8] S. Rozental, reference 5. In order that the matrix element may become of the form desired the constant η connected with the direct couplings between nucleons and light particles is here put equal to 0.

[9] G. Gamow and E. Teller, Phys. Rev. **49**, 895 (1936). B. O. Grönblom, Phys. Rev. **56**, 508 (1939).

[10] R. F. Christy and S. Kusaka, Phys. Rev. **59**, 414 (1941); J. R. Oppenheimer, Phys. Rev. **59**, 462 (1941); see also L. W. Nordheim, Phys. Rev. **59**, 554 (1941).

Letters to the Editor

PROMPT publication of brief reports of important discoveries in physics may be secured by addressing them to this department. Closing dates for this department are, for the first issue of the month, the eighteenth of the preceding month, for the second issue, the third of the month. Because of the late closing dates for the section no proof can be shown to authors. The Board of Editors does not hold itself responsible for the opinions expressed by the correspondents.

Communications should not in general exceed 600 words in length.

The Energy Spectrum of the Primary Cosmic Rays

HU CHIEN SHAN
Physics Department, National Wu-Han University, Kia-Ting, Sze-Chuan, China
August 7, 1941

AS it is impossible to send a cloud chamber to the top of the atmosphere, we cannot obtain the energy spectrum of primary cosmic rays as one can for secondaries at sea level. This important problem has been attacked by Bowen, Millikan and Neher[1] by indirect methods with some success. They calculated from their ionization-altitude curves obtained in 1936 and in 1937 the rough distribution of the energy carried into the atmosphere per cm² per sec. by the primaries of energy E, and concluded a sharp band structure of the primary cosmic rays. For many purposes, a knowledge of the number of primaries as a function of their energy is very desirable. This induces the author to make the following calculation.

Let the number of primaries of energy between E and $E+dE$ be $N(E)dE$. Bowen, Millikan and Neher found the values of the areas $\int_{E_1}^{E_2} N(E)EdE$ to be 0.11, 0.44, 0.87 and 0.94 billion ev per cm² per sec. for the limits E_1 and E_2 set at 1.4 and 2.9, 2.9 and 6.7, 6.7 and 17, and 17 and 40 billion ev, respectively. Dividing the areas by the average and by the difference of the corresponding energy limits, we obtain the average numbers per billion ev energy range of primaries having energies lying between E_1 and E_2. From this we get the solid circles shown in Fig. 1.

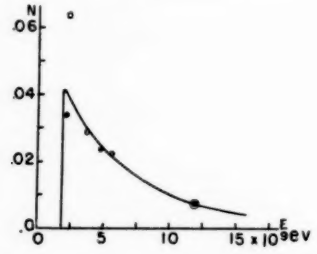

FIG. 1. The energy spectrum of primary cosmic rays.

Later Millikan and Neher[2] discovered that the ionization-altitude curve at one place changes with time. This introduces considerable ambiguity in the result. The curves obtained in 1938 were added in the new analysis. They found then the areas $\int_{E_1}^{E_2} N(E)EdE$ to be 0.14, 0.16, 0.28 and 0.87 billion ev per cm² per sec. for the energy intervals from 2 to 2.9, from 2.9 to 4.5, from 4.5 to 6.7, and from 6.7 to 17 billion ev, respectively. Using these data and making the above calculation again, we get the open circles shown in the figure.

Although the accuracy is low, the curve in the figure probably represents the energy spectrum of primary cosmic rays. The sudden cut-off at the low energy end ($\sim 2\times 10^9$ ev) is exceedingly remarkable. This is very likely to be due to the blocking effect of the solar magnetic field. The curve in the figure is well represented by the exponential equation

$$N = Ae^{-\alpha E}$$

with $\alpha \doteqdot 0.176$, but it is to be noticed that the primaries contain both electrons and protons, as most of us believe, and the energy distribution may be different for electron and proton primaries.

[1] I. S. Bowen, R. A. Millikan and H. V. Neher, Phys. Rev. **53**, 855 (1938).
[2] R. A. Millikan and H. V. Neher, Proc. Am. Phil. Soc. **83**, 409 (1940).

Latitude Effect and the Decay of Mesotrons

R. T. YOUNG, JR.
Worcester Polytechnic Institute, Worcester, Massachusetts
September 16, 1941

DATA on the latitude effect reported in a paper in 1937[1] give some additional information on the decay of the mesotron. In that paper are given measurements with an ionization chamber on cosmic-ray intensities within 20° of the vertical under shielding thicknesses up to 19.4 cm Pb at altitudes corresponding to 76, 51 and 45 cm Hg barometric pressure at geomagnetic latitudes of about 50°N and 1°S. It was pointed out that whereas the latitude ratios I_N/I_E of the northern to the equatorial intensities decrease from 1.30 to 1.16 as the thickness of the atmosphere increases from 45 to 76 cm Hg, the ratio at a given altitude is independent of thickness of lead up to 20 cm. At that time we could give no adequate explanation of this phenomenon. It can now be explained by the decay of the mesotron. The decay of mesotrons is given by the relation: $dn/dz = n\mu_0/p\tau_0$ where dn/dz is the loss of mesotrons per cm of path due to spontaneous disintegration, n the number of mesotrons at a depth z below the top of the atmosphere, μ_0 the rest mass, p the momentum and τ_0 the "proper" lifetime of the mesotron. According to this relation the loss of mesotrons due to spontaneous disintegration is inversely proportional to their momentum. Since the average energy of the radiation getting through the blocking effect of the earth's magnetic field is greater at the equator than in higher latitudes we should expect that the decrease of intensity of the cosmic radiation due to spontaneous decay of the mesotron should be less at the equator than at higher latitudes. This is borne out by the facts quoted above. Interposition of equal masses of lead at both latitudes reduces the radiation in exactly the same way, but interposition of equal masses of air reduces

the radiation more strongly in northern latitudes than at the equator.

Integration of the equation for mesotron decay gives $\log n_2/n_1=\mu_0(z_2-z_1)/p\tau_0$ where n_2 and n_1 are the numbers of mesotrons at depths z_2 and z_1 below the top of the atmosphere. The term p, held constant in the integration, must be interpreted as the "effective" momentum between the depths considered. An expression for p is given by Rossi and Hall.[2] The ratio of the effective momenta for the two latitudes is: $p_E/p_N=\log(n_2/n_1)_N/\log(n_2/n_1)_E$. This ratio is independent of the values taken for the mass or the lifetime of the mesotron. A method of separating the penetrating component from the secondary component is described in reference 1. It was found that under 19.4 cm Pb at northern latitudes about 80 percent of the radiation at sea level, and 50 percent at 51 cm Hg was due to the penetrating component. Since the absorption curves are similar at both latitudes the same percentages may be applied to the equatorial data. Using the data of Table III, reference 1, we obtain:

$$p_E/p_N=\log(0.74/1.62)/\log(0.64/0.80)=1.5.$$

For the energy ranges involved the momenta can be considered proportional to the energies. The ratio of the energies corresponding to these momenta is thus approximately 1.5. The ratio of the minimum energies required for primary electrons at the vertical to break through the earth's magnetic field is $E_E/E_N=4.5$; for protons, 6.5. The variation of energy of mesotrons which penetrate the earth's atmosphere between 51 and 76 cm Hg barometric pressure and have residual ranges greater than 19.4 cm Pb is hence much less than the variation of the lower cut-off of the energy spectrum of the primary radiation which arrives at the earth.

[1] R. T. Young, Jr. and J. C. Street, Phys. Rev. **52**, 552 (1937).
[2] Bruno Rossi and David B. Hall, Phys. Rev. **59**, 223 (1941).

An Explanation of the Diminished Acoustic Velocity in Fluids at High Frequencies

B. V. Raghavendra Rao and D. S. Subba Ramaiya
Department of Physics, University of Mysore, Bangalore, India
September 22, 1941

THE existence of dispersion of acoustic velocity with frequency in gases and the accompanying anomalous damping of high frequency acoustic waves have been definitely established. A satisfactory theory has also been worked out to explain these two phenomena in gases.

In the case of liquids, however, the anomalous damping of ultrasonic waves of high frequency was the first to be observed. A search has been made by a number of investigators to find the accompanying dispersion of acoustic velocity with frequency. So far, in the ultrasonic region at any rate, the experimental results have been inconclusive for the reason that the expected changes in the ultrasonic velocity, a couple of meters per second, are of the same order of magnitude as the errors due to changes in the temperature of the liquid during the course of the experiment.

Early in 1937[1] and subsequently in 1938,[2] one of us experimentally established the dispersion of acoustic velocity in liquids, carbon tetrachloride and acetone, in the hypersonic region. It is now known that it is only at such high frequencies that one should expect measurable changes in the velocity of liquids, a fact subsequently mentioned by Kneser,[3] Bergmann,[4] and others.

What appeared surprising at that time was the fact that in the case of carbon tetrachloride the hypersonic velocity was greater than the ultrasonic velocity, while the reverse was the case in acetone. On a comparison with similar phenomena in gases it is easy to understand the result in the case of carbon tetrachloride. But until now the case of acetone where the hypersonic velocity was less than the ultrasonic velocity required explanation. Further work[5] by interferometric examination of light scattered by liquids in the manner already mentioned has shown that a few other liquids behave similar to acetone in this respect.

In looking for an explanation of the result, one has to consider the effect of high frequency acoustic wave propagation on the liquid medium. Usually the reason for applying Laplace's formula in preference to Newton's in calculating the acoustic velocity in liquids and gases is that the pressure changes in the medium are so rapid that they are taken to be adiabatic. But a closer examination will show, as envisaged by Herzfeld and Rice[6] and by Condon,[7] that this assumption becomes less and less justifiable as the acoustic wave-length approaches 10^{-5} cm for gases and 10^{-8} cm for liquids. In the case of any given fluid the pressure changes due to acoustic wave propagation can be considered completely adiabatic over a range starting from a minimum frequency up to a certain high frequency. Above this, the acoustic velocity begins to diminish due to the enhancement of heat conduction at such high frequencies.

From the relation $\nu=v^2\rho s/4\pi k$ where v is the acoustic velocity, ρ the density, s the specific heat and k the coefficient of thermal conductivity, one can calculate ν the frequency of acoustic waves, at which the departure of the pressure changes in the medium due to acoustic wave propagation from the adiabatic state is a maximum and the corresponding velocity a minimum. But at precisely what frequency of the acoustic wave the adiabatic formula does not hold can at present only be determined by experiment. From the work of one of us on the determination of acoustic velocity in the hypersonic region and from the work of Richardson[8] on the acoustic velocity in gases we get evidence for diminished velocity at a frequency of 10^9 cycles per sec. for liquids and 10^6 for gases under the conditions of the experiment.

This new point of view put forward to account for the diminished acoustic velocity in liquids in the hypersonic region, satisfactorily accounts for the results of Richardson with CO_2 and N_2O where he finds evidence for diminished velocity at a frequency of 10^6 cycles per sec.

[1] B. V. Raghavendra Rao, Nature **139**, 885 (1937).
[2] B. V. Raghavendra Rao, Proc. Ind. Acad. Sci. **A7** 163 (1938).
[3] H. O. Kneser, Physik. Zeits. **39**, 800 (1938).
[4] L. Bergmann, *Ultrasonics* (John Wiley & Sons, New York, 1938). English translation, p. 137.
[5] B. V. Raghavendra Rao, work in course of publication.
[6] K. F. Herzfeld and F. O. Rice, Phys. Rev. **31**, 691 (1928).
[7] E. U. Condon, Am. Phys. Teacher **1**, 18 (1933).
[8] E. G. Richardson, Proc. Roy. Soc. **A146**, 56 (1934).

The Polarization of Luminescence of Ruby

B. V. THOSAR
Physics Department, College of Science, Nagpur, India
August 23, 1941

THE state of polarization of the two intense red lines (λ6927 and 6947) emitted by ruby when optically excited has been investigated. I used a single crystal of synthetic ruby, cut parallel to the optic axis. This was mounted in a glass cell filled with a liquid of nearly the same refractive index as the crystal. The ruby was excited by a narrow beam of light, suitably filtered and the luminescent light was analyzed in the transverse direction.

With the optic axis of the crystal along the vertical, say along OZ, and denoting the direction of incident light by OY, and that of observation by OX, all being mutually perpendicular, I found that the red luminescence is very strongly polarized, as much as 95 percent of the intensity being due to the vibration along OY, i.e., along the direction perpendicular to the optic axis. The intensity of luminescence due to vibration along OZ, the optic axis, is extremely feeble. When the crystal is mounted so that the optic axis was along OX, i.e., parallel to the direction of observation, the intensity of luminescence due to both the vibrations, OZ and OY, is the same, both these directions being perpendicular to the optic axis. Thus it is found that the direction of vibration in nearly the whole of the red emission is confined to one definite plane in the crystal, perpendicular to the optic axis. There is no preferred direction of vibration within this plane.

The crystal of ruby is dichroic. It has a well defined absorption band (from about λ5300–5800) in the green-yellow region, when the incident light is plane-polarized with the direction of vibration perpendicular to the optic axis. There is no such absorption band shown when the direction of vibration in the incident light is parallel to the optic axis. Also there is no selective absorption noticeable for the red region. It thus appears that the process of absorption as well as of luminescence is confined to the same definite plane in the crystal—the plane perpendicular to the optic axis. Also these two processes are definitely related. For, with the exciting light plane-polarized the intensity of red luminescence is greatest when the optic axis is so oriented that the crystal has the strongest absorption for the green-yellow region.

In my previous contributions to the subject,[1,2] I have shown that the fluorescent chromium ion Cr^{+++}, in ruby which emits the sharp red lines, must be replacing in random locations the aluminum ions of the mother-lattice —of corundum, Al_2O_3. In this picture of the structure of ruby, the chromium ions which enter the corundum lattice as impurity become regular components of the lattice, being all situated along the optic axis which is the symmetry axis of the crystal. It is also shown from magnetic considerations that the L vectors of the fluorescent chromium ions must have the same fixed direction in the crystal. If this fixed direction is the optic axis, the orbital moment in all the ions would be along this direction and the electronic orbits would lie in the plane perpendicular to the optic axis. The processes of absorption and emission of light by the chromium ion would then naturally be confined to this orbital plane. The observations reported above, namely, the red luminescence being all due to vibrations in one plane of the crystal and also its dichroism are well explained on this hypothesis.

I am at present engaged in investigating other bands of ruby from this point of view and also the scattering of light in the crystal and its dichroism.

[1] B. V. Thosar, Phys. Rev. **54**, 233L (1938).
[2] B. V. Thosar, Phil. Mag. **26**, 878 (1938).

Absorption Coefficient of β-Rays

DA-TCHANG TCHENG AND JENG-TSONG YANG
Institute of Radium, Shanghai, China
July 10, 1941

MANY authors[1-3] have shown that the absorption of natural heterogeneous β-rays is really not exponential. They are usually more absorbable for large thickness of absorbers. Thus the mass absorption coefficient of UX_2 as measured by certain experimenters varied from a minimum[4] of $\mu/\rho=4.1$ (in Al absorbers) to a maximum[5] of the generally accepted value of $\mu/\rho=6.7$. It is thought that this discrepancy is possibly due to the fact that the absorption curve is not exponential, so that when the measurement was made at different thickness of the absorber, it gave different values of μ/ρ.

We have measured the complete absorption curve of UX_2 from only a few mg/cm² to the ultimate range of UX_2. It is definitely established that its entire logarithmic curve is not exactly a straight line, but can be well defined as a broken line composed of four to five segments (according to the conditions of measurement as shown below) of straight lines. (See Fig. 1.) The slope of each segment represents a definite value of absorption coefficient for a certain range of absorber thickness.

The intersection of the segments usually occurs at definite points corresponding to definite values of screen thickness, no matter what the measuring condition might be, but the slopes of the separate segments are not in-

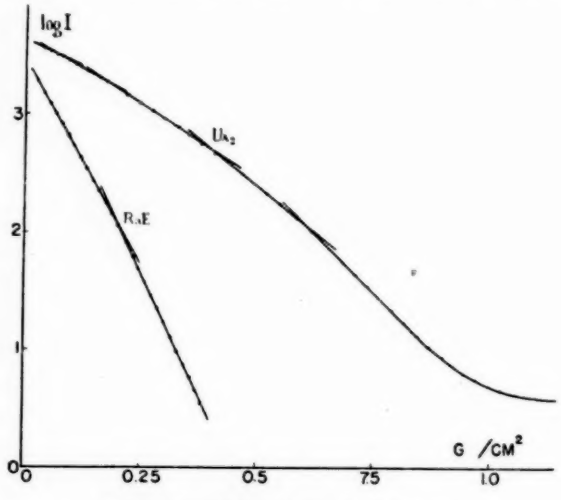

FIG. 1. Absorption of β-rays in aluminum.

TABLE I. *Values of* μ/ρ.

Source	Absorbing Screen							
UX_2	Celluloid	Range (mg/cm²)	0 – 116	– 300 –	460 –	600 –	limit of β-ray	
		μ/ρ	3.6	5.3	6.6	8.2	10.1	
UX_2	Al	Range (mg/cm²)	0 – 70	– 160 –	385 –	610 –	limit of β-ray	
		μ/ρ	4.2	4.8	6.0	7.4	8.9	
UX_2	Cu	Range (mg/cm²)	0 – 75	– 230 –	470 –	limit of β-ray		
		μ/ρ	3.1	6.3	7.4	9.2		
RaE	Celluloid	Range (mg/cm²)	0 – 170	– limit of β-ray				
		μ/ρ	16.6	19.7				
RaE	Al	Range (mg/cm²)	0 – 200	– limit of β-ray				
		μ/ρ	16	19.4				
RaE	Cu	Range (mg/cm²)	0 – limit of β-ray					
		μ/ρ	19					

different to the condition of measurement. When the absorbers are thin, the material of the disk, upon which the UX preparation is placed and which acts as a reflector of the radiations, is quite influential for the determination of μ. Disks made from heavy and thick materials give large values of μ, and lighter materials give smaller ones.

The absorption screens were placed on a cylindrical support, which on account of its simultaneous action as a canalizer, is mostly responsible for the alteration of the values of μ under various conditions. According to our experiments, the slopes of absorption curves are usually more flat, especially at large thickness of absorbers, when made with thin screen supports so that the complete logarithmic absorption curve shows only four segments; while it shows five segments with increased values of μ when made with thicker screen supports. However no indication of further increase of μ is observed if the support is thicker than 800 mg/cm². The radius and the material of the screen support have no appreciable effect on μ.

The distance between the active source and the screen (that is, the height of the screen support) and that between the former and the window of the ionization chamber, play also a considerable role in the value of μ thus determined especially when the screen is not thicker than 150 mg/cm². Low screen supports or large distances between the source and the ionization chamber often give small values of μ.

The variation of μ with measuring conditions and the resolution of the complete absorption curve into segments occur in using copper or celluloid screens as well as in using aluminum screens, but with different values. It is independent of the instrument used in measuring and of the method applied. The same phenomenon also happens when RaE is used instead of UX_2.

If a sufficiently thick ebonite disk is used to hold the source, if the screen support is 6 mm high and is thicker than 800 mg/cm², and if the preparation is about 4 cm distant from the ionization chamber, Table I shows the different values of μ/ρ of UX_2 and RaE.

It is worth while to note that the value of μ/ρ as obtained by most observers is very near to the mean value of those given above.

[1] J. A. Gray, Proc. Roy. Soc. **A87**, 487 (1912).
[2] Kovarik and McKeehan, Physik. Zeits. **15**, 434 (1914).
[3] V. Douglas, Roy. Soc. Canada Trans. **16**, Section 3, 113 (1922).
[4] Geiger, Trans. Faraday Soc. **5**, 505 (1910); Jungfeld, Physik. Zeits. **14**, 507 (1913).
[5] A. F. Kovarik, Phys. Rev. [2] **3**, 150 (1914); Phys. Rev. [2] **6**, 419 (1915).

Temperature Study of X-Ray Diffraction by Diamond

K. LONSDALE AND H. SMITH
Davy Faraday Laboratory, London, England
October 2, 1941

SIR C. V. Raman and Dr. P. Nilakantan have recently[1] suggested that observations on the temperature changes in the intensity of diffuse diffraction by diamond should provide a crucial test as to whether the optical or acoustical vibrations are involved in the occurrence of such diffraction in crystals generally. They also state that, in fact, the intensity of the diffuse maxima found for diamond is practically unaffected by cooling the crystal down to liquid air temperatures.

We have shown,[2] by experiment on a number of diamonds kindly provided by Professor W. T. Gordon, that the diffuse maxima are of two kinds. The "primary" diffuse diffraction, common to all diamonds examined, is really diffuse. It consists of a broad maximum accompanying the sharp Laue spot over an angle of incidence varying by not more than about $\pm 3°$ from the Bragg angle, and it is quite strongly *temperature-sensitive* over a range of 650°C⇄30°C⇄−180°C.[3] This type of diffuse maximum, which increases in diffuseness as the angle of incidence diverges from the Bragg angle, corresponds to that found for all other crystalline substances examined.[4] The "secondary" diffuse diffraction is not really diffuse at all. It consists, according to the diamond orientation, of a sharp spot overlaying the primary diffuse maximum, sometimes accompanied by well-defined streamers of uneven intensity; or of three small sharp spots surrounding the primary diffuse maximum; or of other related groups of spots and streaks. Geometrically it corresponds in reciprocal space to the existence of sharp horns of reflecting power extending out from the lattice points along cube directions. This secondary diffraction is *structure-sensitive*, in that its intensity varies markedly with the diamond used. For the strain-free, mosaic diamonds classed as of type II[5] it is entirely absent; diamonds of type I, even if of uniform size and shape, may show it in very varying intensity. It is also temperature-sensitive (tested over the same range) but much less so than the primary diffraction. It persists over a range of angles of incidence more than three times as great as the range of primary diffuse diffraction, and the sharpness of the secondary maxima not only does not diminish but indeed increases as the angles of incidence and diffraction diverge.

It appears, from the description given by Raman and Nilakantan of the sharpness, persistence and relatively small temperature-sensitiveness of the effects observed by them, that they have only observed the secondary diffraction, and that only on a diamond or diamonds which show this secondary effect strongly. The photographs published by them[6] indicate further that they were using a rather large slit or a large diamond or both. The best conditions for observation of the primary maxima are (1) a fine slit and small diamond (our best photographs were taken with a 0.5-mm slit and an octahedron weighing 1 mg), (2) a crystal orientation in which the primary and secondary

maxima are separated, or (3) a diamond in which secondary effects are weak or absent, (4) a high temperature. Provided that conditions (1) and (2) are fulfilled, however, the primary maxima are easily observable not only for the {111} planes but also for the {220}{113}[{004}{331}] planes of diamonds, with filtered or unfiltered radiation from an iron or copper target. If diamond is to be taken as a typical crystal, it is certainly these diffuse, temperature-sensitive primary maxima which must be discussed.

As far as the secondary phenomena are concerned it is clear that these maxima, which, though slightly temperature-sensitive, are only present in diamonds showing signs of considerable internal strain (type I), cannot be regarded as due entirely, or even mainly, to temperature movements. Further, attempts to explain the effects in terms of any theory, static or dynamic, classical or quantum-mechanical, have so far been complicated by the fact that the {220}{113}{004} and {331} secondary groups are unexpectedly incomplete. *All* the theories, given suitable initial hypotheses, predict spots in geometrically identical positions, and in the case of the {111} planes these spots are found; but they also all predict spots associated with other planes some of which have not been found.

Full details of our experimental work await publication.

[1] C. V. Raman and P. Nilakantan, Phys. Rev. **60**, 63 (1941).
[2] K. Lonsdale and H. Smith, Nature **148**, 112 (1941).
[3] K. Lonsdale and H. Smith, Nature **148**, 257 (1941).
[4] K. Lonsdale and H. Smith, Proc. Roy. Soc. London **A179**, 8 (1941) [with 28 plates].
[5] R. Robertson, J. J. Fox and A. E. Martin, Phil. Trans. Roy. Soc. London **A232**, 463 (1934).
[6] C. V. Raman and P. Nilakantan, Proc. Ind. Acad. Sci. **A11**, 389 (1940); Curr. Sci. **10**, 242 (1941).